

Winter 2011

# Detection of Mortality in Tropical Forests Using Remote Sensing: From Treefall Gaps to Large Disturbances

Fernando Del Bon Espirito-Santo  
*University of New Hampshire, Durham*

Follow this and additional works at: <https://scholars.unh.edu/dissertation>

---

## Recommended Citation

Espirito-Santo, Fernando Del Bon, "Detection of Mortality in Tropical Forests Using Remote Sensing: From Treefall Gaps to Large Disturbances" (2011). *Doctoral Dissertations*. 637.  
<https://scholars.unh.edu/dissertation/637>

This Dissertation is brought to you for free and open access by the Student Scholarship at University of New Hampshire Scholars' Repository. It has been accepted for inclusion in Doctoral Dissertations by an authorized administrator of University of New Hampshire Scholars' Repository. For more information, please contact [nicole.hentz@unh.edu](mailto:nicole.hentz@unh.edu).

DETECTION OF MORTALITY IN TROPICAL FORESTS USING  
REMOTE SENSING: FROM TREEFALL GAPS TO LARGE  
DISTURBANCES

BY

Fernando Del Bon Espírito-Santo

B.S. in Forest Engineer, Federal University of Lavras (UFLA), Brazil, 2000  
M.S. in Remote Sensing, National Institute of Space Research (INPE), Brazil, 2003

DISSERTATION

Submitted to the University of New Hampshire  
in partial fulfillment of  
the requirements for the degree of

Doctor of Philosophy

in

Earth and Environmental Science

December 2011

UMI Number: 3500783

All rights reserved

INFORMATION TO ALL USERS

*The quality of this reproduction is dependent upon the quality of the copy submitted.*

In the unlikely event that the author did not send a complete manuscript and there are missing pages, these will be noted. Also, if material had to be removed, a note will indicate the deletion.



UMI 3500783

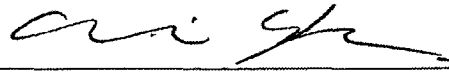
Copyright 2012 by ProQuest LLC.

All rights reserved. This edition of the work is protected against unauthorized copying under Title 17, United States Code.



ProQuest LLC  
789 East Eisenhower Parkway  
P.O. Box 1346  
Ann Arbor, MI 48106-1346

This dissertation has been examined and approved.



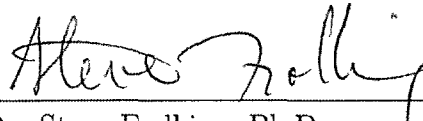
---

Dissertation Director, Dr. Michael Keller, Ph.D.  
Affiliate Professor, University of New Hampshire.



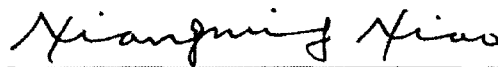
---

Dr. Bobby Braswell, Ph.D.  
Research Associate Professor, Univ. of New Hampshire



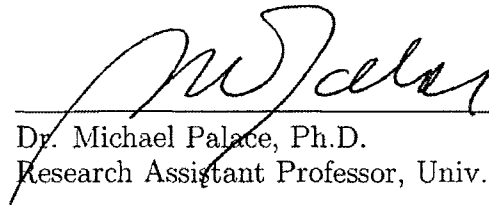
---

Dr. Steve Froking, Ph.D.  
Research Professor, University of New Hampshire



---

Dr. Xiangming Xiao, Ph.D.  
Professor, University of Oklahoma



---

Dr. Michael Palace, Ph.D.  
Research Assistant Professor, Univ. of New Hampshire

September 15, 2011  
Date

# DEDICATION

To my Parents: Papai, Mamãe, Madrinha, Renata, Medi, Menezes, Dona Aurea, little Duda, Niga, Pank and Negão eu dedico.

*"The whole history of science shows us that whenever the educated and scientific men of any age have denied the facts of other investigators on a priori grounds of absurdity or impossibility, the deniers have always been wrong"*

- Alfred Russel Wallace -

# ACKNOWLEDGMENTS

My special gratitude goes to Dr. Michael Keller who opened a huge door in my scientific life. Although Michael has never been physically present in my doctorate, we interacted quite very well by the modern web communication tools. Michael gave me a lot support and important directions, how an adviser should be, a good adviser. I also would like to express my special thanks to Michael for showing me how a young and exciting scientist should persuade its academic life enterprise.

My special thanks also go to the Embrapa Santarém team, Dr. Raimundo Cosme de Oliveira Junior, Mr. Cleuton Pereira and Mr. Francisco Alves de Freitas (Chico). Cosme, always very happy, coordinated with efficiency the logistics of all my field work activities Cleuton and Chico worked in the field with distinguished ecological knowledge of years of practice. They also made my life very easy and fun in the forest which I will remember our moments and adventures forever.

This research had a incredible number of local people from Brazil that physically help me in four long field work trips to the Tapajós National Forest (4 field campaigns of approximately 3 months) which I hope remember all in this list: Galo, Xaropinho, Renilson, Nem, Vavá, Ehrly Pedroso, Coronel and all from Ambé (Tapajós local selective logging community) team.

I would like to thank: the LBA-Santarém Office, Dr. Rodrigo da Silva, Mr. Daniel Amaral and Mr. Idelvandro Fonseca for their support; Dr. Yosio Shimabukuro (INPE) who gave me a lot advice regarding several matters of remote sensing; Dr. Bruce Nelson (INPA) for sharing his beautiful house in Manaus and helping me with several scientific discussions regarding large disturbances; Mr. Cleber de Oliveira (INPE) for teaching me all

the complicated steps of the orthorectification process of high resolution satellite images, Dr Carlos Souza (IMAZON) for sharing his contacts in Acre where I also conducted an additional month of field work, Ms Tara Woodcock and Ms Veronika Leitold (University of Arizona) who were very kind to help me in the last days of my field activities, Dr Plínio Camargo (CENA/ESALQ/USP) for coordinating easily several field work activities together, Dr Emmanuel Gloor from University of Leeds for helping me with several statistical analyses of forest disturbances and for sharing his lovely house in England, and Dr Oliver Phillips also from Leeds for let me work closely with the Rainfor Group

Another special thanks go to Dr Thomas Milliman (UNH, Morse Hall), my best colleague at Complex Systems Research Center, for help me with several if not thousands experiences of computer programming and Dr Ernst Linder (UNH, Department of Mathematics and Statistics) for teaching me a lot about geo-statistics

My acknowledgments are extended to the members of my doctoral committee Dr Steve Frolking, Dr Xiangming Xiao, Dr Michael Palace, and Dr Bobby Braswell for all the guidance and Dr Scott Saleska and Dr George Hurtt during my qualification

Finally I would like to thank João, my friend and English professor from my home town in Brazil who unfortunately passed way during my doctorate João without any business interest, that I still do not understand, has been made it possible for me to learn English and to bear the challenge to have part of my education in a prestigious foreigner university

I have been VERY fortunate to share my personal and academic life with Dr Isabel Maria Anna Dregely and I thank her for her understanding, patience and love during the past years in New England Mein Deutsch ist immer noch schlecht, aber ich werde lernen weil ich dich liebe! I also would like to thanks my closest Brazilian friends in US, Jose Carlo and Neide Lanzoni and Adilson and Rafaela Gal, for sharing so many pleasurable moments together

This research was supported by the NASA Earth System Science Fellowship (NESSF) (Grant # NNX07AN84N) and the NASA Terrestrial Ecology Program contribution to the Large Scale Biosphere-Atmosphere Experiment in the Amazon (LBA).



# CONTENTS

DEDICATION . . . . .	iii
ACKNOWLEDGMENTS . . . . .	iv
LIST OF TABLES . . . . .	xi
LIST OF FIGURES . . . . .	xii
ABSTRACT . . . . .	xv
<b>1 INTRODUCTION</b> . . . . .	<b>1</b>
1.1 Natural Disturbances in Tropical Forests . . . . .	1
1.2 Problem Definition . . . . .	4
1.2.1 Landscape Scale Questions . . . . .	5
1.2.2 Regional Scale Questions . . . . .	5
1.2.3 Relation of Forest Disturbance to Carbon Cycling . . . . .	6
1.3 Objectives . . . . .	6
1.4 Scope and Organization . . . . .	7
<b>2 GAP FORMATION AND CARBON CYCLING IN THE BRAZILIAN AMAZON: MEASUREMENT USING HIGH-RESOLUTION OPTICAL REMOTE SENSING AND STUDIES IN LARGE FOREST PLOTS</b> . . . . .	<b>11</b>
2.1 Introduction . . . . .	12
2.2 Material and Methods . . . . .	15
2.2.1 Study Area and Large Forest Survey Plots . . . . .	15
2.2.2 Gap-Formation and Canopy Openness . . . . .	16
2.2.3 Geostatistics Analysis of Light Environments . . . . .	20

2 2 4	Coarse Woody Debris (CWD) of the Tree-Fall Gaps	21
2 2 5	Remote Sensing Image Processing	22
2 2 6	Linking Ground Disturbance to Satellite Image	25
2 3	Results	27
2 3 1	Gap Geometry, CWD and Tree Mortality	27
2 3 2	Linking Gap Geometry and Light Penetration to C stocks	28
2 3 3	Remote Sensing and Forest Light Environments	28
2 4	Discussion	37
2 5	Conclusion	44
<b>3</b>	<b>STORM INTENSITY AND OLD-GROWTH FOREST DISTURBANCES IN THE AMAZON</b>	
	REGION	46
3 1	Introduction	47
3 2	Methods	48
3 2 1	Data and Study Area	48
3 2 2	Severe Storms in the Amazon Region	48
3 2 3	Digital Classification of the Blow-downs	50
3 2 4	Land Cover Mapping of the Undisturbed Amazon Forest	51
3 2 5	Modeling Spatial Point Patterns of Blow-downs	52
3 2 6	Recurrence Intervals of Blow-downs	55
3 3	Results	56
3 3 1	Size Class Distribution of Large Disturbances	56
3 3 2	Unmixing Spectral Properties of Blow downs	56
3 3 3	Mask of the Antropogenic Disturbances	58
3 3 4	East-West Distribution of Disturbances and Severe Storms	59
3 4	Estimate of Return Frequency of Large Disturbances	65

3.5	Discussion . . . . .	65
3.6	Conclusions . . . . .	68
<b>4</b>	<b>PAN AMAZON FOREST DISTURBANCE SPECTRUM AND IMPLICATIONS FOR THE TROPICAL OLD-GROWTH FOREST CARBON SINK</b>	<b>70</b>
4.1	Introduction . . . . .	71
4.2	Methods . . . . .	73
4.2.1	Forest Inventories and Remote Sensing . . . . .	73
4.2.2	Spatial Distribution of Large Disturbances . . . . .	76
4.2.3	Return Time versus Disturbance Severity . . . . .	77
4.2.4	Forest Aboveground Biomass Simulation . . . . .	78
4.3	Results and Discussion . . . . .	79
4.3.1	Size Frequency and Spatial Clustering . . . . .	79
4.3.2	Occurrence spectrum and return time . . . . .	79
4.3.3	Implications on Basin-Wide Old-growth Forest Carbon Sink . . . . .	82
4.4	Concluding Remarks . . . . .	83
<b>5</b>	<b>CONCLUSIONS</b>	<b>85</b>
5.1	The Balance of Natural Disturbances Processes in the Amazon . . . . .	85
5.2	Open Questions on Disturbance Area and Severity . . . . .	89
5.3	An Equation to Relate Disturbance Area and Biomass Loss . . . . .	91
5.4	Limitations and Future Work on Natural Disturbances for Carbon Cycling .	91
	APPENDICES	93
	APPENDIX A FREQUENTLY USED ABBREVIATIONS	94
	APPENDIX B SUPPLEMENTAL MATERIAL FOR CHAPTER 2	95

APPENDIX C SUPPLEMENTAL MATERIAL FOR CHAPTER 4	107
C.1 Data Integration . . . . .	107
APPENDIX D DOCTOR PUBLICATIONS (2005 - 2011)	115
D.1 Articles in Preparation . . . . .	115
D.2 Articles Submitted Recently . . . . .	115
D.3 Peer-Reviewed Journal Articles . . . . .	115
BIBLIOGRAPHY	117

# LIST OF TABLES

2.1	Geometrical characteristics of canopy gaps and its responses . . . . .	29
3.1	Frequency, disturbed area and recurrence interval of blow-downs . . . . .	66
4.1	Statistical summary of the four data sets . . . . .	75

# LIST OF FIGURES

1-1	Schematic outlines of the main processing steps . . . . .	10
2-1	Location of Tapajós National Forest (TNF), Pará State, Brazil . . . . .	17
2-2	Diagram summarizing methods . . . . .	26
2-3	Correlation coefficients of ground gap parameters . . . . .	30
2-4	IKONOS-2 image processing of 114 ha plot at TNF . . . . .	31
2-5	IKONOS-2 image processing of 53 ha plot at TNF . . . . .	32
2-6	Empirical and fitted semivariogram models for CO and LAI . . . . .	34
2-7	Interpolated ground collections (n=731) of CO and LAI . . . . .	35
2-8	Interpolated ground collections (n=2315) of CO and LAI . . . . .	36
2-9	Distribution of ground gaps over IKONOS-2 image . . . . .	38
3-1	General diagram of image processing and spatial statistics . . . . .	49
3-2	Frequency distribution of blow-downs in the studied area . . . . .	57
3-3	Example of an unmixing Landsat image with occurrence of large disturbances	57
3-4	Land cover mapping of the undisturbed Amazon forest . . . . .	58
3-5	Complete spatial randomness tests for large disturbances in Amazon . . . . .	59
3-6	Intensity of blow-downs occurrences using a Gaussian smoothing kernel . . .	60
3-7	K-function and simulated envelopes of the spatial distribution of blow-downs	61
3-8	Spatial distribution of blowdowns overlaid on the Landsat images . . . . .	62
3-9	Annual frequency of intense storms in the Amazon and blow-down clusters	63

3-10	Numbers, frequency and quantile-quantile plot for blowdowns and storms . . . . .	64
3-11	Scatter plot of storm frequency and blow-down occurrence . . . . .	65
4-1	Spatial distribution of forest disturbance data in the Amazon . . . . .	74
4-2	Intensity maps of blow-downs of Brazilian Amazon . . . . .	80
4-3	Natural forest disturbance spectrum from the Amazon basin . . . . .	81
5-1	Total data gathered to evaluate natural disturbances in the Amazon . . . . .	88
5-2	Relation between disturbance area and aboveground biomass loss . . . . .	90
B-1	GPS ground validation of the ortorectification IKONOS image . . . . .	95
B-2	Freq. distribution of ground collection of LAI-2000 PCA in the 114 ha plot	96
B-3	Freq. distribution of ground collection of LAI-2000 PCA in the 114 ha plot	97
B-4	Spatial distribution of gap fraction . . . . .	98
B-5	Spatial distribution of gap fraction in 114 (spatial trends removed) . . . . .	98
B-6	Spatial distribution of LAI in 114 ha plot . . . . .	99
B-7	Spatial distribution of LAI in 114 ha (spatial trends removed) . . . . .	99
B-8	Spatial distribution of gap fraction in 53 ha plot . . . . .	100
B-9	Spatial distribution of LAI in 53 ha plot . . . . .	100
B-10	Semivariograms of 114 ha plot . . . . .	101
B-11	Semivariograms of 53 ha plot . . . . .	101
B-12	Interpolated canopy openness and leaf area index . . . . .	102
B-13	Uncertainty of CO and LAI interpolation . . . . .	102
B-14	Contour map of CO and LAI in 114 ha plot . . . . .	103
B-15	Contour map of CO and LAI in 53 ha plot . . . . .	104
B-16	Linear regression analysis between gap area and CWD . . . . .	105

B-17	Linear regression analysis between gap area and dead trees . . . . .	106
C-1	Relation between disturbance area and severity . . . . .	109
C-2	Schematic outline to integrate several sources of disturbance data . . . . .	110
C-3	Spatial distribution of 72 Landsat scenes with blow-downs . . . . .	110
C-4	Gaussian kernel smoothing algorithm . . . . .	111
C-5	K-function and monte carlo simulation . . . . .	111
C-6	Frequency, probability density function for area . . . . .	112
C-7	Frequency, probability density function for change in biomass . . . . .	113
C-8	Probability density function for area and severity . . . . .	114



## ABSTRACT

DETECTION OF MORTALITY IN TROPICAL FORESTS USING REMOTE SENSING:  
FROM TREEFALL GAPS TO LARGE DISTURBANCES

by

Fernando Del Bon Espírito-Santo  
University of New Hampshire, December, 2011

The frequency, severity, and intensity of natural disturbances in tropical forests continually re-shape forest structure. At small scale, branch or tree-falls gaps and subsequent recovery are important mechanisms for carbon cycling. At landscape scale, large disturbances (blow-downs) may also play a role on the structure and composition of tropical forests. Quantitative studies of natural disturbances across the occurrence spectrum (branch fall-gaps to blow-downs) are rare for the Amazon. Remote sensing coupled with intense field work data collection provides the means to analyze the dynamic of tropical forests at multiple scales. In this dissertation three aspects of natural disturbances were examined: (1) formation and detection of small scale disturbances investigated in the field and with high resolution remote sensing; (2) mapping and spatial analysis of large disturbances (blow-downs) caused by convective cloud drafts; and (3) a quantitative characterization of the large spectrum of natural disturbances in tropical ecosystems. For small scale disturbances, two large plots of 114 and 53 ha were established and surveyed in unmanaged tropical forest of the Amazon. Data of gap area, canopy openness (CO), leaf area index (LAI), coarse woody debris (CWD) and tree mortality were collected in both plots. The relation between CO and LAI of gaps coupled with high resolution satellite images IKONOS-2 was investigated using geostatistics. Based on field plot measurements, tree-fall gaps account

only about 30% of the flux of annual tree mortality. Most mortality does not result in gap formation. On average, gap formation accounted for a minor proportion of the stocks (about 5% of the total fallen CWD) and fluxes (about 23%) of CWD carbon. There was no significant correlation between remote sensing products and variables of CO and LAI in both large plots, probably due to high shadow fraction in high-resolution images. For large scale disturbances, a spatial pattern analysis of blow-downs apparently caused by severe storms was discovered using 27 Landsat images and daily precipitation from NOAA satellite data. In this image mosaic from 1999 to 2000, there are 279 patches (from 5 ha to 2,223 ha) characteristic of blow-downs. A total of 21,931 ha of forest were disturbed. There was a strong correlation between occurrence of blow-downs and frequency of heavy rainfall (Spearman's rank,  $r^2=0.84$ ,  $p<0.0003$ ). We provided the first spectrum analysis of disturbances, at several scales of severity by combining data collected for this dissertation with previously published information from a variety of sources: (1) Large plot surveys, (2) mapped blow-downs, (3) RAINFOR permanent plots, (4) historical blow-downs  $\geq 30$  ha, and (5) the published mean above-ground biomass map of the Amazon. We found two disjointed disturbance regimes - small-scale tree-fall gaps and larger-scale blow-down disturbances - suggesting that there may be other missed disturbance mechanisms in the Amazon may also play a role in the dynamics of tropical forest ecosystems.

# CHAPTER 1

## INTRODUCTION

### 1.1 Natural Disturbances in Tropical Forests

Tropical forests account for 40% of carbon stored globally in terrestrial vegetation and contribute as much as 36% of the net exchange between atmosphere and terrestrial vegetation [Melillo et al., 1993]. The Amazon basin forests may contribute substantially to observed inter-annual variations in the global carbon cycle [Chambers et al., 2001]. Changing dynamics in tropical forests influence inter-annual and long term variations in the tropical forest carbon cycling [Malhi and Wright, 2004].

While it may be convenient to consider old-growth tropical forests to be in steady-state, recent studies suggest that they may be changing rapidly. Phillips and Gentry [1994] and Phillips et al. [1998] observed an increased turnover of trees and carbon uptake (between 0.1 to 0.5 MgC ha<sup>-1</sup> yr<sup>-1</sup>) through time in many permanent plots of neotropical and paleotropical forests. This increased turnover may be associated with the increase of atmospheric CO<sub>2</sub> [Phillips and Gentry, 1994] and with an observed increase in the growth of lianas [Phillips et al., 1998]. In addition, micrometeorological techniques and inverse modeling of atmosphere also suggest accumulation rate of biomass associated with the hypotheses of CO<sub>2</sub> enrichment [Grace et al., 1995] in South American forests of 0-3 PgC yr<sup>-1</sup> [Malhi and Grace, 2000]. However, recent study with biometric measurements and eddy covariance at the central East Amazon has shown a reduction of carbon sequestration (lower biomass accumulation) with substantial contributions to ecosystem respiration by large stocks of

coarse woody debris (CWD) likely because of recent episodic disturbances or tree mortality [Saleska et al , 2003]

The amount of carbon held in the tropical ecosystems varies spatially and temporally as a result of natural and human activities [Houghton et al , 2000] Much attention has been focused recently on human-induced changes in the vegetation cover of the Amazon such as deforestation [Skole and Tucker, 1993], selective logging [Souza and Barreto, 2000, Asner et al , 2005] and fires [Cochrane, 2003] Human activities are directly responsible for the losses of biomass and consequentially for the alteration of terrestrial carbon stocks [Houghton, 2005] Small natural disturbances due to mortality of trees, on the other hand, are an important dynamic component of carbon cycle [Shugart, 1984] Tree mortality reduces the stock of aboveground biomass and the resulting necromass is re-mineralized leading to carbon dioxide emission to the atmosphere [Saleska et al , 2003, Rice et al , 2004] In addition, tree mortality changes the structure of the canopy through the creation of gaps [Hubbell et al , 1999] Gaps increase the spatial heterogeneity of light conditions in the understory [Denslow, 1987] and alter the interaction between vegetation and the atmosphere turbulent exchanges [Bolzan et al , 2002] In addition to small gaps, large natural disturbances (e.g. blow-downs) have been detected in intact Amazon forests [Nelson et al , 1994]

Modal rates of tree mortality in old-growth tropical forests range from 0.5 to 2% per year [Lieberman et al , 1985, Denslow, 1987, Phillips and Gentry, 1994] Permanent plot data on tree mortality has been used to estimate stand turnover rates However, existing forest inventory plots in old-growth neotropical forests are few in number, limited in size, almost always sited in a non-random fashion with little or no replication, and they do not document spatial dependencies of vegetation elements across the entire landscape [Clark et al , 2004a] Most of the permanent plots in tropical forest were not designed to study carbon budgets

[Rice et al , 2004] The interpretation of plot data provokes numerous ecological debates [Phillips and Gentry, 1994, Sheil et al , 1995, Clark, 2002, Phillips et al , 2002]

At the plot scale, tropical forest dynamics are governed by occurrences of small gaps [Denslow, 1987] A study in 50 ha plot of old-growth moist forest on Barro Colorado Island (BCI), Panama, where all plants with stem diameter bigger than 1 cm were measured, found 1284 gaps across a range of gap sizes 25-49 m<sup>2</sup> (n=894), 50-99 m<sup>2</sup> (n=283), 100-199 m<sup>2</sup> (n=65), 200-399 m<sup>2</sup> (n=33), and  $\geq 400$  m<sup>2</sup> (n=9) Most the disturbances in the BCI forest (894 gaps of 25-49 m<sup>2</sup>) were produced by the death of one to several trees [Hubbell et al , 1999] However, the high frequency these of small gaps produced a total disturbance area of 22,350 m<sup>2</sup> or 2.2 ha of 50 ha forest plot over a 13-year period Estimates of tree mortality from permanent plot studies differ from estimates made from gap formation rates For example, a snapped-off tree may not die even though most of its biomass would be lost Forest turnover rates based on tree mortality can be about half those based on gap dynamics in the same area [Leigh, 1975, Lieberman et al , 1985] Consequently, use of permanent plot data for the estimation of regional carbon dynamics may lead to biases at sub-decadal time-scale

Large natural disturbances in old-growth tropical forests (area  $\geq 1$  ha) are caused by a variety of mechanisms such as landslides [Walker et al 1996], floods [Wittmann, Anhof, and Junk, 2002], fires [Cochrane, 2003], wind [Nelson et al , 1994], and cyclonic storms [Lugo, 1995] Forest disturbance caused by hurricanes (powerful tropical cyclonic storms in the Atlantic) are very common in tropical forest of the Caribbean islands and coastal areas in the region of 10°- 20° [Lugo, 1995] In these regions, catastrophic forest disturbances are common, usually in the form of large storms that damage hundreds of square kilometers [Vandermeer et al , 2000] Consequently, kilometers of tree-fall areas are created and easily detect by satellite images [Ramsey III et al , 2001] In continental regions of tropical forests

such as huge areas of Brazilian Amazon, hurricanes do not occur. However, using Landsat TM images across of the Amazon Nelson et al [1994] detected large natural gaps greater than 30 hectares with fan-shape form (blow-downs) produced by high-velocity downburst winds [Garstang et al , 1998]. Nelson et al [1994] evaluated Landsat data covering most of the Brazilian Amazon and found that the TM scene with the greatest total blow-down-affected area contained 16 blow-downs totaling 8,600 ha or 0.31% of the scene area. The largest single blow-down covered 3,370 ha, with the most frequent size classes falling between 30 and 100 ha. These blow-down events occurred preferentially in the central portion of the Brazilian Amazon.

## 1.2 Problem Definition

Natural disturbances in tropical forests are dynamic and complex. Understanding these phenomena is difficult because of the unpredictability of these events in time and space. Natural disturbances across of the Amazon landscape range in size from single tree fall gaps [Hubbell et al , 1999] to large disturbances [Nelson et al , 1994]. Quantitative studies of natural disturbances in the Amazon are rare. Remote sensing provides a means to analyze disturbances and to study the dynamics of tropical forests at multiple scales. In this thesis, I study natural disturbances and their effects on carbon cycling in tropical forests using remote sensing, spatial statistical modeling and field work.

I propose the following general questions to guide the thesis work. The questions deal with two scales of disturbance that I have identified as related to landscapes and regions. Disturbance processes cross these scales and the differentiation is based on practical concerns for analysis.

### 1.2.1 Landscape Scale Questions

At the local landscape scale and in the domain of gap sizes of square meters to hectares, what is the mean coarse woody debris (CWD) or biomass change and tree mortality observed in small and large scale disturbances? What is the pattern of CWD observed across several disturbances size classes and its implication for the carbon cycling? Can one analyze forest dynamics by observation of gap formation instead of a conventional analysis of individual tree mortality? What remote sensing sensors and digital processing techniques can be used to detect and to monitor gap creating disturbances in tropical forest?

Mortality of individual trees has been related to the creation of new necromass pools. However, substantial biomass loss can also be caused by sub-lethal disturbances [Lieberman et al., 1985]. What elements of the carbon stock (tree, branch or litterfall) lost to the necromass flux can be detected by remote sensing? Can high spatial and spectral resolution satellite images improve the understanding of gap formation in tropical forests?

### 1.2.2 Regional Scale Questions

At the regional scale, in the domain of thousands of square kilometers, what remote sensing approaches can be applied to detect large disturbances, especially blow-downs in the Amazon? Can temporal information improve traditional multi-spectral remote sensing classification? How does the frequency of these events vary across the Amazon landscape? What is the effect of blow-downs on carbon flux in the Amazon?

Although the occurrence of blow-downs has already been analyzed [Nelson et al., 1994], a multi-spectral analysis of remote sensing involving modern techniques of image processing has not been developed to improve the detection of these disturbances. Current digital image processing techniques would allow us to reduce the minimum spatial dimension of a blow-down disturbance below the 30 ha threshold used by Nelson et al. [1994].

### 1.2.3 Relation of Forest Disturbance to Carbon Cycling

What is the relative importance of disturbance at the local landscape scale versus disturbance at the regional scale to the dynamics of the carbon cycle in the Amazon? Is there some mechanistic process that can explain the variation and the frequency of these disturbances at local and regional scales? How can we reduce the uncertainties in carbon budgets by improvement of our knowledge of the rate of formation of small gaps and large disturbances in Amazon forests?

## 1.3 Objectives

The availability of published studies quantifying the rates of natural disturbances in tropical forests is limited. Only a small portion of that literature has incorporated remote sensing techniques. Limited knowledge of the mechanisms for large scale disturbances makes it difficult to model their occurrence. Much of our knowledge of tropical forest dynamics comes from studies conducted in permanent plots in Panama [Condit et al., 2004], Costa Rica [Clark and Clark, 1996], Puerto Rico [Lugo and Helmer, 2004], Guiana Shield [ter Steege and Hammond, 2001], Borneo [van Nieuwstadt and Sheil, 2005] and other areas of Asia [Baxter and Getz, 2005]. In the Amazon few studies with permanent plots have been developed [Malhi et al., 2002]. Permanent plots and networks of plots provide valuable information. However, in the Amazon where plots are extremely scarce, it is difficult to scale from plot work to the regional scale. The goal of this thesis is to examine and to quantify the dynamic processes of forest disturbances in the Brazilian Amazon by use of remote sensing and field work information coupled with a spectrum analysis of the frequency distribution of disturbances from branch-fall to landscape blow-downs.



## 1.4 Scope and Organization

Although much of this research work will involve remote sensing image processing, this thesis will be fundamentally concerned with developing new data analysis methods to improve the estimation of rates of disturbance in Amazon forests. Use of remote sensing data can provide information of forest dynamics across Amazon landscapes and regions. With spatial and temporal information of forest disturbances at different levels, it will be possible to improve terrestrial ecosystem modeling to understand the carbon cycle in the Amazon.

The proposed thesis will be divided into five chapters that are directly linked. Across all chapters, the central topic of disturbances in tropical forest will be studied in different contexts and at different scales. A short overview of each chapter is presented in the following paragraphs. A schematic outline of the steps towards completion of this study is illustrated in the Fig. 1-1.

**Chapter 1.** *Introduction*, concerns and importance of the study of Tree Mortality in Tropical Forests: From Tree-fall Gaps to Landscape Changes. This introductory chapter provides a review of approaches of tree mortality studies in tropical forests including remote sensing and field work across the Amazon, and identifies the research questions.

**Chapter 2.** *Gap Formation and Carbon Cycling in the Brazilian Amazon: Measurement Using High Resolution Optical Remote Sensing and Studies in Large Forest Plots*. This chapter will focus on the use of high resolution spatial remote sensing (IKONOS-2 satellite images) to identify and quantify canopy opening at tropical forest sites. Few studies, if any, have attempted to relate the occurrence of natural disturbances with production of CWD which contributes a large pool of carbon [Denslow, 1987]. In this study we present the survey results of two large forest inventory plots of 114 and 53 ha installed in unmanaged tropical forest of the Amazon. In those plots all gaps were mapped and light availability (canopy

openness and leaf area index) were collected with a very intense protocol of collections. Moreover, all coarse woody debris (CWD) and tree mortality in each ground gap was measured. This chapter will provide the first quantitative estimation of the relation between the gaps area with the amount of CWD produced by natural tree or branch fall disturbances in two large plots installed and surveyed in the central Amazon.

**Chapter 3.** *Storm Intensity and Old-Growth Forest Disturbances in the Amazon Region.*

The occurrence of blow-downs have been associated with heavy rain are relatively frequent in the Amazon. Nelson et al. [1994] used a historical series of Landsat image to register and quantify these events. However, the blow-down classification map was restricted to 30 ha and a single time slices. At that time, Nelson et al. [1994] carried out a visual classification of the blow-down phenomenon. Since then, no study has been conducted to follow up on this work on the Amazon landscape. This chapter will focus on the use of remote sensing classification techniques to improve the estimation of blow-downs in the Amazon central. To evaluate the relation between severe storms and large disturbances in the Amazon, two regional data sets will be integrated: (1) a multitemporal data set of Real-Time Rainfall (RTR) of the north continental area of South America, and (2) a mosaic of ETM+ Landsat images covering the precipitation gradient east to west across the Amazon basin.

**Chapter 4.** *Pan Amazon Forest Disturbance Spectrum and Implications for the Tropical Old-Growth Carbon Sink.* The dynamic processes of biomass accumulation [Malhi et al., 2002] and forest turnover [Phillips and Gentry, 1994; Phillips et al., 1998] have already been developed for small plots. Despite the critical importance of disturbances in forests, a complete characterization and understanding of the spectrum of natural disturbances in tropical ecosystems is missing. Indeed, natural disturbances across of the Amazon landscape have a range of scales from tree-fall gaps [Brokaw, 1982; Denslow, 1987] to large blow-downs

areas [Nelson et al , 1994, Garstang et al , 1998] The goal of this chapter is produce a spectrum analysis of different size class areas of disturbances (from tree-fall gaps to blow-downs) and its relation with carbon cycling To provide this spectrum analysis, data will be integrated from different sources of field work and remote sensing (1) several RAINFOR permanent plots over the Amazon basin [Phillips and Gentry, 1994, Phillips et al , 1998, Lewis et al , 2004, Malhi et al , 2006], (2) two large plots surveyed in this study (Chapter 2), (3) data sets of blow-downs with class size  $\geq 5$  ha covering the central Amazon region (Chapter 3), (4) original historical raw dataset of blow-downs  $\geq 30$  ha provided by Dr Bruce Nelson [Nelson et al , 1994], and (5) the mean above-ground biomass over the South America continental area [Saatchi et al , 2007, 2011]

**Chapter 5. *Conclusions*** This chapter will provide an overview of the balance of natural disturbance processes in the Amazon The overall relation between severity (area) and intensity (change in aboveground biomass) of disturbances from small tree fall-gaps to blow-downs will be presented and discussed Moreover, limitation and future work of natural disturbances will be addressed regarding its importance for the carbon cycling

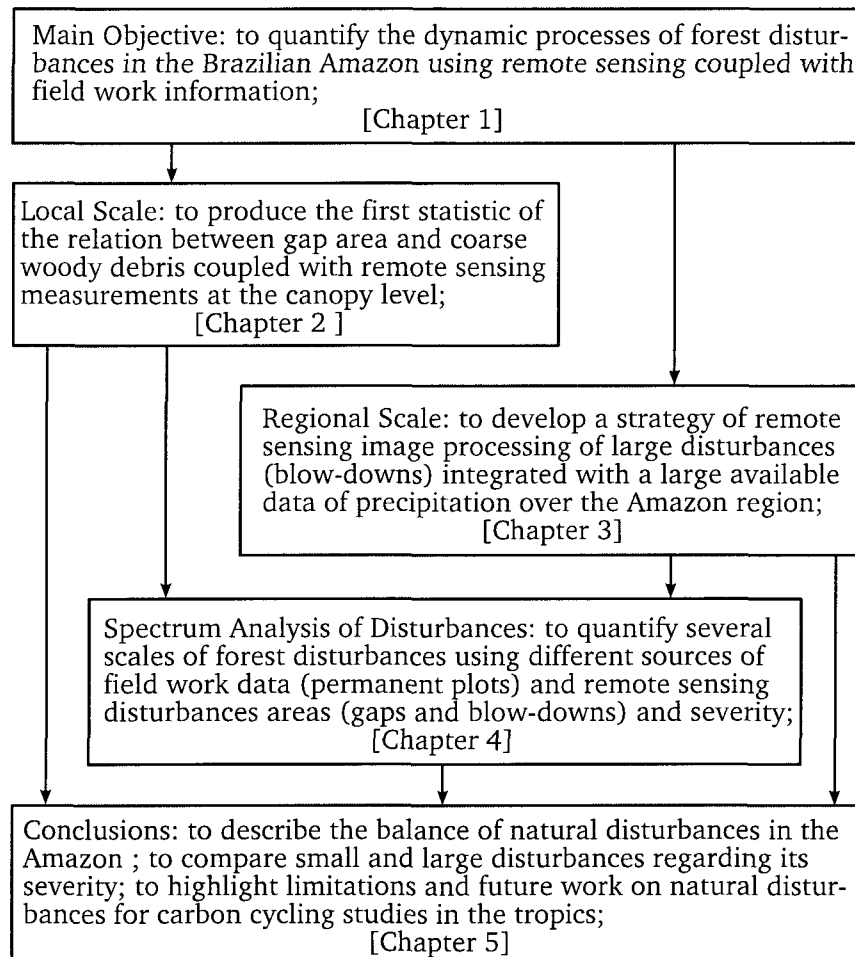
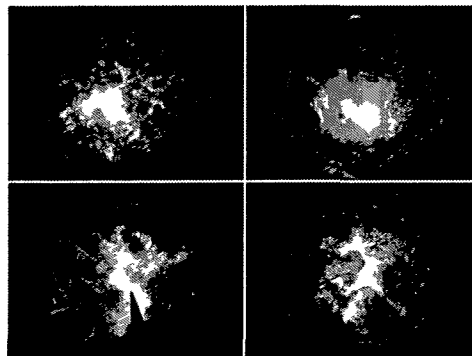


Figure 1-1: Schematic outlines of the main processing steps carried out in this thesis to achieve main objectives.

## CHAPTER 2

# GAP FORMATION AND CARBON CYCLING IN THE BRAZILIAN AMAZON: MEASUREMENT USING HIGH-RESOLUTION OPTICAL REMOTE SENSING AND STUDIES IN LARGE FOREST PLOTS



Dissertation chapter in preparation for Journal of Geophysical Research - Biosciences

## 2.1 Introduction

The formation of gaps in tropical forests continually re-shapes forest structure [Whitmore, 1989, Brokaw and Scheiner, 1989, Shugart, 2000] and is considered an important mechanism for the maintenance of biodiversity [Denslow, 1987, Whitmore, 1989, Brokaw and Scheiner, 1989, Hubbell et al , 1999] Gaps produced by tree-falls and subsequent regrowth create the patchwork structure characteristic of all old-growth tropical forests [Brokaw, 1982, Uhl et al , 1988] and are important to forest dynamics and carbon cycling [Shugart, 1984] The impact of gap formation on tropical forest carbon cycling can be measured by tree mortality at the plot level [Phillips et al , 1998, 2004, Clark and Clark, 2000, Laurance et al , 2004], by measurement of the stocks of coarse woody debris (CWD) [Delaney et al , 1997, Clark et al , 2002, Rice et al , 2004, Keller et al 2004, Baker et al , 2004, Chambers et al , 2004, Palace et al , 2007] or more rarely by measurement of the flux of CWD [Palace et al , 2008]

Gap size and frequency varies across the tropical forest landscape [Clark and Clark, 2000] In a 50 ha area of old-growth tropical forest in Panama, censused in 1982, 1985, 1990, and 1995, only 9 of the 1284 gaps were larger than 400 m<sup>2</sup> [Hubbell et al , 1999] In contrast, at La Selva in Costa Rica, a substantial portion of total gaps registered [ $>21\%$ ] had areas greater than 400 m<sup>2</sup> [Denslow, 1987] The average area of gaps at La Selva was reported to be of 0.01 to 0.02 ha [Clark and Clark, 2000], with only 23% of the gaps exceeding 200 m<sup>2</sup> [Sanford, Braker, and Hartshorn, 1986] The size and frequency of tree-fall gaps is one of the causes of the high variance in biomass estimates at small plot sizes [Shugart, 1984, Bormann and Likens, 1994] At La Selva, the inter-sample variance in biomass estimates began to stabilize for plots sizes above 0.25 ha, about 18 times greater than the estimated median gap size, or 6 times larger than the estimated size of the largest gap class (0.04 ha) in that reserve area of only about 1,000 ha of old growth forest [Clark and Clark, 2000]

Few studies of canopy dynamics have attempted to map the distribution of small gaps

in tropical forests [Hubbell et al., 1999] and few, if any, have attempted to relate the occurrence of natural disturbances with production of CWD which contributes a large pool of carbon [Denslow, 1987; Clark et al., 2002; Rice et al., 2004; Keller et al., 2004; Chambers et al., 2004; Palace et al., 2007] and nutrients [Clark et al., 2002]. We are unaware of any study in the tropical forest literature that estimates the relation between the area of gaps (area, perimeter or any gap geometry) with the amount of CWD produced by natural tree or branch fall disturbances. Relations between disturbance area and its biophysical consequences (e.g. CWD or tree mortality) are valuable for the quantification of the effects of disturbance on carbon cycling in forest ecosystems [Turner, 2010].

Forest disturbances caused by tree-falls and or branch-falls can be described either in terms of the numbers of dead trees or with regard to the sizes and rates that canopy gaps are produced [Van der Meer and Bongers, 1996]. Physically, gaps have been defined in many ways but we find that these divide into two categories: (1) gap-formation at the canopy top level; and (2) gap-formation at the ground level. The first definition describes gaps as a vertical hole in the forest canopy defined by a plumb line extending from the foliage at the gap edge down to a selected height above ground (e.g. 2 m) [Brokaw, 1982]. The second defines a gap as the ground area under a canopy opening extending to the bases of the surrounding the canopy trees, with a minimum trunk diameter (e.g. 20 cm) and height (c.g. 10 to 20 m) [Runkle, 1981]. The definition of Runkle [1981] includes areas directly and indirectly affected by the canopy opening by light enhancement at the forest floor. Depending on the definition used, the area measured can easily vary by a factor of 2. This frustrates interpretation of data on tree fall disturbance regimes not accompanied by a clear gap definition [Brokaw, 1982]. Although gaps can be detected and mapped using these definitions, Lieberman and Lieberman [1989] have argued that disaggregating forest environments into gap and non-gap is unrealistic and difficult to implement with rigor and

consistency. Instead, they argue that the forest light environments should be treated as a continuum.

In order to evaluate the role of Amazon forest dynamics in relation to the global carbon budget, it is necessary to understand the effects of natural disturbances at regional scale. Natural disturbances such as large wind-throw or blow-downs caused by convective cloud downdrafts [Gartang et al., 1998] have been studied for threshold areas greater than 30 ha [Nelson et al., 1994] and 5 ha [Espírito-Santo et al., 2010] based on studies that interpreted  $3.9 \times 10^6 \text{ km}^2$  and  $0.75 \times 10^6 \text{ km}^2$  of Landsat imagery respectively. Recently, Negrón-Juárez et al. [2010] estimated that a single large storm that propagated across the Amazon may have killed 542 million trees. They based their finding on the direct interpretation of only  $0.034 \times 10^6 \text{ km}^2$  of satellite imagery in one contiguous region (0.8% of the total study area) and extrapolated to the larger region based on meteorological data, indicating that  $4.5 \times 10^6 \text{ km}^2$  were potentially affected by squall lines.

Remote sensing provides a means to analyze gap-formation at multiple scales. Data from high-spatial-resolution sensors such as IKONOS (GeoEye Inc.) have been used in tropical forests to measure tree crown sizes [Asner et al., 2002; Clark et al., 2004b], to estimate mortality in dominant trees [Clark et al., 2004a], to detect the effects of selective logging [Read et al., 2003] and in other ecological applications [Hurt et al., 2003]. However, high-resolution images have rarely been used to estimate gap-formation or natural disturbances in tropical forests, with the exception of demographics studies of emergent tree mortality in Costa Rica [Read et al., 2003; Clark et al., 2004b,a].

The aim of this study is to improve the quantification of the area affected by, and the carbon cycle effects of, natural gap-phase disturbances in a tropical forest of Brazilian Amazon. We link gap-formation with carbon cycling through analysis of the coarse woody debris (CWD) within gaps and link gap area measurement to the quantity of CWD. Working



in a large contiguous plot, we investigate how remote sensing can be used to estimate tree-fall and/or branch-fall disturbances and attempt to establish the limits of detection of small disturbances using high resolution satellite imagery. We compare the detection of gaps using high-resolution remote sensing and detailed ground-based forest survey supplemented by instrumental measurements of light penetration.

## 2.2 Material and Methods

### 2.2.1 Study Area and Large Forest Survey Plots

The study was conducted in the area of Tapajos National Forest (TNF) Para State (Brazil), between the coordinates 2°32' and 4°18' S and 54°30' and 55°29' W (Fig. 2-1a-c). According to Koppen classification, the climate in the region is predominantly AmW type [Eidt, 1968] with a mean annual temperature of 25°C. From the historical data (1950-2000) of the Belterra weather station located at the km 20 of BR-163 Highway, the TNF and region has two well defined seasons. The wet season occurs from January through May with 70% of the annual rainfall. The TNF region is characterized by two geomorphological units: the Low Plateau of the Amazon (LPA) and the Tapajós-Xingu Plateau (TXP) [RADAMBRASIL, 1976]. The LPA presents dissected relief and a mean elevation around of 100 m. The TXP, where our studies were conducted, occurs in flat relief and with elevations from 120 to 170 m. Two kinds of soil are common for these geomorphological classes. One is the dystrophic yellow latossol with clay and medium clay (Oxisol) characteristic of the TXP [Silver et al., 2000]. The other is clay red-yellow podzolic soil (Ultisol) that characterizes the LPA.

We installed and surveyed two large forest inventory plots of 114 and 53 ha, in unmanaged forest area at the TNF (Fig. 2-1a-g). The 114 ha plot was installed between August and September of 2008 and the 53 ha plot between August and October of 2009. In both plots the design and the measurement approach was inspired by tropical tree demography

studies of the Center of Tropical Forest Science (CTFS), Smithsonian Institution, which has installed large plots between 25 and 100 ha around the world [Ashton, 1995; Condit et al., 1996; Hubbell et al., 1999; Nascimento et al., 2005; Baltzer et al., 2007].

We modified the concept of those large field surveys to focus on natural disturbances and their connection with the carbon cycle. Our design anticipated up-scaling. All ground measurements were used to calibrate high-resolution satellite images (IKONOS-2) acquired within 2 months of the field campaigns. We adopted an intense protocol of ground measurements of gap-formation and canopy openness and we related those areas with the amount of CWD measured in each gap.

### 2.2.2 Gap-Formation and Canopy Openness

We mapped all gaps in both large plots using the gap definition of Runkle [1981] that includes areas directly and indirectly affected by the canopy opening. Runkle's gap definition includes all gap areas that experience significant forest floor light enhancement. accounts for the direct ecological impact of gap-formation, and is practical to implement. Nonetheless, we recognize that the constraint of any binary definition (gap vs non-gap, c.f. Lieberman and Lieberman [1989]) is unrealistic, so we collected data on light availability (canopy openness) and estimated leaf area index (LAI) for the whole large plot area. We collected the following information for each gap: (1) mode of formation, (2) disturbance age, (3) gap area and perimeter at the ground level, (4) proportion of canopy openness (CO) and (5) LAI.

We defined the modes of gap-formation based on the type of disturbance: (a) partial or complete crown-fall (from either live or dead standing trees), (b) snapped bole-fall, and (c) uprooted tree-fall. We classified all gaps into two age classes: (a)  $< 1$  year, for gaps caused by recent disturbances, and (b)  $\geq 1$  year. For each gap identified in the field we collected a central GPS coordinate using an average of 53 way-points (collection time of

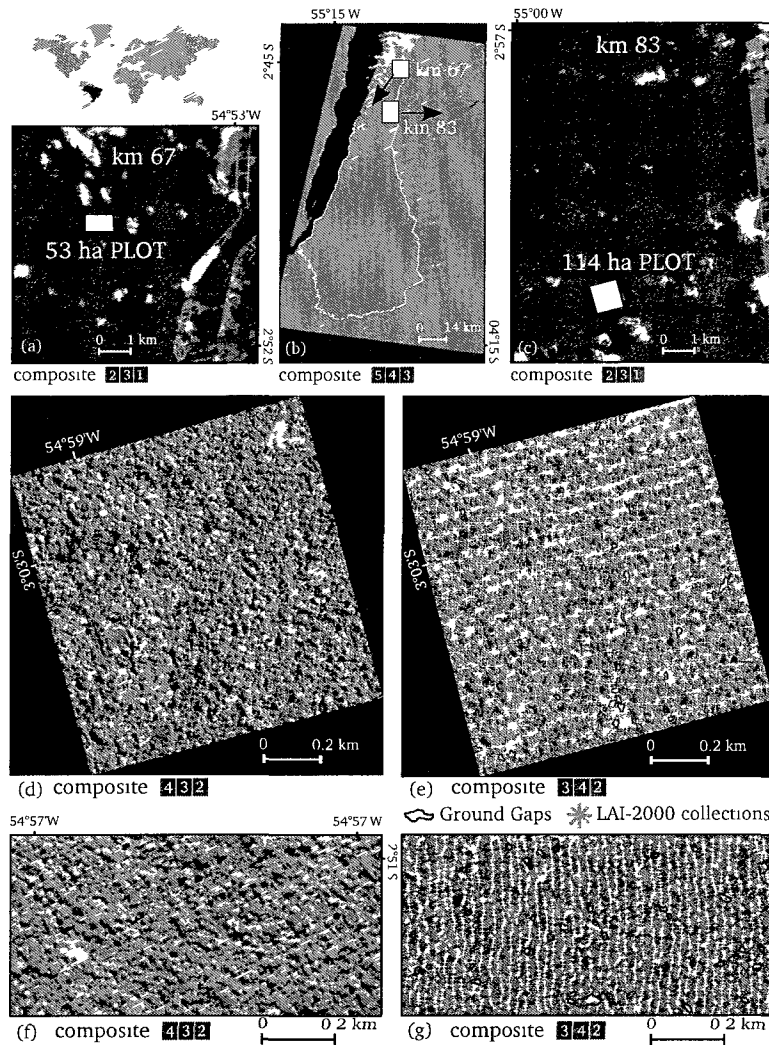


Figure 2-1: Large plot of 53 ha (white box) overlapped in an IKONOS-2 image of 8 August 2009 (a). Location of Tapajós National Forest (TNF) in a TM Landsat 30 July 2001 of Pará State, Brazil (b) and the overlapped IKONOS-2 images. Large plot of 114 ha (white box) overlapped in the IKONOS-2 of 23 June 2008 (b). Forest canopy details of the 114 ha plot survey in the 4 meters multispectral IKONOS-2 bands (d). Ground collections of gaps ( $n=55$ , Runkle's gap definition), hemispherical photos ( $n=110$ , two photos per gap) and biophysical data of canopy openness (CO) and leaf area index (LAI) collected with LAI-2000 plant canopy analyzer ( $n=980$ ) in 114 ha overlapped in a 4 m multispectral IKONOS-2 image (e). Forest canopy details of the 53 ha plot survey in IKONOS-2 multispectral images (f). Ground collections of gaps ( $n=41$ ), hemispherical photos ( $n=82$ ), LAI-2000 ( $n=2315$ ) in 53 ha overlapped in a visible multispectral band composition of IKONOS-2 images (g). Color compositions of Landsat image at full-width wavelength for the three bands are: (3) Red  $0.63-0.69 \mu\text{m}$ ; (4) Near IR  $0.76-0.90 \mu\text{m}$ ; and (5) Mid-IR  $1.55-1.75 \mu\text{m}$ . For the IKONOS2 image the wavelength bands are: (1) blue  $0.45-0.52 \mu\text{m}$ ; (2) green  $0.51-0.60 \mu\text{m}$ ; (3) red  $0.63-0.70 \mu\text{m}$ ; and (4) NIR:  $0.76-0.85 \mu\text{m}$ .

about 2 minutes) with a GPS receiver (GPSMAP 76CSx). From the center of each gap we estimated the distance and the azimuth of each large tree (DBH > 20 cm) along the gap edge. The distance and the azimuth were collected using a laser rangefinder (Impulse-200LR, Laser Technology Corp.) and magnetic compass, respectively, where the temporal magnetic declination of our compasses were corrected using the geomagnetic database model of NOAA [NOAA, 2010]. We collected at least 8 points of the edge of each gap to delimit the gap ground area, according with the geometry and the size of canopy opening. Large gaps required more edge points.

We quantified the CO and LAI for each gap using indirect measurements of hemispherical photographs. We also examined the spatial distribution of sky opening for the whole large plots using diffuse non-interceptance (DIFN) canopy and LAI estimates produced by the LAI-2000 [LI-COR, 1992] plant canopy analyzer (PCA). According to Frazer et al. [2000 and personal communication] the measurements are not exactly the same for hemispherical photos and PCA, considering that LAI-2000 has a limited field of view and different sine weightings. However, in both instruments, the CO is a sine-weighted measure that represents to the relative amount of sky that is unobstructed (open) from a point beneath the forest canopy [Frazer et al., 2000, 2001]. Two photos were taken at the center of each gap, 1.5 m above of the forest floor, with a true color digital camera Nikon Coolpix 950 and FC-E8 sheye lens (180°field of view). The photographs were taken using a tripod and collected in the early morning, and/or late afternoon, or when clouds eclipsed the sun [Rich, 1989]. The lens was facing skyward and camera body was oriented with magnetic north, allowing superposition of solar tracks. The CO of the photos was analyzed using the image processing software Gap Light Analyzer (GLA), version 2 [Frazer, Canham, and Lertzman, 1999]. Considering the substantial color blurring or chromatic aberration associated with digital cameras [Frazer et al., 2001], we used an automatic threshold algorithm for hemispherical

canopy-photographs based on edge detection [Nobis and Hunziker, 2005] to separate canopy and sky elements, producing a binary black and white image. The automatic threshold was applied to all images using the edge value mode [Nobis and Hunziker, 2005]. All photographs were saved in gray scale (BMP format) and CO was extracted following ?. In order to reduce the artifact of image processing and sky condition, we averaged the CO of the two photos collected in each gap.

Using the LiCor PCA, we estimated the CO and LAI in both plots where the CO represents values of DIFN collected with LAI-2000 PCA at a height of 1.5 m. We used two intercalibrated LAI-2000 PCA sensors; one sensor was installed in an open area without obstruction close of the experiment area (above unit) to measure the instantaneous diffuse solar radiation and the other was used to collect the data along the forest transects (below unit) [Welles and Norman, 1991; LI-COR, 1992]. Both sensors were oriented in the same direction, pointed away from the sun with a compass. The measurements were done in the early morning (5:30 AM) or late afternoon (5:30 PM) to minimize the incidence of direct sun on the sensor. We omitted ring 5 measurements of the LAI-2000 because of the large variability in measurements introduced by that ring because of the potential for exaggerated influence of understory plants near the sensor.

In the 114 ha plot the LAI and CO measurements were made along 21 transects of 1 km length with a separation of 50 m. Along each 1 km line we collected biophysical data from the LAI-2000 and GPS coordinates at points separated by approximately 15 m along the transect to produce a grid of CO and LAI data with  $\sim 15 \times 50$  m spatial resolution. We used this data to map all gaps by light availability near the forest floor. For the 53 ha plot we adopted a more intensive data collections of light availability. There measurements were made along 41 transects of 0.5 km length with a separation between lines of 25 meters (double the density of the 114 ha plot). Along each 0.5 km line we collected data of LAI-2000

and its GPS coordinates points separated by approximately 15 m along the transects. In both large plots for cases where the gaps occurred between the lines, we explicitly collected ground data of LAI-2000 at the center and edge of these gaps in order to obtain the maximum spatial variance of CO and LAI. In total, 21 days were needed in each plot to measure the DIFN by LAI 2000 PCA considering the small temporal collection window of this instrument.

For the 114 ha plot we collected 980 measurements of DIFN data from LAI-2000 plant canopy analyzer for the whole area (Fig. 2-1e). However, from the 980 samples, only 731 ground data were used for the geostatistical analysis of canopy openness (CO) and LAI in the 114 ha. We eliminated 249 points with DIFN=0 where inspection of the data revealed that the LAI-2000 devices failed producing large number of consecutive zero values. These 249 samples represent all of 15 transect lines and a few points with DIFN=0 in the darkest regions of the forest plot. Along those 15 transect lines we have only 3 small and old gaps (> 1 year old) that have a minor impact on our analysis of light variability at this plot. In the 53 ha plot we applied a more intensive LAI-2000 data collections with 2315 measurements for the total plot area and no data were excluded (Fig. 2-1g).

### 2.2.3 Geostatistics Analysis of Light Environments

We interpolated all collections of CO and LAI from LAI-2000 PCA of the two large plots using Kriging [Krige, 1951, Journel, 1986, Cressie, 1993]. The difference between neighborhood values (semivariances) is used to represent the spatial autocorrelation structure of the variable [Journel, 1986, Cressie, 1993]. We used a semivariogram  $\gamma(h)$  to calculate the kriging weights of CO ground collections, given by

$$\gamma(h) = \frac{1}{2} \text{Var}[z(s_i + h) - z(s_i)] \quad (2.1)$$

where  $\gamma(h)$  is an estimated semivariance value given a lag ( $h$ ) considering a variable

with the spatial location  $z(s_i)$  and its neighboring at distance  $s_i + h$ . All the geostatistical analyses were executed using `geoR` [Ribeiro and Diggle, 2001] and `Fields` [Fields-Team, 2006] packages of R language [R-Team, 2005].

We fit several theoretical semivariogram models (linear, spherical, exponential, Gaussian and power) using the weighted least squares method and we selected the model with smallest RMSE and the best correlation. Three parameters were used to fit the semivariogram: (1) range equal to the maximum distance of spatial dependence of a variable; (2) sill a variance related to the spatial structure of the data; and (3) nugget equal to the residual variation at the shortest sampling interval. Finally, we used the following ordinary kriging estimator ( $Z$ ) of a number of measurements of CO and LAI ( $z_i$ ) and its corresponding weightings ( $w_i$ ) to predict the spatial distribution of CO over the sample areas:

$$Z(x, y) = \sum_{i=1}^n w_i z_i \quad (2.2)$$

Considering the skewed frequency distribution of DIFN, we applied a square root transformation on the raw data of CO in both large forest inventory plots. No transformation was applied to LAI because the square root transformation did not markedly affect its skewness (see Sup. Material, B2-3).

#### 2.2.4 Coarse Woody Debris (CWD) of the Tree-Fall Gaps

We measured the volume of all CWD in each ground gap. CWD were separated into categories of complete dead trees or wood pieces. For snapped bole-falls and uprooted tree-falls, dead trees with diameter  $> 10$  cm were recorded for diameter. For complete crown-falls only crown-fall trunks were recorded; measuring all fallen branches would have been exceedingly time consuming. The majority of CWD production in this area was caused by single or multiple tree-falls. We used the allometric equation developed by ? as

approximation of wood biomass losses by fresh treefalls and snapped bole falls. For gaps with partial crown-fall we recorded the diameters of all wood pieces greater than 10 cm (the end diameters of the logs) and length of the woody material. CWD in the gaps were classified according to its decomposition status [Harmon et al , 1995] into five classes from freshest (class 1) to most rotten (class 5) [Keller et al , 2004, Palace et al , 2007, 2008]. We used an average of wood density measured for each decay class specifically developed for this site [Keller et al , 2004]. We calculated the sectional volume of each segment of CWD using Smalian's equation, cross-sectional average areas from the ends of the segment

$$V_s = h(AL + AU)/2 \quad (2.3)$$

where  $V_s$  is the segment volume ( $m^3$ ) of a CWD,  $h$  is the segment length (m),  $AL$  is the cross-sectional area at lower end section (large diameter) and  $AU$  is the cross-sectional area at the upper end section (small end diameter)

The mass of section of CWD ( $M_i$ ) was determined from the product of the volume of material ( $V_i$ ) and the respective density for the material class ( $\rho_i$ ) [Keller et al , 2004, Palace et al , 2007, 2008]

$$M_i = \rho_i V_i \quad (2.4)$$

### 2.2.5 Remote Sensing Image Processing

We investigated the relation between CO and LAI of gaps and remote sensing data of 114 and 53 ha plots installed in 2008 and 2009, respectively. Two images of the commercial satellite IKONOS-2 were acquired over field plots. The first acquisition was in June 23, 2008 (~ 2 months before of the field work campaign) with a nominal collection elevation and sun angle elevation of  $66.77^\circ$  and  $56.81^\circ$ , respectively. The second acquisition was in



August 11, 2009 (at the same period of field work activities) with a nominal collection elevation and sun angle elevation of 66.74° and 54.49°, respectively. IKONOS-2 is a satellite sensor that produces 11-bit radiometric images in panchromatic (PAN) and multi-spectral (MS) with 1 and 4 m spatial resolution, respectively [Goward et al., 2003; Dial et al., 2003]. The PAN image uses a wide portion of visible and near-infrared electromagnetic spectrum (0.45-0.90  $\mu\text{m}$ ). The multispectral wavelength bands at full-width and half-maximum are: blue (0.445-0.516  $\mu\text{m}$ ), green (0.506-0.595  $\mu\text{m}$ ), red (0.632-0.698  $\mu\text{m}$ ) and NIR (0.757-0.853  $\mu\text{m}$ ). The image was radiometrically transformed from digital numbers (DN) to in-band radiance physical units ( $\text{mW cm}^{-2} \text{sr}^{-1}$ ). Subsequently the image in radiance was corrected to the top-atmosphere or apparent reflectance ( $\rho_a$ ) using the mean solar exoatmospheric irradiance and the post-calibration gain and off-set of the IKONOS sensor [Taylor, 2009], by application of Markham and Barker [1987] algorithm:

$$L_\lambda = L_{min\lambda} + \left( \frac{L_{max\lambda} - L_{min\lambda}}{QCAL_{max\lambda}} \right) QCAL \quad (2.5)$$

where  $L_\lambda$  is spectral radiance,  $L_{min\lambda}$  is minimum spectral radiance,  $L_{max\lambda}$  is maximum spectral radiance,  $QCAL_{max\lambda}$  is digital number range, and  $QCAL$  is digital number.

The apparent reflectance ( $\rho_a$ ) is calculated by:

$$\rho_a = \frac{\pi L_\lambda d^2}{E_{sum\lambda} \cos\theta_s} \quad (2.6)$$

where  $L_\lambda$  is spectral radiance ( $\text{mWcm}^{-2}\text{sr}^{-1}\mu\text{m}^{-1}$ ),  $d$  is Sun-Earth distance in astronomical units,  $E_{sum\lambda}$  is exoatmospheric average spectral radiance ( $\text{mWcm}^{-2}\mu\text{m}^{-1}$ ) and is Sun zenith angle.

We ortho-rectified the IKONOS images using an empirical 3-D rational function model [Toutin, 2001, 2004] over the rational polynomial coefficients (RPCs) from satellite ephemeris

and altitude data (Geo-Eye product). The rational polynomial method is similar to a simple polynomial method, except that it involves a ratio of polynomial transformations and it also takes ground elevation into consideration. RPCs reduce the numbers of ground control points (GCPs) needed for the ortho-rectification [Fraser et al., 2001; Dial and Grodecki, 2005]. We extracted the Z-terms related to the third dimension of the terrain from an available DEM extracted from the Shuttle Radar Terrain Mission (SRTM) for the region. Although the spatial resolution of SRTM [Smith and Sandwell, 2003] is relatively coarse ( $\sim 90$  m for South America) for high-resolution satellite images, this has a minimal effect in our flat study area. In addition we used highly accurate GCPs with differential GPS collected in the field to check and improve the ortho-rectification quality. A cross-check of GCPs revealed a root mean square (RMS) error  $\sim 4$  meters after the ortho-rectification process (see Sup. Material, B-1).

We applied a spectral mixture analysis (SMA) using a linear mixture model [Shimabukuro and Smith, 1991] in all 4 IKONOS MS bands of both images to produce fractional images base on three end-members: green vegetation (GV), nonphotosynthetic vegetation (NPV), and shade (SD). The spectral pure end-members (GV, NPV and SD) were determined using pure end-members as determined using the pure pixel index (PPI) [Boardman, 1993; Boardman et al., 1995]. A spectral library was then built to estimate the fractional proportions (NPV, GV and SD) of each pixel [Shimabukuro and Smith, 1991]. Considering the high percentage of shadow in high resolution forest canopy images [Asner and Warner, 2003] we also produced simple Normalized Difference Vegetation Index (NDVI) [Tucker, 1979] from the IKONOS bands red (0.632-0.698  $\mu\text{m}$ ) and NIR (0.757-0.853  $\mu\text{m}$ ) for both images.

### 2.2.6 Linking Ground Disturbance to Satellite Image

We applied an ordinary least square (OLS) regression to assess the relationship between canopy openness (disturbances) and a high-resolution satellite image. The continuous variables of CO and LAI interpolated by kriging (114 and 53 ha plot areas) were used to evaluate the remote sensing IKONOS-2 products, fractions (NPV, GV and SD) and NDVI images. For the 114 ha plots we used a total interpolated grid of 71 416 pixels of 4 meters (the same spatial resolution of IKONOS 2 multispectral bands) of CO and LAI to evaluate patterns of disturbance signals of ground remote sensing in the satellite image products of 2008. In the 53 ha plot a total grid of with 33,020 pixels of 4 meters were used to detect disturbances of tree fall-gaps over the satellite image products of 2009. Following the regression analyses we determined the best remote sensing threshold from IKONOS-2 image to quantify the disturbances at the plot scale and for the whole image. In total we statistically tested 16 variables where four are ground remote sensing data (grids of CO and LAI for both plots) and four are satellite products (NPV, GV, SD and NDVI). We also applied a secondary approach to detect areas with a high density of ground disturbances. Using the interpolated grids of CO and LAI from both plots, we selected ground thresholds from those variables that were found to cover all mapped polygons of tree-fall gaps. The selected grid pixels of 4 meters from those thresholds were then submitted to analysis of regression with remote sensing products. We empirically estimated the amount of CWD produced by small scale of disturbances based on this derivative remote sensing threshold and on the relation between biophysical canopy gap (CO and LAI) and CWD. Our methodological approach is summarized in Figure 2-2.

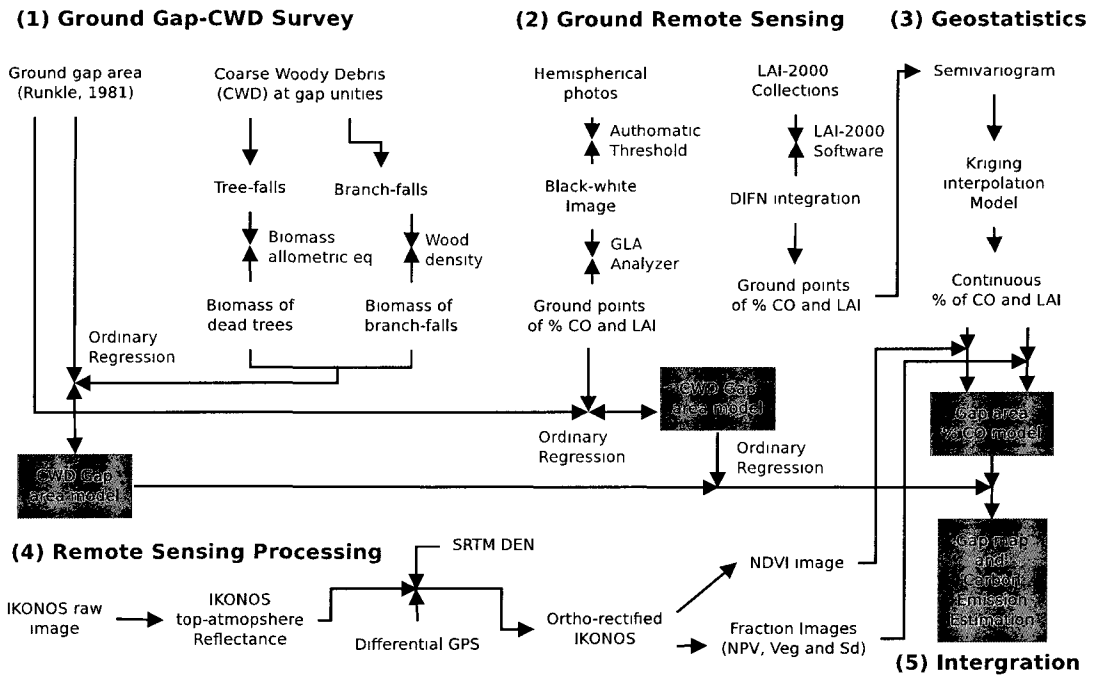


Figure 2-2: Diagram summarizing methods for ground gap-CWD survey and remote sensing, geostatistics, image processing and data integration applied in this study.

## 2.3 Results

### 2.3.1 Gap Geometry, CWD and Tree Mortality

In two large forest inventory plots (114 and 53 ha) we found 96 gaps. We removed 4 samples (outliers) reducing our total sample to  $n=92$  (Table 2.1). Outliers were identified as samples with large differences from the mean, high variability of residuals when the variables were plotted in stepwise scatter plot pairs and high scores of leverage (the impact on the fitted values when  $i$ th cases is dropped from the regression models) [Crawley, 2007]. These 4 outliers had high amount of CWD and number of dead trees for a small proportion of opened area. The correlation between CWD and gap area increased from  $r=0.61$  to  $r=0.73$  with the exclusion of outliers. Also, removing these outliers increased the correlation between number of dead trees and gap area from  $r=0.69$  to  $r=0.75$ .

For the total areas of the two plots (167 ha) we found 16 gaps produced by partial or complete crown-fall (from either live or dead standing trees), 44 by snapped bole-fall and 32 by uprooted tree-fall (Table 2.1). In total those disturbances represented a sum area of 2.37 ha or 1.42% of the total plot. Only 1.36 ha or 0.81% of the plots was affected by recent disturbances < 1 yr old. The recurrence interval or turnover for these events is about 123 years for all gap-formation types. The mean gap size was 257 m<sup>2</sup> (95% confidence limit between 219 and 294 m<sup>2</sup>). The minimum gap size is 32 m<sup>2</sup> (crown-fall) and the maximum 1,313 m<sup>2</sup> (uprooted tree-fall). The average length of these gaps is 26 m where the geometry of uprooted gaps had the largest length (81 m) and consequently the largest disturbance area (1,313 m<sup>2</sup>).

Coarse woody debris amounts depended of the type of gap formation, crown-falls contained 0.11 Mg C ha<sup>-1</sup> of CWD, snapped tree falls 0.65 MgC ha<sup>-1</sup> and uprooted tree falls 0.70 MgC ha<sup>-1</sup>. In total, all 92 gaps contained a stock of 1.45 MgC ha<sup>-1</sup> of necromass for the study area. The flux of CWD caused by the gaps is 0.76 MgC ha<sup>-1</sup> y<sup>-1</sup>. All those

natural disturbances accounted for a mortality average of 6.47 trees (DBH  $\geq$  10 cm) per gap or a sum of 596 individual trees ( $3.57 \text{ ha}^{-1}$ ;  $> 10 \text{ cm DBH}$ ) for the total 167 ha plot area. From those total dead trees contained in the gaps of all ages, we estimated a mean annual tree mortality of  $2.38 \text{ trees ha}^{-1} \text{ y}^{-1}$  (Table 2.1).

### **2.3.2 Linking Gap Geometry and Light Penetration to C stocks**

A section of reported values of C stocks by different gap-formation mode is listed in Table 2.1 and summarized in Fig. 2-3. There is a strong correlation between production of CWD and gap geometry ( $r=0.73$  for area,  $r=0.80$  for perimeter and  $r=0.78$  for length) (Fig. 2-3 and Sup. Material B-16). Gap area and perimeter both correlated even more strongly ( $r=0.75$  and  $0.77$ , respectively) with the number of dead trees (Fig. 2-3 and Sup. Material B-17).

A total of 184 hemispherical photos were collected (2 for each gap) and analyzed with GLA [Frazer, Canham and Lertzman, 1999] to estimate CO ( $n=92$ ) and LAI ( $n=92$ ) for each gap. We found a weak correlation between CWD and ground hemispherical photo measurements of CO and LAI ( $r=0.22$  and  $r=0.12$ , respectively). Slightly higher correlation was found between the number dead trees and the same variables ( $r=0.57$  for CO and  $r=0.41$  for LAI)

### **2.3.3 Remote Sensing and Forest Light Environments**

Based on the high resolution multispectral bands of the IKONOS-2 acquired close to the dates of our forest surveys we produced the remote sensing products NDVI and spectral unmixing fractions images (GV, NPV and SD) for the 114 (Fig. 2-4) and 53 ha (Fig. 2-5) large plots.

Geostatistical analysis of CO and LAI in the 114 ha plot ( $n=731$ ) revealed a spatial auto-correlation of both variables (Fig. 2-6) to a range of 56 and 71 meters for CO and

Table 2.1 Geometric characteristics of ground tropical canopy gaps (n=92) and biophysical responses of those disturbances in two large plot (114 and 53 ha) forest surveys at Tapajós National Forest (PA), Brazil

Gap Parameters	Gap Mode Formations			
	Crown-Fall	Snapped	Uprooted	All Gaps Types
Frequency of gap formation mode	16	44	32	92
Proportion of gap formation mode*	17%	48%	35%	
Gap area (ha)	0.26	1.18	0.93	2.37
Proportion of area under gap process**	0.15%	0.71%	0.56%	1.42%
Gap area (ha) with < 1 yr old in 167 ha	0.14	0.90	0.32	1.36
Proportion of area under gaps < 1 yr old	0.08%	0.54%	0.19%	0.81%
Frequency of gaps > 500 m <sup>2</sup>	0	4	2	6
Max gap size (m <sup>2</sup> )	266	658	1313	1313
Min gap size (m <sup>2</sup> )	32	92	100	32
Mean gap size (m <sup>2</sup> )	160	268	290	257
Median gap size (m <sup>2</sup> )	187	233	252	221
Standard deviation gap size (m <sup>2</sup> )	67.6	146.8	243.0	182.1
Max gap perimeter (m)	72	123	192	192
Min gap perimeter (m)	22	37	40	22
Mean gap perimeter (m)	50	69	74	67
Median gap perimeter (m)	54	62	70	65
Standard deviation of gap perimeter (m)	13.9	21.9	31.8	25.9
Max gap length (m)	32	49	82	82
Min gap length (m)	7	13	15	7
Mean gap length (m)	19	25	31	26
Median gap length (m)	19	24	27	24
Standard deviation of gap length (m)	6	9	15	12
Max gap width (m)	18.5	29.0	33.0	33.0
Min gap width (m)	4.4	7.2	6.1	4.4
Mean gap width (m)	12	14	13	13
Median gap width (m)	13	14	13	13
Standard deviation of gap width (m)	3.9	4.4	5.6	4.8
Max CWD per gap (Mg C)†	2.85	8.79	17.55	17.55
Min CWD per gap (Mg C)†	0.06	0.14	0.40	0.06
Mean CWD per gap (Mg C)†	1.12	2.45	3.63	2.63
Median CWD per gap (Mg C)†	1.18	1.46	2.94	1.61
Standard deviation of CWD per gap (Mg C)†	0.74	2.23	3.47	2.70
CWD in gaps (Mg C ha <sup>-1</sup> )†	0.11	0.65	0.70	1.45
CWD flux in gaps (Mg C ha <sup>-1</sup> y <sup>-1</sup> )††	0.00	0.00	0.00	0.01
Max number of dead trees per gap‡	10	24	26	26
Min number of dead trees per gap‡	0	1	1	0
Mean number of dead trees per gap‡	2.7	7.8	6.6	6.5
Median number of dead trees per gap‡	1.5	6.5	5.0	5.0
Standard deviation of dead trees per gap‡	2.65	5.87	6.03	5.77
Dead trees in the gaps per hectare‡	0.3	2.0	1.3	3.6
Annual tree mortality per hectare‡‡	0.2	1.7	0.5	2.4

\*Proportion = (sum area of gaps in all ages – by total plot area) × 100%, \*\*Proportion = (sum area of gaps < 1 yr old – by total plot area) × 100%, †Only pieces of CWD ≥ 10 cm of diameter were measured in gaps area of all ages, ††Only pieces of CWD ≥ 10 cm of diameter were measured in gaps area < 1 yr old, ‡Only dead trees ≥ 10 cm of diameter at breast height were measured in the gap area of all ages, ‡‡Only dead trees ≥ 10 cm of diameter at breast height were measured in the gap area < 1 yr old

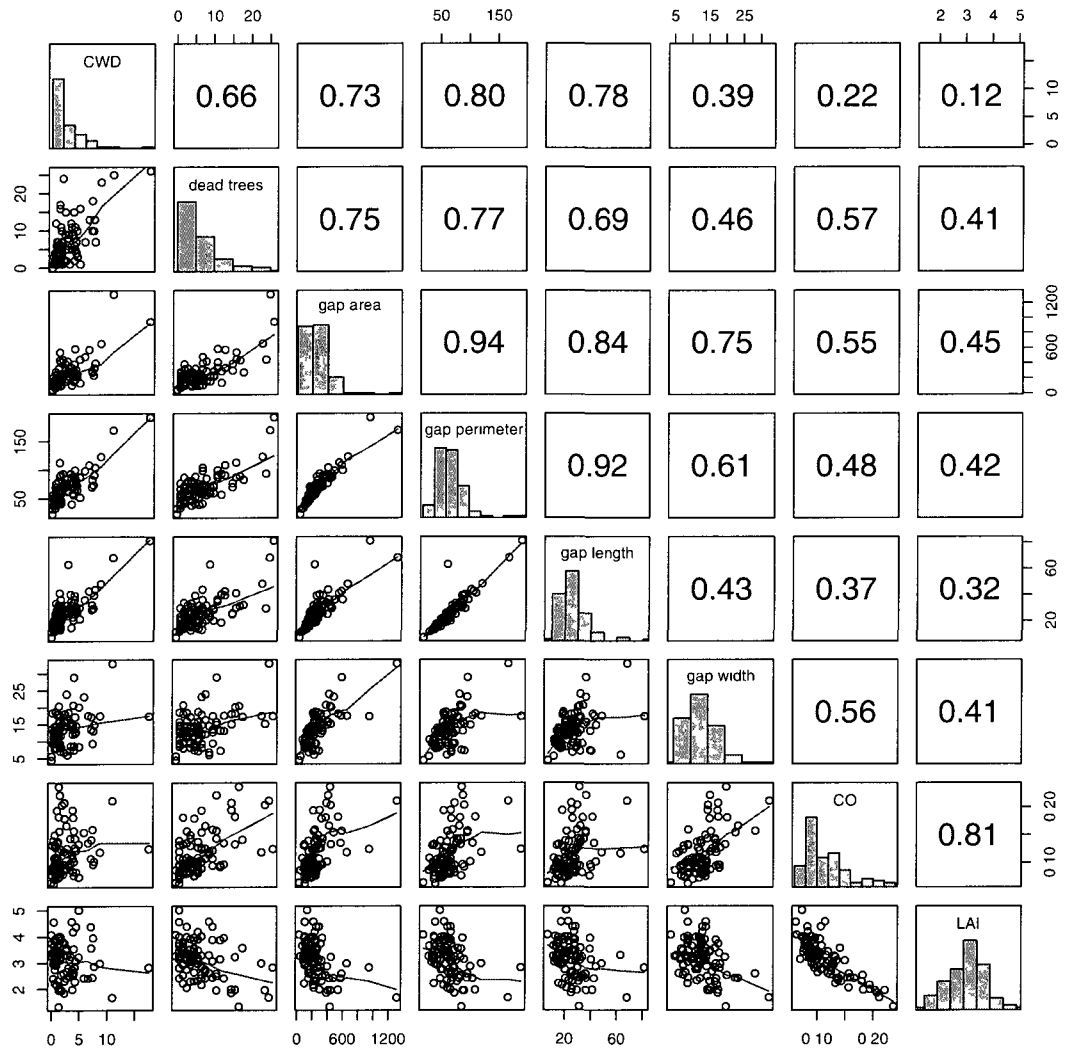


Figure 2-3: Bivariate Pearson correlation coefficients ( $r$ ) between pairs of ground gap parameters (CWD, number of dead trees > 10 cm of DBH, gap area in  $m^2$ , gap length in m, gap width in m, CO proportion of canopy openness and LAI leaf area index) of gap survey ( $n=92$ ) in two large forest plot areas (114 and 53 ha). The upper half of the graphs gives the linear correlation coefficients and the lower half graphs are scatter plots fitted with a non-linear parametric smoothing function.



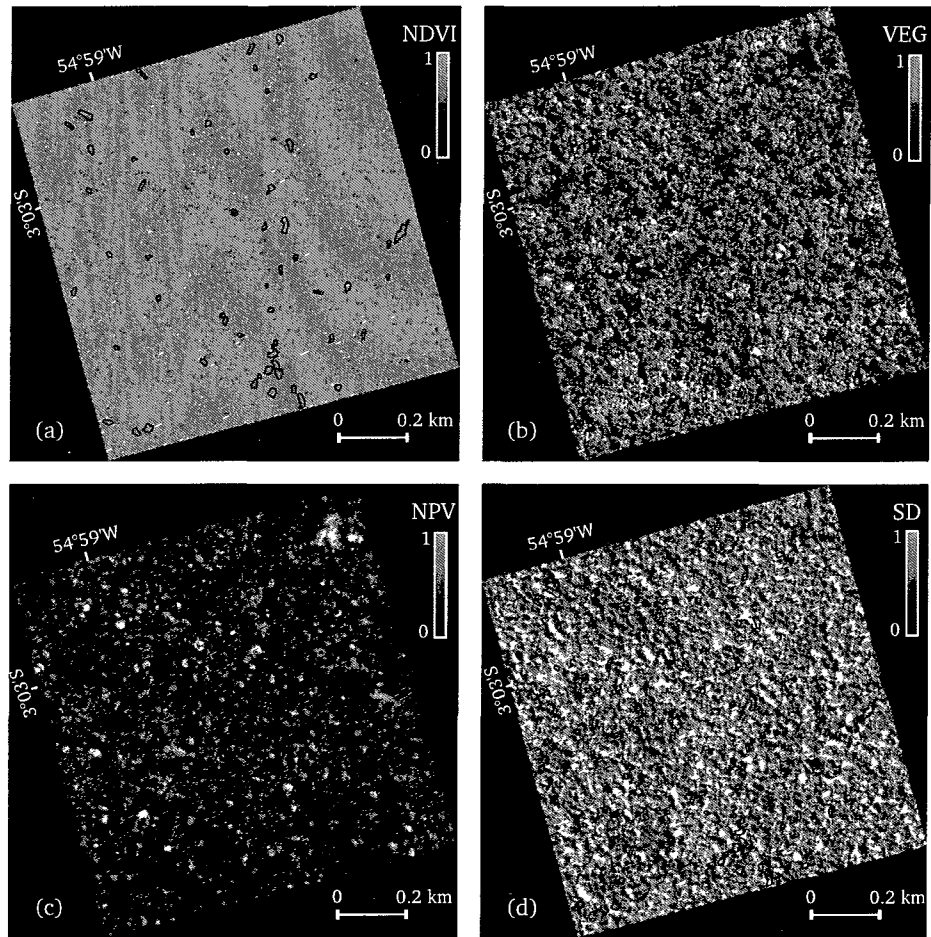


Figure 2-4: IKONOS-2 image processing of 114 ha plot at Tapajós National Forest (Brazil). Normalized Vegetation Index (a) and unmixing fraction images of vegetation (b), nonphotosynthetic vegetation (c) and shade (d). Ground gaps (n=55) are overlaid in red.

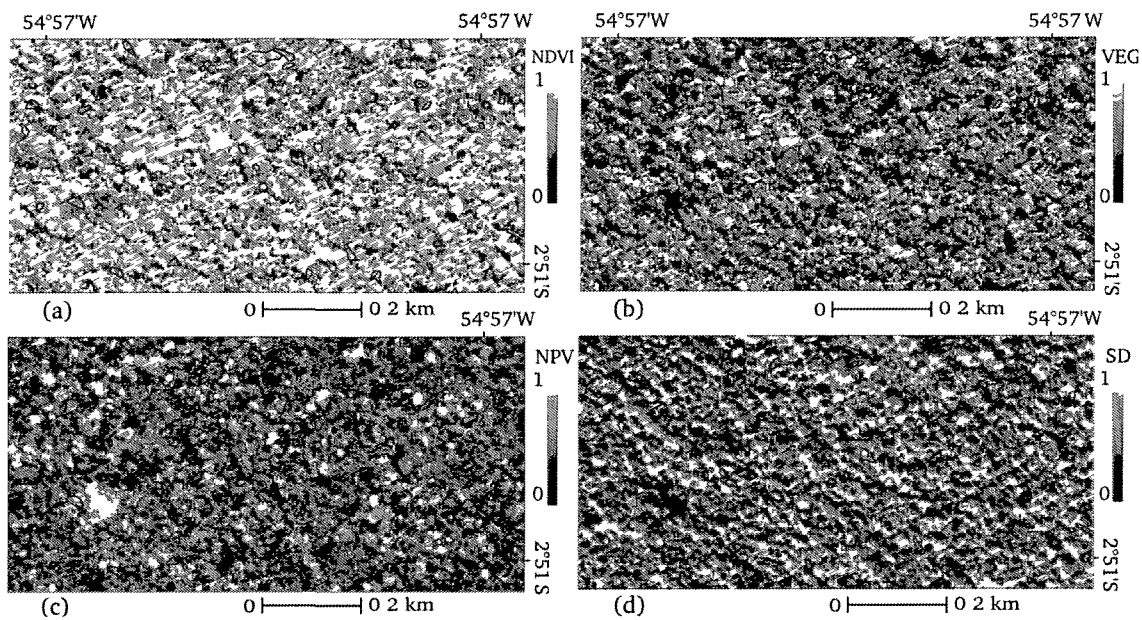


Figure 2-5 IKONOS-2 image processing of 53 ha plot at Tapajós National Forest (Brazil) Normalized Vegetation Index (a) and unmixing fraction images of vegetation (b), nonphotosynthetic vegetation (c) and shade (d) Ground gaps (n=41) are overlaid in red

LAI, respectively (Fig. 2-6a-b). For the 53 ha plot (n=2315) a stronger pattern of spatial auto-correlation was found to a range of 57 and 60 meters for CO and LAI, respectively (Fig. 2-6c-d). We found a spatial trend in both CO and LAI for the data of 114 ha plot probably related with the dissected relief, but no spatial trend of (CO and LAI) for the 53 ha plot (see Sup. Material, B-4-9). Experimental semivariograms of the data of both large plots showed a periodic variance every 50 meters (see Sup. Material, B10-11) aliasing the spacing between transects. Based on the smallest RMSE for both types of data we selected and fitted an isotropic exponential semivariogram model  $\gamma(h) = c_0[1 - \exp(-h/a_0)]$ , where  $\gamma(h)$  is the semivariance at the lag  $h$ ,  $c_0$  is the variance asymptote, and  $a_0$  a lag distance or range.

A clear pattern of light penetration was found around of the ground gaps of the large plot of 114 ha (Fig. 2-7a,f) and 53 ha (Fig. 2-8a,f), although high uncertainty of interpolation was found at the 114 ha plot considering the smaller number of data collection parts in that plot (see Sup. Material, B-13 and B-14). The geostatistical interpolation of canopy openness (square root of CO) and LAI clearly showed that the occurrence of gaps increases light penetration on the forest floor in both plots (Fig. 2-7a and Fig. 2-8a). Tree fall gaps increased the amount of opened sky and inversely reduced total LAI (Fig. 2-7f and Fig. 2-8f). We found that most gaps are in areas with  $CO \geq 0.25$  and  $LAI \leq 4$  indexes in both plots.

We were unable to find any significant correlation between remote sensing spectral products (NDVI and GV, NPV and SD unmixing images) and the continuous biophysical variables of CO (Fig. 2-7b-e) and LAI (Fig. 2-7g-j) of 114 ha plot (total grid with n=71,416 pixels of 4 meters). The same lack of correlation was also found for remote sensing products and CO (Fig. 2-8b-e) and LAI (Fig. 2-8g-j) for 53 ha plot area (total grid with n=33,020 pixels of 4 meters). Also we were unable to find any significant correlation between same

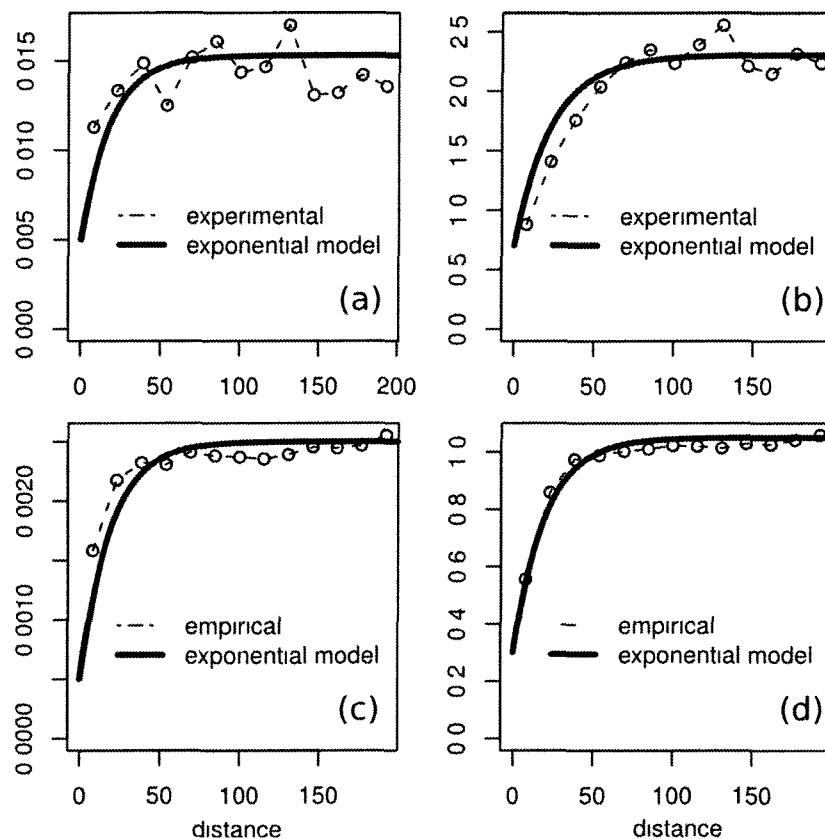


Figure 2-6 Empirical and fitted exponential semivariogram models for canopy openness - CO (a) and leaf area index - LAI (b) for the 114 ha plot (n=731). For the 53 ha plot (n=2315) a fitted exponential semivariogram models was also applied for CO (c) and LAI (d). Kriging parameters used to interpolate CO and LAI in 114 ha plot were, respectively direction (isotropy in both), nugget (0.0055 and 0.4586), sill (0.0103 and 1.603) and range (56.1 and 71.16). For the 53 ha kriging plots of CO and LAI we used direction (isotropy in both), nugget (0.0026 and 0.3922), sill (0.0028 and 0.7507) and range (57.26 and 60.26). A square root transformation was applied for the raw data of CO or (DIFN) to reduce its skewed frequency distribution in both plots.

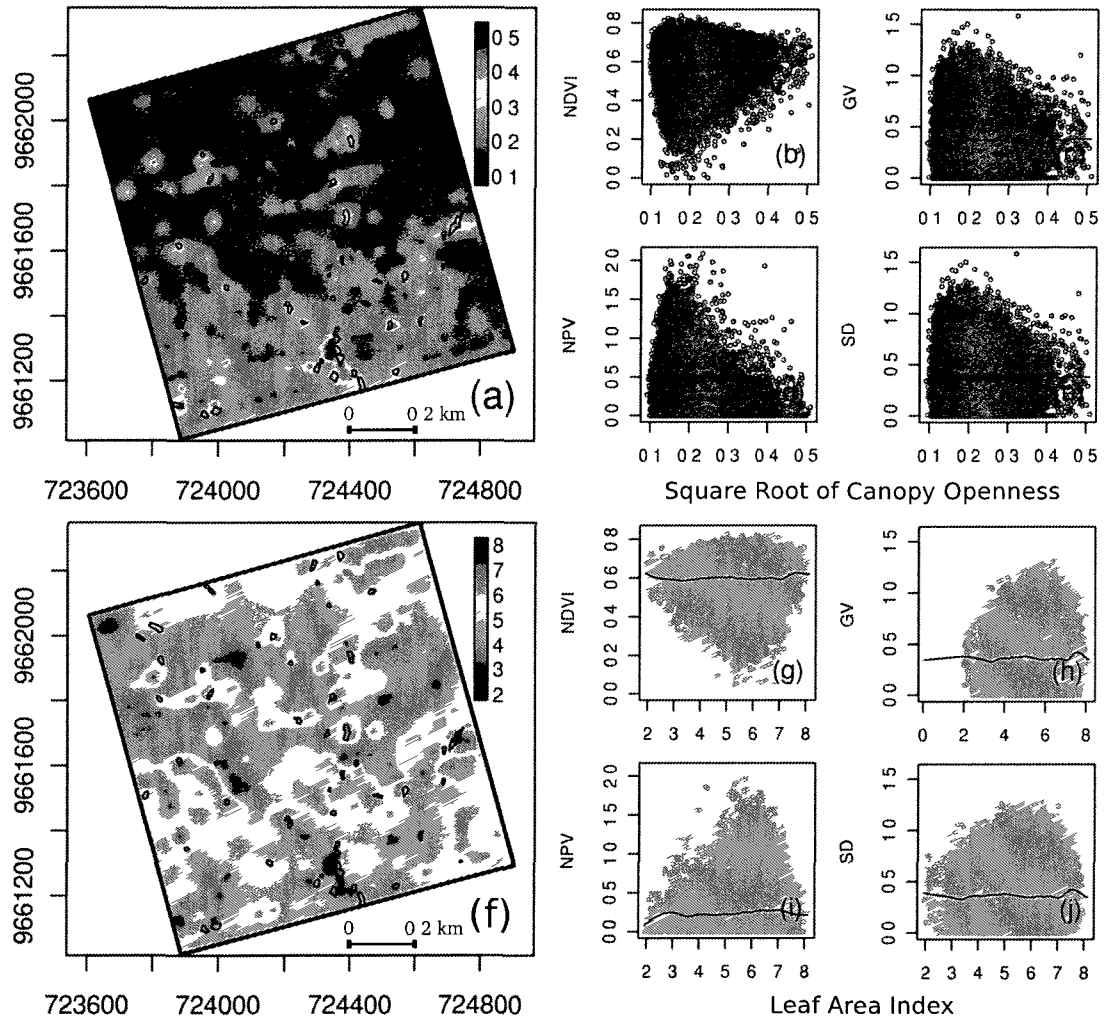


Figure 2-7 Interpolated ground collections ( $n=731$ ) of canopy openness (square root of CO) (a) and leaf area index (LAI) (f) in 114 ha forest area (4 meter grid plot) using kriging with an exponential semivariogram model. Gaps (black polygons) are present in areas of high CO (a) and low leaf area index (f). Scatter plots of canopy openness grid and remote sensing products (4 m spatial resolution) NDVI (b), green vegetation (c), nonphotosynthetic vegetation (d) and shade (e). For LAI grid plot the scatter plots with the same remote sensing products are NDVI (g), green vegetation (h), nonphotosynthetic vegetation (i) and shade (j).

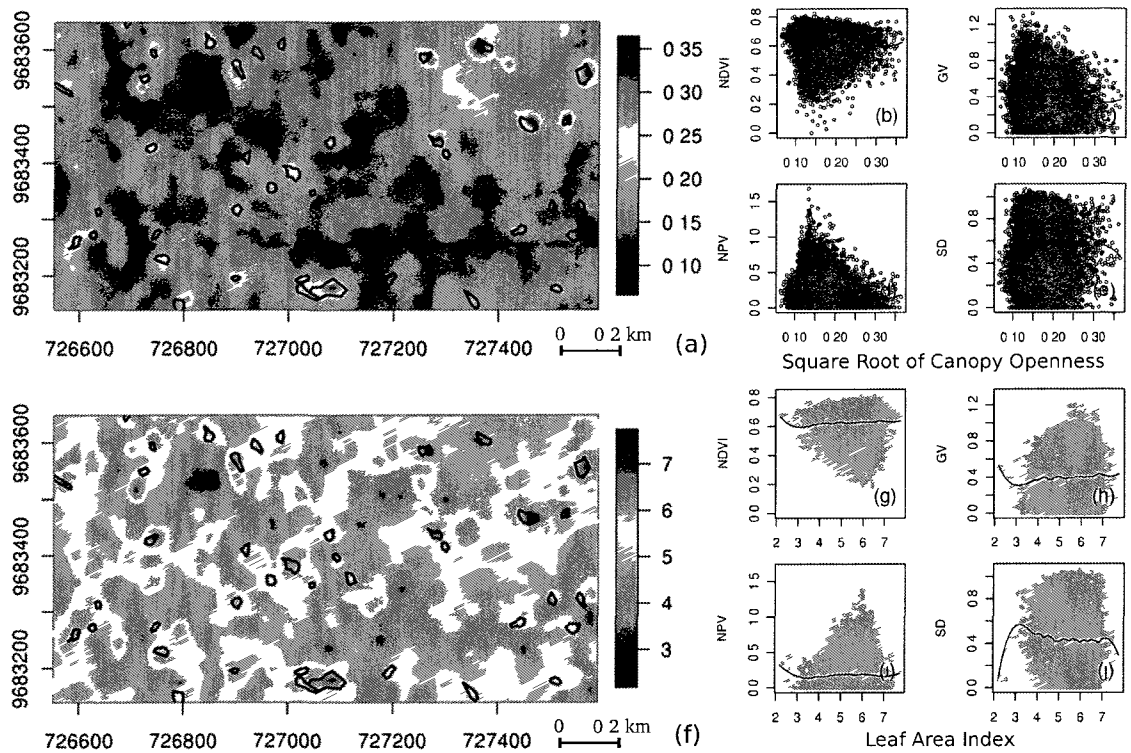


Figure 2-8 Interpolated ground collections ( $n=2315$ ) of canopy openness (square root of CO) (a) and leaf area index (LAI) (f) in 53 ha forest area (4 meter grid plot) using kriging with an exponential semivariogram model. Gaps (black polygons) are present in areas of high opened sky (a) and low leaf area index (f). Scatter plots of canopy openness grid and remote sensing products (4 m spatial resolution) NDVI (b), green vegetation (c), nonphotosynthetic vegetation (d) and shade (e). For LAI grid plot the scatter plots with the same remote sensing products are NDVI (g), green vegetation (h), nonphotosynthetic vegetation (i) and shade (j).

remote sensing products and raw ground data points (CO and LAI) in 114 ha (n=731) and 53 ha (n=2315) (data not shown).

Gaps produced high variability of light environments, so thresholds of CO and LAI were selected for both large grids to test for covariation with remote sensing products. For 114 ha plot the comparison between  $CO \geq 0.30$  areas (Sup. Material, B-14a) and remote sensing products also showed no correlation (Sup. Material, B-14b-e). The same lack of correlation was found between  $LAI \leq 4$  (Sup. Material, B-14f) and remote sensing products (Sup. Material, B-14g-j). For 53 ha plot the regression analysis between  $CO \geq 0.23$  areas (Sup. Material, B-15a) and remote sensing products also showed also no correlation (Sup. Material, B-15b-e). The same lack of correlation was again found between  $LAI \leq 5$  (Sup. Material, B-14f) and remote sensing products (Sup. Material, B-14g-j).

The overlay of the ground gaps of 114 ha plot over the 1 m spatial resolution panchromatic IKONOS-2 image (Fig. 2-9a,c) and its 4-m multispectral unmixing images of VG, NPV and SD (Fig. 2-9b,d) revealed that most of the ground gaps are located in areas high fraction of shade fraction (SD) (Fig 2-9d). Conversely, shade areas are not uniquely associated with gaps because of the complex structure of this old growth forest. Emergent trees produce shade even where there is no canopy gap. We found the same pattern of high proportion of shadow component in areas of tree-fall gaps over the second high-resolution image of the 53 ha plot (Figure not shown).

## 2.4 Discussion

The interaction between atmosphere and forest canopy reshapes the structure of forests [Lawton and Putz, 1988; Garstang et al., 1998; Turner, 2010]. In the Tapajós National Forest the major mode of gap-formation was snapped bole tree fall (Table. 2.1, n=44 from total 92 gaps) suggesting that tall trees of the forest canopy were killed by winds associated

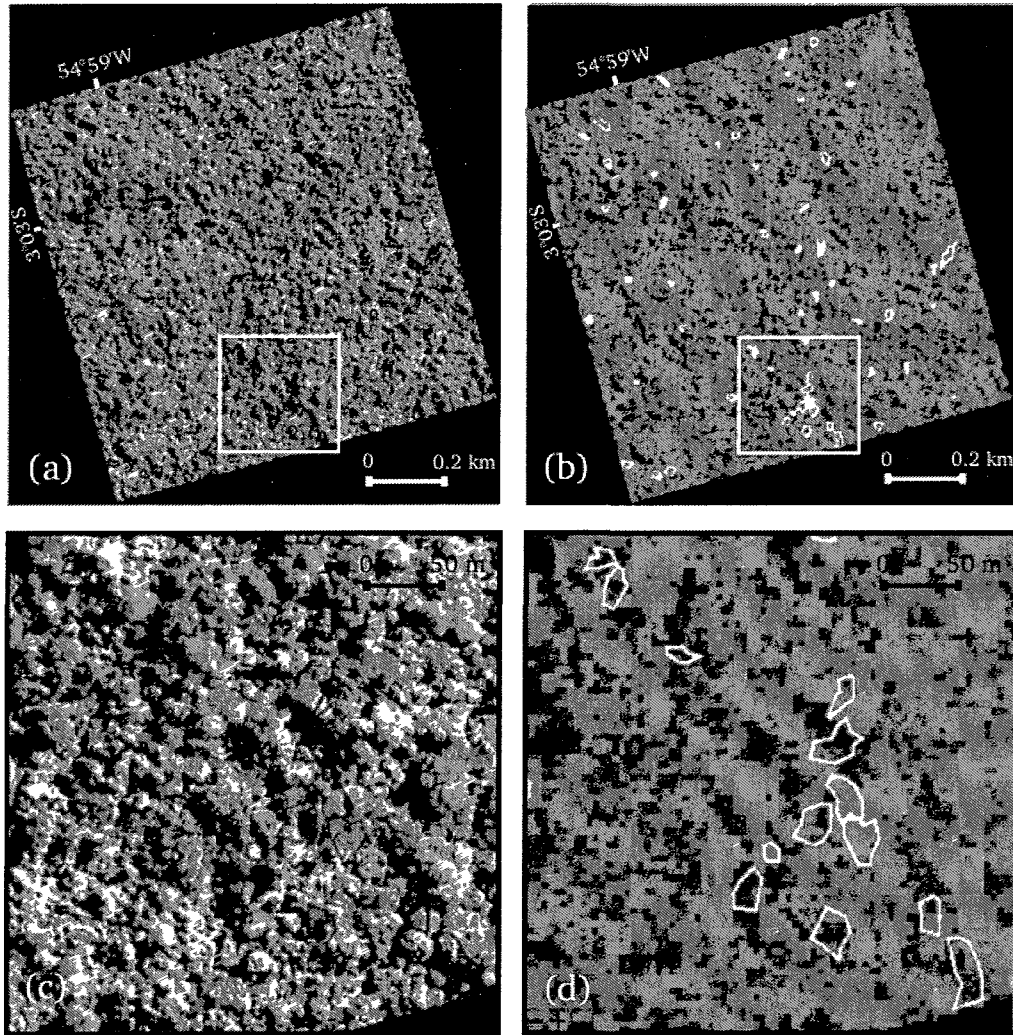


Figure 2-9. Distribution of ground gaps ( $n=55$ ) over 1 m spatial resolution pan-chromatic IKONOS-2 image of 23 June 2008 with full-width wavelength  $0.45\text{-}0.90\ \mu\text{m}$  (a) and RGB color composition of the unmixing images of green vegetation, nonphotosynthetic vegetation and shade (b), respectively. Spatial details of ground gaps in the pan-chromatic high resolution image (c) and spectral details of the gaps in the unmixing images (d)



with the rainy season [Garstang et al , 1998] or the low-level winds driven by the mesoscale circulations of the Amazon and Tapajós rivers [Lu et al , 2005] Several large trees (DBH  $\geq$  50 cm) had their trunks broken at the height around of 5 to 8 meters, which suggest strong patterns of wind gusts at forest canopy

The effects of natural disturbances on carbon cycle have not being quantified because of the diversity of scales and severity or intensity of natural processes [Turner, 2010] In tropical regions the impact of large scales regional disturbances e.g hurricanes [Lugo et al , 1983, Whigham et al , 1991, Chambers et al , 2007b] or and blow-downs [Nelson et al , 1994, Garstang et al , 1998, Chambers et al , 2009b, Espirito-Santo et al , 2010, Negron-Juárez et al , 2010] have received some attention At a fine scale –  $\sim$  100 m or tree-fall disturbances – few studies monitored gap dynamics [Hubbell et al , 1999] and related fine scale disturbances to carbon cycling through (tree mortality and fluxes of CWD) In our study of two large plots of 114 and 53 ha, we found tree mortality depended upon the gap size and the mode of gap formation From the sample of 92 gaps only 16 disturbances had downed a single tree Most of the gaps had multiple fallen trees with an average mortality of 6.47 trees ( $>$  10 cm DBH) per gap (Tab 2.1) As expected, more fallen trees produced larger gaps We found a high correlation between number of dead trees and gap area ( $r=0.75$ ) or gap perimeter ( $r=0.77$ ) (Fig 2-3 and Sup Material B-17) The recurrence interval or turnover for these events is about 123 years for all gap-formation types, closely of the average range of 100-125 years of others studies [Denslow, 1987, Brokaw, 1982, Van der Meer et al , 1994] depending of the gap definition

We provide the first statistics of CWD production based on gap size and mode of gap formation in the tropical forest literature and we estimate an empirical relation between the production of CWD and gap size (Fig 2-3 and Sup Material B-16) Gap formation as result of uprooted tree-falls produced 1.5 more CWD than snapped trees and 3 times

more than crown-falls. Uprooted tree falls disturbed larger gap areas (average  $\sim 290 \text{ m}^2$ ) than the other types of gap formation. Estimates of carbon fluxes based on tree mortality from permanent plot studies differ from estimates made from gap-formation rates [Leigh, 1975]. For example, a snapped-off tree may not die even when much of its biomass is lost. Conversely, a tree that dies standing may not ever form a gap. We compared our results to permanent forest plots [Pyle et al., 2008] for tree mortality measurements and repetitive line intercept transects for monitoring of CWD flux [Palace et al., 2008] in the Tapajós National Forest. In our study plots gap disturbances accounted for a mortality average of 6.47 stems ( $\text{DBH} \geq 10 \text{ cm}$ ) per gap or mean tree mortality of  $2.38 \text{ stems ha}^{-1} \text{ y}^{-1}$ . In comparison, Pyle et al. [2008] found about mortality of  $8.38 \text{ stems ha}^{-1}$ . The total stock of CWD in gaps represents between 4.9% and 5.8% of the total stock of fallen CWD, when compared with Palace et al. [2008] and Pyle et al. [2008], respectively. The production of CWD in the recent gaps  $0.76 \text{ Mg C ha}^{-1} \text{ y}^{-1}$  by our measurements of gaps less than one year old, was only 29% as large as the flux of carbon from annual tree mortality measured by Pyle et al. [2008] or 23% of the total flux of CWD.

Optical remote sensing data have been used to estimate large areas of tropical forest disturbance [Nelson et al., 1994; Chambers et al., 2007b, 2009b; Espírito-Santo et al., 2010] rather than its biophysical responses (e.g. amount of CWD or tree mortality). The strong correlation between gap area and its disturbance responses found in this study may be useful to relate disturbance areas detected by satellites to carbon emissions from CWD and tree mortality at large scales [Chambers et al., 2007b]. However, we caution that only about 30% of normal mortality created gap conditions that could be measured on the ground.

While a great deal of research on canopy disturbance regimes and responses of individual species to gap has been documented, there has been little research on the nature of forest regimes in and around gaps [Canham et al., 1990]. In our study we quantified the regimes

of light penetration in and around of gaps of the understory forest floor and found that gaps played a role on the dynamics of light environments of tropical forests, rarely quantified at large scales. Despite the differences of sample design between plots (50×15 m vs. 25×15 m) and number of data points (n=731 vs. n=2315), the geostatistical interpolation of canopy openness (square root of CO) and LAI revealed that occurrence of tree-fall gaps increased the amount of opened sky (Fig. 2-7a and Fig 2-8a) and reduced the total LAI (Fig. 2-7f and Fig. 2-8f). Most gaps are present in areas with  $CO \geq 0.23$  and  $LAI \leq 4$  thresholds (Sup. Material, B-14 and B-15).

The ecologically altered area at the forest floor is often larger than the size of the gap at the forest canopy level [Popma et al., 1988]. Runkle's gap size is normally assumed to be a reasonable measure of the gap size on the forest floor and Brokaw's gap size is used for the forest canopy [Clark. 1990]. It is normally assumed that gap from Brokaw definition is between 2 and 3 smaller than Runkle's gap area [van der Meer et al., 1994]. Comparing our instrumental measurement of light penetration and the definition of ground gaps of Runkle [1981], which theoretically includes areas directly and indirectly affected by the canopy opening by light enhancement at the forest floor, we found that the area measured by LAI-2000 PCA are twice as large as the areas defined by Runkle's or as much as a factor of 4 using the conservative gap definition of Brokaw [1982]. Over the 167 ha area of our study plots, 1.42% of this plot is in gap phase process (Tab. 2.1). Using the empirical threshold of light penetration of  $CO \geq 0.30$  (114 ha plot) and  $CO \geq 0.23$  (53 ha plot) where most the gaps are geographically located (Sup. Material B-14a and B-15a), the total area in gap phase process is 2.57 and 3.33% for 114 and 53 ha plot, respectively. We favor the opinion of Lieberman and Lieberman [1989] that the dichotomous definition of forest environments into gap and non-gap is unrealistic and difficult to implement with rigor and consistency.

Our ground measurements of understory light regimes and responses of gap tree-fall

disturbances not only raises the question of the importance of gap area definition [Clark, 1990], but also provide a methodological opportunity for the future studies of light regimes coupled with important elements of the carbon cycle process (tree mortality and CWD) in other forest areas. The recent use of the LiDAR technology to detect and understand forest gap dynamics in the tropics seems promising [Kellner and Asner, 2009] considering the direct evaluation of the canopy height. However, given that LiDAR returns waveforms signals into a zenith projection [Parker et al., 2004, Lefsky et al., 2005], light penetration can go further than the vertical hole at the gap edge to a given distance. Consequently, measurements of light enhancements at the forest floor estimated by LiDAR instruments will tend to follow the gap definition of Biotkaw [1982] or much bigger if a given tree height threshold is used as cut off [Kellner and Asner, 2009]. Our spatially explicit exploration of light environments emphasized the need to understand the dynamics of light penetration as a continuum.

One of the main goals of this study was to compare high resolution satellite images (Fig. 2-3 and 2-4) with ground-based light measurements to detect patterns of tree-fall gap mortality. As expected NDVI and GV have similar biophysical propriety to monitor changes of canopy green vegetation [Hall, Shimabukuro, and Huemmrich, 1995] and NPV is potential useful to detect patterns of CWD changes of non-vegetation components of the forests [Asner, Wessman, and Schimel, 1998]. However, we were not able to find significant correlations between those ground remote sensing measurements and satellite images in both large grids plots of CO and LAI (Fig. 2-7 and 2-8). Moreover we found no correlation between remote sensing products (NDVI, GV, NPV and SD) even in regions of the plot with high fraction of CO or opened sky and low LAI where most of the ground gaps were found in the plot (Sup. Material B-14 and B-15). The lack of correlation between ground measurements from LAI 2000 plant canopy analyzer (PCA) and remote sensing

has been pointed out as a problem of signal saturation of optical remote sensing in high biomass forests [Toan et al., 2004; Aragão et al., 2005]. Moreover this problem raises others questions: if the index saturation of the biophysical variables (CO and LAI) exists, was it the result of saturation of the remote sensing spectral products (NDVI and GV), PCA ground measurements or both? We expected to find some useful signal of recent disturbances between ground data and remote sensing products in those areas, but we were unable to detect it (Sup. Material B-14 and B-15).

We believe that, for this area of the Amazon with high canopy density, the lack of correlations between ground measurements of PCA and remote sensing products (16 covariates) was caused because of the high shadow fraction in the high resolution images caused by stratified tropical vegetation (Fig. 2-9). Tropical forest shadow fractions represent roughly 30% ( $\pm 10\%$  SD) and so they exert a major control over spatial variability in canopy reflectance at both the local and regional levels [Asner and Warner, 2003]. Considering that in our large experimental plots most of the gaps were present in areas of high proportion of shadow (Fig. 2-9), it was not possible to uniquely detect gaps using the high resolution IKONOS-2 images. Shadows are also abundant in non-gap areas of the heterogeneous forest canopy.

We note that IKONOS-1 images have been used to detect and map recent man-made canopy gaps caused by reduced-impact selective logging activities by application of NDVI thresholds and visual interpretation [Miller et al., 2007]. Despite the recognition that NDVI is an effective index to reduce remote sensing artifacts (from solar geometry effects, acquisition image angles, noise and atmosphere contaminations, shadow and topography [Tucker, 1979], we still found that NDVI filtering alone was insufficient to enable gap detection. It is possible that some areas mapped from the simple IKONOS thresholds ( $NDVI < 0.4$ ) in Miller et al. [2007] are artifacts or pixels of shadow components.

Our spectral approach to image interpretation may not be the only approach to extracting information on gaps from the high-resolution images. Modern techniques of image processing or computer vision using textural metrics [Kayitakire, Hamel, and Defourny, 2006; Malhi and Román-Cuesta, 2008] currently available could be very useful to detect patterns of disturbances in high resolution satellite images [Malhi and Román-Cuesta, 2008].

## 2.5 Conclusion

The dynamics of gaps play a role in the regimes of tree mortality, production of CWD and light variability on the understory forest floor. In surveys of two large plots (114 and 53 ha) of an Amazon tropical forest, we found clear patterns of tree mortality and CWD production dependent upon the gap size, geometry and the mode of gap formation (crown-fall, snapped trunks, and uprooted trees). Tree-fall gaps caused only about 30% of the flux of annual tree mortality. Most mortality does not result in gap formation. On average, gap formation accounted for a minor proportion of the stocks (between 4.9% and 5.8% of the total fallen CWD) and fluxes (about 23%) of CWD carbon. We caution that even if adequate remote sensing measurements are developed to detect gaps, gap detection alone appears insufficient to provide reliable measurements of tree mortality.

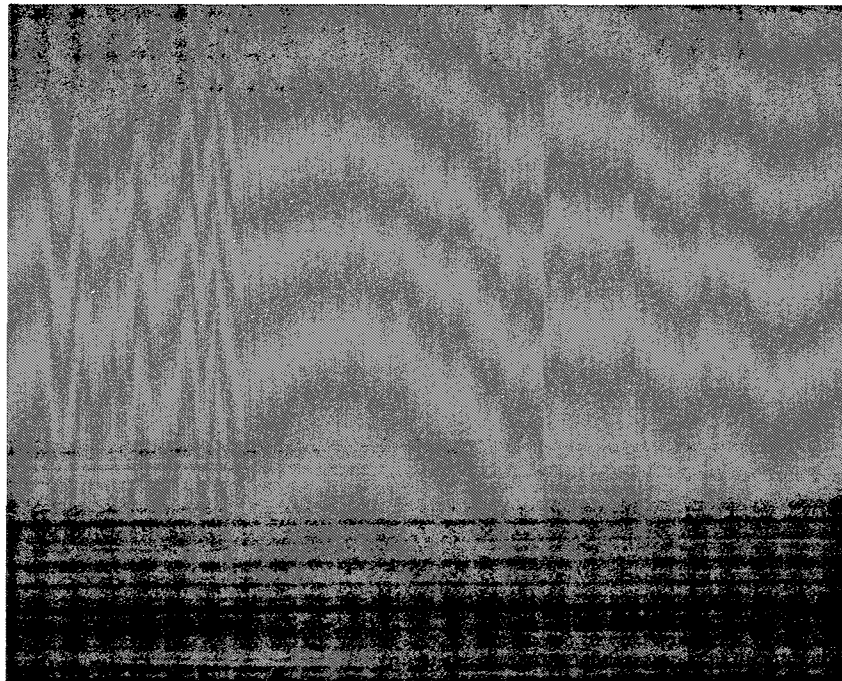
The forest understory light environment was shaped by the occurrence of tree-fall gaps. From the 96 ground mapped disturbances, tree-fall gaps increased light on the forest floor and reduced total leaf area index. Quantitative light penetration thresholds of  $CO \geq 0.23$  and  $LAI \leq 4$  closely matched disturbances found in the ground. Accepting thresholds of  $CO \geq 0.30$  for 114 ha plot and  $CO \geq 0.23$  for 53 ha plot, light penetration by our ground-based measurements suggests that gap influences are twice as large as the areas measured by Runkle's gap definition. From a remote sensing perspective, small changes in canopy structure (e.g. defoliation) are detected in ground measurements of CO or LAI. LAI-2000

biophysical data are likely be more related to recent changes in forest canopy than Runkle's gap definition

We found little correlation between spectral remote sensing products (NDVI and GV, NPV and SD) and ground-based measurements of CO and LAI. Probably, the high proportion of shadow in high-resolution images renders effective gap detection impossible using spectral approaches. While textural approaches using passive optical high-resolution sensors or active sensors (e.g. LiDAR, RADAR) may provide more effective approaches to measurement gap formation, our studies suggests that remote sensing estimates of mortality and the carbon flux that results from mortality remains a challenge in the tropical forest environment because only a small proportion of mortality and associated carbon fluxes (~30%) are linked to gap formation.

CHAPTER 3

STORM INTENSITY AND OLD-GROWTH  
FOREST DISTURBANCES IN THE  
AMAZON REGION



Dissertation chapter published at Geophysical Research Letters, v37, L11403,

doi:10.1029/2010GL043146, 2010



### 3.1 Introduction

Are old-growth tropical forests in steady-state? Recent studies of permanent tree plots suggest that tropical forests are changing rapidly. Increases in the rate of turnover of trees and increasing carbon uptake (between 0.1 and 0.5 MgC ha<sup>-1</sup> y<sup>-1</sup>) have been observed in permanent plots of neotropical and paleotropical forests [Phillips and Gentry, 1994]. There is accumulating evidence that old-growth tropical forests may be growing faster, experiencing changing patterns of recruitment and mortality [Phillips and Gentry, 1994], and increasing their stock of above-ground biomass [Malhi et al., 2006].

Local openings in the forest canopy ( $\pm 100$  m<sup>2</sup>) are widely recognized as an important factor affecting the dynamics of tropical forests [Hubbell et al., 1999]. Larger disturbances caused by cyclonic storms (hurricanes) also change the structure of tropical forests, damaging up to hundreds of square kilometers [Lugo et al., 1983; Lugo, 1995]. In continental equatorial regions of the Amazon, hurricane damage does not occur. However, Nelson et al. [1994] used Landsat images of the Brazilian Amazon to detect large natural gaps (> 30 ha) with fan-shape forms (blow-downs), probably caused by high-velocity wet downburst winds [Garstang et al., 1998]. Nelson et al. [1994] identified 330 blow-downs in 137 Landsat TM between 1987 and 1989 of the Amazon, with a total disturbed area of 90,000 ha. The TM scene with the greatest total disturbance affected area had 16 blow-downs totaling 8,600 ha or 0.31% of the scene. The largest single blow-down covered 3,370 ha, with the most frequent size classes falling between 30 and 100 ha. Most of these large blow-down areas ( $\geq 30$  ha) occurred in the west-central basin of the Amazon, where annual precipitation is high.

Forest damage by storms is most often associated with the intensity of wind gusts [Lugo et al., 1983]. In the Amazon region wind gusts greater than 10 m s<sup>-1</sup> accompanied by rainfall have been recorded [Garstang et al., 1998]. Heavy rainfall caused by convective storms

ought to correlate with strong winds and microbursts [Fujita, 1985]. In this study, we examine a regional mosaic of Landsat images and estimates of daily precipitation retrieved from satellite images to determine if there is a coherent spatial relation between heavy precipitation and large disturbances in old-growth forest in the Amazon. Earlier work [Nelson et al., 1994, Chambers et al., 2009b] strongly suggests that severe convective storm activity associated with heavy rains causes intense winds that in turn lead to forest disturbance through blow-downs. We hypothesize that the weather patterns that cause blow-downs in the Amazon lead to different rates of forest turnover in the eastern and western Amazon basin.

## **3.2 Methods**

### **3.2.1 Data and Study Area**

To evaluate the relation between severe storms and large disturbances in the Amazon, two regional data sets were integrated: (1) a multitemporal data set of Real-Time Rainfall (RTR) of the north continental area of South America, and (2) a mosaic of ETM+ Landsat images [TRFIC, 2001] covering the precipitation gradient east to west across the Amazon basin from the east ( $2^{\circ}13'S$  and  $51^{\circ}51'W$ ) to west ( $6^{\circ}29'S$  and  $66^{\circ}49'W$ ). Using these two data sets we applied several steps of remote sensing image processing and spatial statistical analysis (Fig. 3-1).

### **3.2.2 Severe Storms in the Amazon Region**

The frequency of severe storms was determined by the integration of the RTR daily images produced by geosynchronous NOAA (National Oceanic and Atmospheric Administration) satellites [Vicente et al., 1998]. RTR estimates are produced at 4 km spatial resolution using 10.7 mm band data from NOAA 8 satellites with adjustment for cloud top temperature

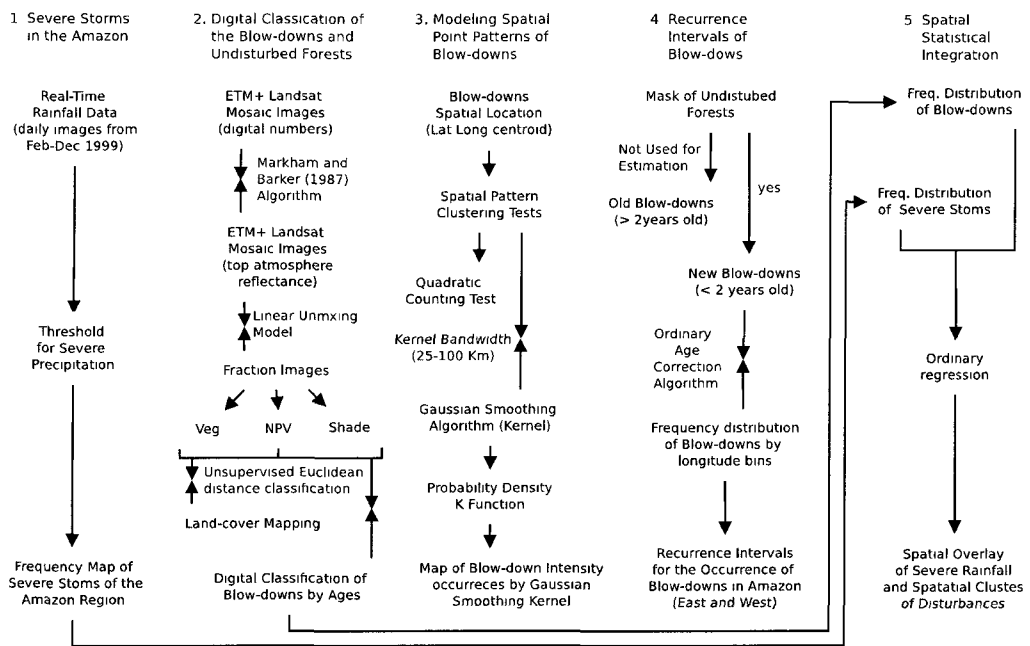


Figure 3-1: General diagram of image processing and spatial statistics applied in this re-search. Top numbes from 1 to 5 are the main objectives for each sequence of steps.

gradients and moisture regimes using fields of precipitable water and relative humidity generated by the National Centers for Environmental Prediction ETA Model [Vicente et al , 1998] RTR daily images were obtained from 01 February to 31 December 1999 No data were obtained during January 1999 because of operational problems We defined heavy rainfall as days with precipitation  $\geq 20 \text{ mm d}^{-1}$

### 3.2.3 Digital Classification of the Blow-downs

We have classified large disturbances as blow-downs based on spectral characteristics and spatial patterns identified previously [Nelson et al , 1994, Chambers et al , 2009b] The number and area of large blow-downs in the Amazon were quantified using digital classification of 27 Landsat ETM+ images from 1999 to 2001 with low cloud cover ( $\leq 20\%$ ) and spatial resolution of  $\sim 28.5 \text{ m}$  All images were orthorectified with a spatial accuracy of  $\sim 15 \text{ m}$  [?] A relative atmospheric correction was applied to the Landsat images using the Markham and Barker [1987] algorithm

We applied a spectral mixture analysis (SMA) [Shimabukuro and Smith, 1991] using all six original ETM+ spectral bands to produce fraction images based on three end-members green vegetation (GV), nonphotosynthetic vegetation (NPV) and shade (SD) Spectrally pure end members were determined using the pure pixel index (PPI) [Boardman et al , 1995, Boardman, 1993]

A semi-automated classification was applied to identify and to classify all blow-down events on the Landsat images A pixel by pixel classification was developed using six bands (GV, NPV and SD, plus the original bands 3, 4 and 5) The pixel groups were labeled using an unsupervised classification of Euclidean distance [Schowengerdt, 1997]

We identified blow-downs when a cluster of more than 55 labeled pixels was observed in old growth forest with no sign of anthropogenic activity in the region Clusters were

generally fan-shaped [Nelson et al., 1994]. Areas of anthropogenic disturbances (agriculture, pastures, secondary forests, roads and cities) or naturally exposed soils (patches of savanna shrubs and trees, savanna herbs, open vegetation on white sand and dry river borders) were excluded from our analysis. The blow-downs were also classified into two age classes (old  $> 2$  y and new  $< 2$  y) according to the relative proportions of GV and NPV.

We used general categories for anthropogenic disturbances and naturally exposed soils in order to avoid confusion of natural and anthropogenic disturbances. The application of these generic land-cover categories allowed us to separate areas of natural forests with high confidence. Using these broad classes, we reduced the thematic classification uncertainty – normally very high for some land-use types in the Amazon – especially among agriculture, pastures and initial regeneration [Numata et al., 2003].

#### **3.2.4 Land Cover Mapping of the Undisturbed Amazon Forest**

We used an unsupervised classification of Euclidean distance [Schowengerdt, 1997] of unmixing fraction images [Shimabukuro and Smith, 1991] plus the original bands 3, 4 and 5 to separate natural forests from other land cover classes. Our classification included five categories: natural forests, anthropogenic disturbances, natural exposed soils, water and cloud cover. The anthropogenic disturbances class included agriculture, pasture, secondary forest, roads and urban areas. Selectively logged areas were not included in this land-cover map because of the small proportion of logging in this region, except in limited areas around the Tapajós National Forest (TNF) in Pará State and areas near of Manaus city. Most selective logging occurs in South Pará and Amazonas States and throughout the States of Mato Grosso and Rondônia [Asner et al., 2005]. Naturally exposed soils occurred in patches of savanna shrubs and trees, savanna herbs, capinaranas and dry river borders observed in the Landsat images, without any sign of anthropogenic disturbances. After the automatic clas-

sification, all images were carefully inspected to correct possible mistakes of the automatic classification.

### 3.2.5 Modeling Spatial Point Patterns of Blow-downs

Are large disturbances clustered spatially? Do the blow-downs present a homogeneous spatial pattern or do they vary from region to region of Amazon forest (inhomogeneous distribution)? Considering that most of blow-downs occurred in the Western Amazon, is there any spatial auto-correlation of these events? To address these questions we carried out a spatial point patterns analysis (SPA) [Ripley, 1981]. A SPA normally includes the assumption that all events with small area dimension can be analyzed as a single point in space. In this study the blow-downs were treated as a single spatial point (the centroid of each classified blow-down) in the domain of 793,076 km<sup>2</sup> of Amazon forest. We investigated the spatial distribution of blow-downs using the SPA approach implemented in the spatstat package [Baddeley and Turner, 2005] of the R language [R-Team, 2005]. A SPA consists of a set of points ( $s_1, s_2$ , etc.) in a defined study region ( $A$ ) divided into sub-regions ( $B$ ).  $Y(B)$  is the number of events that occurred in sub-region  $B$ . In a spatial context, the number of points can be estimated by use of their expected value  $\mathbb{E}(Y(B))$ , and covariance  $COV(Y(B_i), Y(B_j))$ , given that  $Y$  is the number of events in the areas  $B_i$  and  $B_j$ . The intensity of an event ( $s$ ) is the frequency of points of a specific location  $s$ , where  $ds$  is the area of this region. The intensity of events or in our case, blow-downs, can be represented as:

$$\lambda(s) = \lim_{ds \rightarrow 0} \left\{ \frac{\mathbb{E}(Y)(ds)}{ds} \right\} \quad (3.1)$$

We used a Gaussian smoothing algorithm named kernel to explore the intensity distribution of the blow-downs (first order property). We tested bandwidths between 25 and

100 km to produce the spatial clusters of blow-downs and a probability density function  $k$  [Ripley, 1981] to examine the spatial dependence of these events. If a set of points  $N$  are uniformly distributed, then for any sub-region  $B$ , the expected number of points in  $B$  is proportional to the area  $B$  for a point process  $X$ .

$$\mathbb{E}[N(X \cap B)] = \lambda B \quad (3.2)$$

If  $X$  is homogeneous, the constant  $\lambda$  can be estimated as number of points divided by the total window area  $B$  or formally  $\lambda = N(X)/B$ , where the unit for  $\lambda$  is number of points per area [Baddeley and Turner, 2006]. Using this approach we found that the density of blow-down occurrence is small (0.000365 per  $\text{km}^2$  for the entire region). However, considering that the intensity of points varies location to location, we used two others well known approaches to estimate its intensity: quadratic counting and kernel smoothing [Ripley, 1981; Diggle, 1983]. In the quadratic counting, the total window area is divided into sub-regions ('quadrats') and the numbers of points falling in each quadrat are counted. We divided the total studied area by sub-regions of  $10 \text{ km} \times 5 \text{ km}$  to estimate the intensity of blow-downs. In kernel smoothing, the intensity of points is estimated by a probability distribution function, the kernel function [Bailey and Gatrell, 1995]. The intensity of points or blow-downs will vary from region to region, but with kernel smoothing it will follow the assumption that the expected number of points that falling a small region of area  $du$  around a location  $u$  is equal to  $\lambda(u)du$  where  $\lambda(u)$  is the intensity function for the region  $B$  [Baddeley and Turner, 2006]. The expectation of the region  $B$  can be represented as:

$$\mathbb{E}[N(X \cap R)] = \int_B \lambda(u)du \quad (3.3)$$

To test the spatial auto-correlation of blow-downs or second property of SPA, we used

the K-function of Ripley [1981]. Compared to neighbor distance methods that consider only the closest points, the K-function provides a summary of spatial dependence of events over a wider range of scales. Following Bailey and Gatrell [1995] the K-function ( $k$ ) is a function where the intensity ( $\lambda$ ) or mean number of events per unit of area is equal to the expected ( $\mathbb{E}$ ) number ( $\#$ ) of points at an arbitrary radius ( $r$ ) or formally:

$$\lambda k(r) = \mathbb{E}(\#(\text{events})) \quad (3.4)$$

Following the definition of K-function, if  $A$  is the area of  $B$  then the expected number of events in  $B$  is  $\lambda A$  and the expectation of ordered pair of events at the distance at most  $h$  apart in  $B$  will be  $\lambda^2 A k(r)$ . The K-function can be re-written as:

$$\hat{k}(r) = \frac{1}{\lambda^2 B} \sum_{i \neq j} \sum \frac{I_r(d_{ij})}{W_{ij}} \quad (3.5)$$

where  $d_{ij}$  is the distance between the  $i$ th and  $j$ th observed event in  $B$  and  $I_r$  is an indication function which is 1 if  $d_{ij} \leq r$  and 0 otherwise. The ordered pair of events is  $\sum_{i \neq j} \sum I_r(d_{ij})$  and  $W_{ij}$  is an empirical edge correction or a proportion of the circumference around of each point near of the border of  $B$ .

We explored the K-function to detect whether clustering or regularity is present in the spatial distribution of blow-downs in the Amazon. Under regularity, following a homogeneous Poisson process, the expected number of points falling in  $B$  is  $\lambda \pi r^2$  [Ripley, 1981]. In a regular pattern values of  $\hat{k}(r) < \pi r^2$  and under clustering pattern  $\hat{k}(r) > \pi r^2$  [Bailey and Gatrell, 1995]. Thus, a frequent way to have a graphic idea of the K-function is to transform it to a straight line (L-function) which transforms the Poisson K function to the straight line  $\hat{L}(r) = r$ :



$$\hat{L}(r) = \sqrt{\frac{k(r)}{\pi}} \quad (3.6)$$

A common approach to test the K-function under the null hypothesis of Complete Spatial Randomness (CSR) could be done using the Monte Carlo test [Ripley, 1981]. In a CSR model the total number of events are independently and uniformly distributed in  $B$ . The CRS model could be tested using upper  $U(r)$  and lower  $L(r)$  simulation envelopes. Under a CSR model the number of independent simulation  $m$  of  $n$  events could be constructed as:

$$U(r) = \max_{i=1, m} \hat{L}(r) \quad (3.7)$$

$$L(r) = \min_{i=1, m} \hat{L}(r) \quad (3.8)$$

We used 100 Monte Carlo simulations to test the distribution of blow-downs in the Amazon under a CRS model.

### 3.2.6 Recurrence Intervals of Blow-downs

We used the following assumptions to calculate the recurrence intervals of the large disturbances detected in the Amazon: (i) only new blow-downs up to 2 years old were used to calculate the recurrence time, considering that probability of detection decreases with age of the regrowth in older patches; and (ii) disturbances occurred at a constant rate during the two years of detection. The recurrence interval ( $T$ ) was calculated as:

$$T = \frac{A_{forest}}{D_{AR}}, \text{ where } D_{AR} \text{ is:} \quad (3.9a)$$

$$D_{AR} = \frac{A_{new-blowdown}}{Y} \quad (3.9b)$$

where  $A_{forest}$  is the total area of forest,  $D_{AR}$  is the disturbance rate and  $Y$  is 2 (estimated time in years of blow-down recovery).  $D_{AR}$  is estimated from the total area of new blow-downs ( $A_{blow-downs}$ ) during the time interval (maximum interval of detection equal to 2 years). Thus, the recurrence interval can be rewritten as:

$$T = \frac{A_{forest}}{(A_{new-blown-down}/2)} = 2 \left( \frac{A_{forest}}{A_{new-blown-down}} \right) \quad (3.10)$$

### 3.3 Results

#### 3.3.1 Size Class Distribution of Large Disturbances

In 27 Landsat images, we mapped 279 patches as large disturbances that we refer to as blow-downs, accounting for a total of 21,931 ha. Of that area, 17,822 ha (189 patches) were old blow-downs (> 2 years old), and 4,109 ha (90 patches) were recent blow-downs. The largest blow-down covered 2,223 contiguous hectares. The smallest blow-down observed was 5 ha based on the minimum threshold of blow-down detection of  $\sim 55$  pixels. Blow-downs smaller than 50 ha were most frequent (Fig. 3-2a). Blow-downs greater than 101 ha, although rare, accounted for 61.6% of total blow-down disturbance area of this region (Fig. 3-2b).

#### 3.3.2 Unmixing Spectral Properties of Blow-downs

Based on spectral unmixing of each Landsat image (Fig. 3-3a), new blow-downs (Fig. 3-3b and c) had on average 28% of NPV ( $\pm 10.20\%$  sd), 54% of GV ( $\pm 9.53\%$  sd) and 17% of SD ( $\pm 6.20\%$  sd) (Fig. 3-3f). Old blow-downs (Fig. 3-3d and e) had 1 % of NPV ( $\pm 1.34\%$  sd), 94 % of GV ( $\pm 5.46\%$  sd) and 5% of SD ( $\pm 4.75\%$  sd) (Fig. 3-3f).

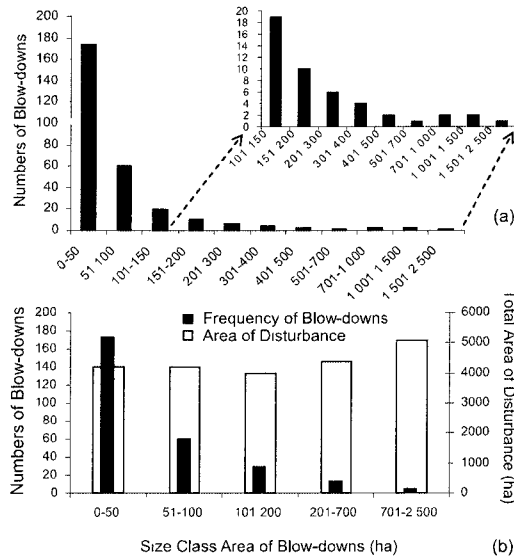


Figure 3-2: Frequency distribution of the 279 classified blow-downs (a) and their corresponding disturbed areas (b) classified in 27 Landsat images of an east-west transect of the Amazon.

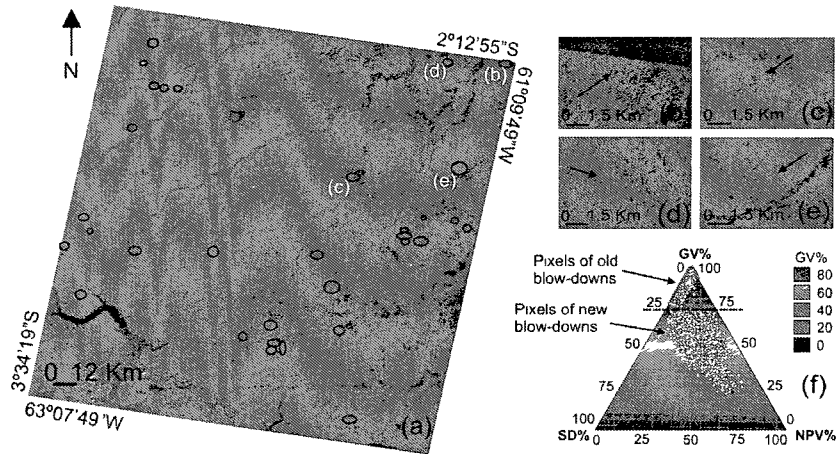


Figure 3-3: Unmixing Landsat image in color composition NPV (R), GV (G) and SD (B) showing the spatial distribution of several blow-downs (a). Close-up view of new blow-downs with probable age < 2 yrs (b and c) and old blow-downs likely > 2 yrs old (d and e). In (f), general fraction image proportions of new (n=3539 pixels) and old blow-downs (n=1869 pixels), sampled from the correspondent unmixed Landsat image (a). Vertices of the ternary diagram (clockwise from top) represent 100% of GV, NPV and SD fraction images.

### 3.3.3 Mask of the Antropogenic Disturbances

Land cover maps for the Amazon are currently available from the Brazilian deforestation project PRODES [INPE, 1998]. These maps do not provide information about natural disturbances. Unfortunately, we could not use the land cover map provide by PRODES as a basis for comparison for our natural disturbance studies because of the temporal mismatch between the PRODES images and the images selected for this studies. By performing our own simple classification, we also avoid sources of error from conversions of cartographic projections, image processing algorithms, and mismatches in the definitions of land-cover types.

Our digital classification of the 27 Landsat scenes in the study area resulted in 88.32% of natural forests, 2.29% of antropogenic disturbances, 0.51% of naturally exposed soils, 5% of water and 3.83% of cloud cover. By contrast, natural blow-down disturbances represented only 0.02% of the total area (Fig. 3-4).

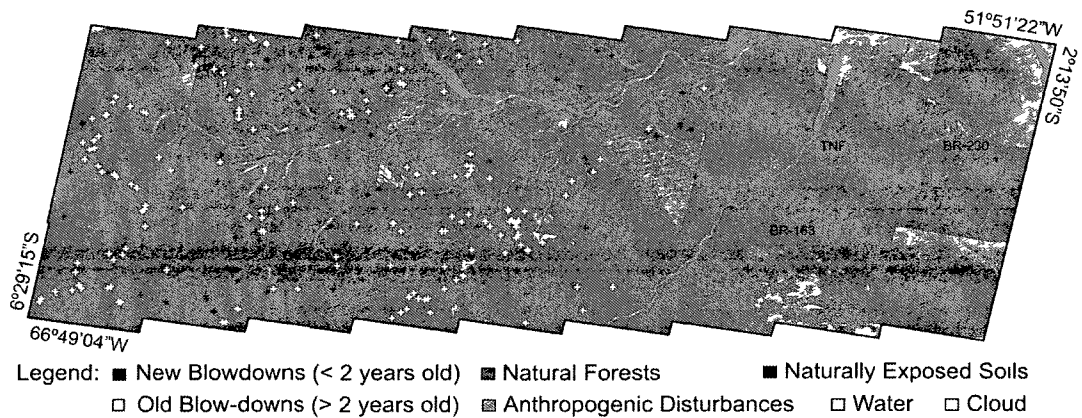


Figure 3-4: Land-cover map and occurrences of large disturbances (blow-downs) in the study region. TNF is the Tapajós National Forest. BR 63 and 230 are major highways that are foci for active land use change.

### 3.3.4 East-West Distribution of Disturbances and Severe Storms

The occurrence of blow-downs ( $\geq 5$  ha) over the Amazon region investigated is not homogeneous in the east-west direction and there is a complete absence of blow-downs in some regions of eastern Amazon (Fig. 3-5). The Gaussian smoothing kernel test for the three bandwidths (25, 50 and 100 km) produced three different spatial patterns maps of blow-down densities (Fig. 3-6). The 25 km of bandwidth (Fig. 3-6a) produced too much local variations of blow-down densities. Using 100 km overly-smoothed the variation of point densities (Fig. 3-6c). We found that a band with of 50 km (Fig. 3-6b) produced a reasonable estimation of intensity of blow-downs, although the choice of optimal bandwidth is still questionable.

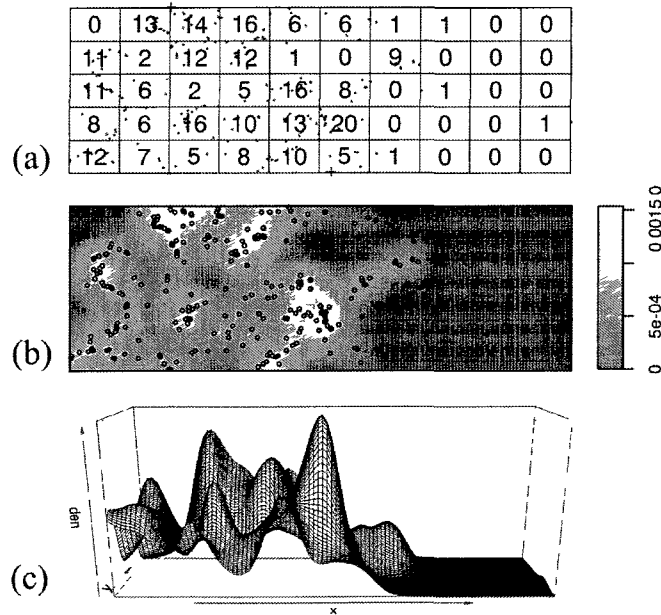


Figure 3-5: Complete spatial randomness tests for large disturbances in Amazon. Intensity of blow-downs estimated by quadratic counting (a) and kernel smoothing with bandwidth of 50 km (b). An east-west perspective graphic of the intensity of blow-downs in the Amazon produced by a smoothing kernel (c).

Despite the bandwidth empirically selected, the 100 Monte Carlo simulation under a

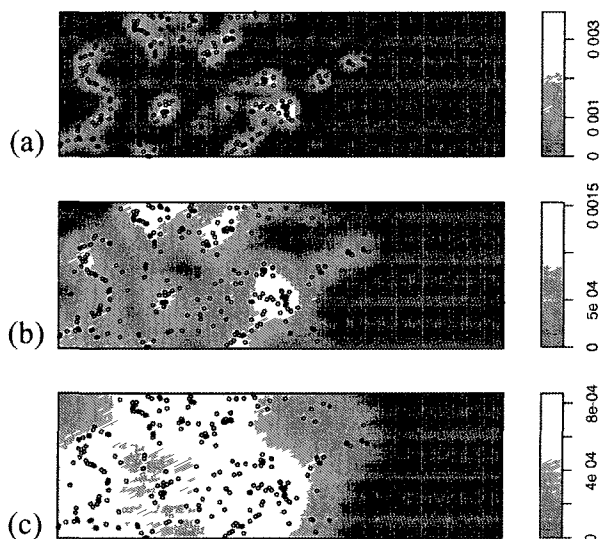


Figure 3-6: Intensity of blow-downs occurrences using a Gaussian smoothing kernel with bandwidth of (a) 25, (b) 50 and (c) 100 km.

CRS model suggested that the occurrence of blow-downs in the Amazon follow a clustering spatial pattern, since the K-function lies well outside the upper simulation envelop (Fig. 3-7).

Most of these large disturbances occurred between  $58^{\circ}00'W$  and  $66^{\circ}49'W$  (Fig. 3-8a). Several clusters of blow-downs were detected in the western Amazon (Fig. 3-8b). Blow-downs were infrequent in the eastern basin ( $51^{\circ}51'W$  to  $58^{\circ}00'W$ ). The greatest area disturbed by blow-downs occurred between the longitudes  $62^{\circ}$  and  $63.99^{\circ}$ , where  $\sim 5,000$  ha of old growth forest were disturbed by 40 large blow-downs (Fig. 3-8c). Old and new blow-downs had similar spatial distributions (Fig. 3-8a,b).

We provide a quantitative linkage between blow-down occurrence and the frequency of heavy daily rainfall in the Amazon region associated with severe convective activity [Garstang et al., 1998]. Blow-down occurrence frequency and the associated disturbance area were greater where severe storms occurred more frequently (Fig. 3-9).

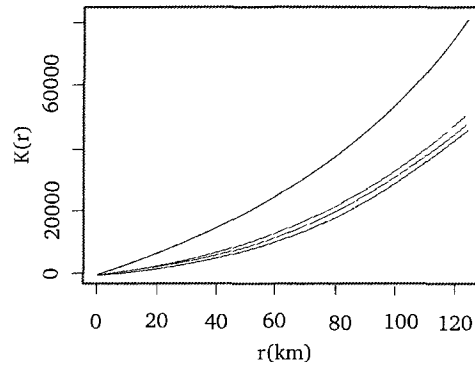


Figure 3-7 K-function and simulated envelopes of the spatial distribution of blow-downs in the Amazon. The black line is the original K-function and the colored lines are the upper and lower envelopes.

The simplest test of normality ('quantile-quantile plot') revealed that a slight S-shape distribution of occurrence blow-downs and storms which suggests evidence of non-normality (Fig. 3-10). The quantile-quantile plot ranks samples from our data distribution against a similar number of ranked quantiles taken from a normal distribution [Crawley, 2007]. If the occurrence of storms and blow-downs are normally distributed the line will be straight.

The relation between storm frequency and blow-down occurrence in the east-west bins is non-linear (Fig. 3-11). Non-linearity in this case is not surprising considering that the data comes from different spatial scales and also there is some temporal mismatch of the data (Real-Time Rainfall NOAA daily images from 1999 and Landsat ETM+ images from 1999 to 2001). Because of the non-linearity, we used the Spearman's rank correlation to test the relation between the two variables. We found a strong rank correlation between frequency of storms and blow-down occurrence (Spearman's rank,  $r^2=0.84$ ,  $p \leq 0.0003$ ). Storms may not be the only independent variable that explains the occurrence of blow-downs in the Amazon (e.g. distribution of soil types may be important). Future research exploring new explanatory variables is still necessary.

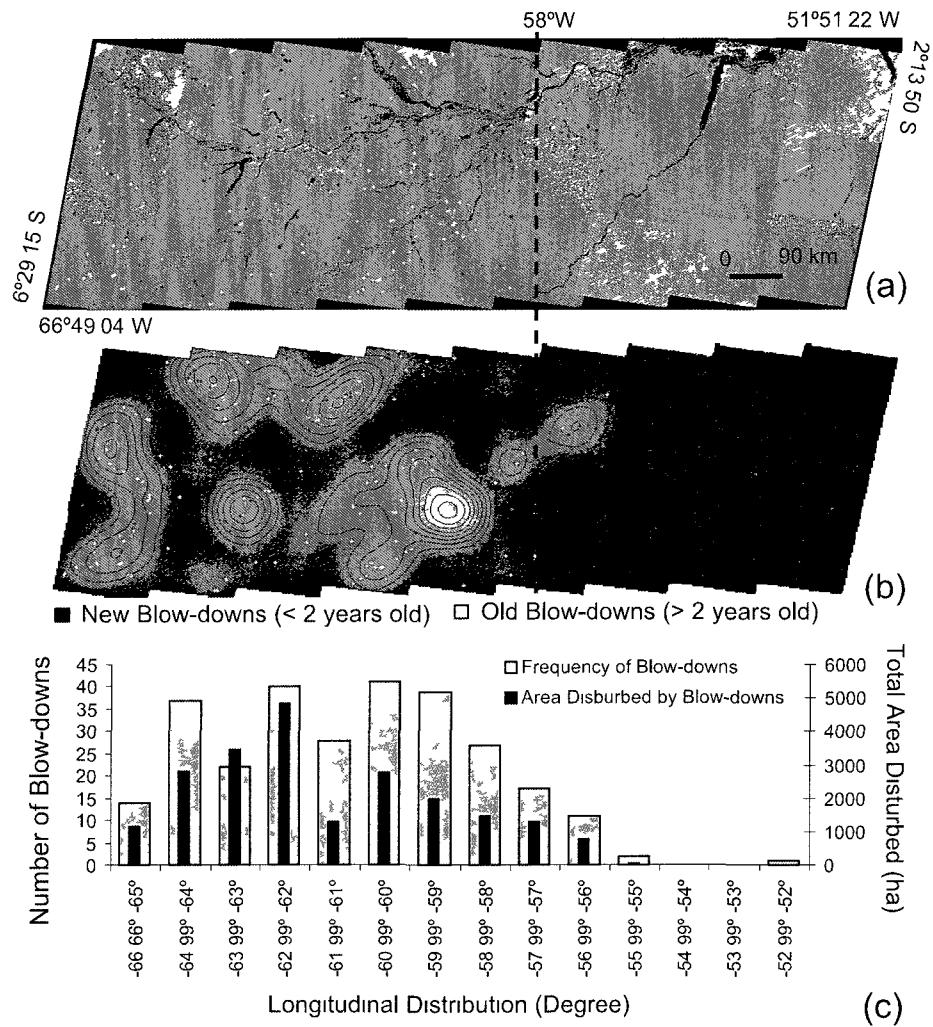


Figure 3-8 Spatial distribution of the 279 blow-down disturbances >5 ha (a) and their spatial clustering (b) observed in the east-west image transect of the Amazon. In (c), east-west distribution of blow-down frequency and area



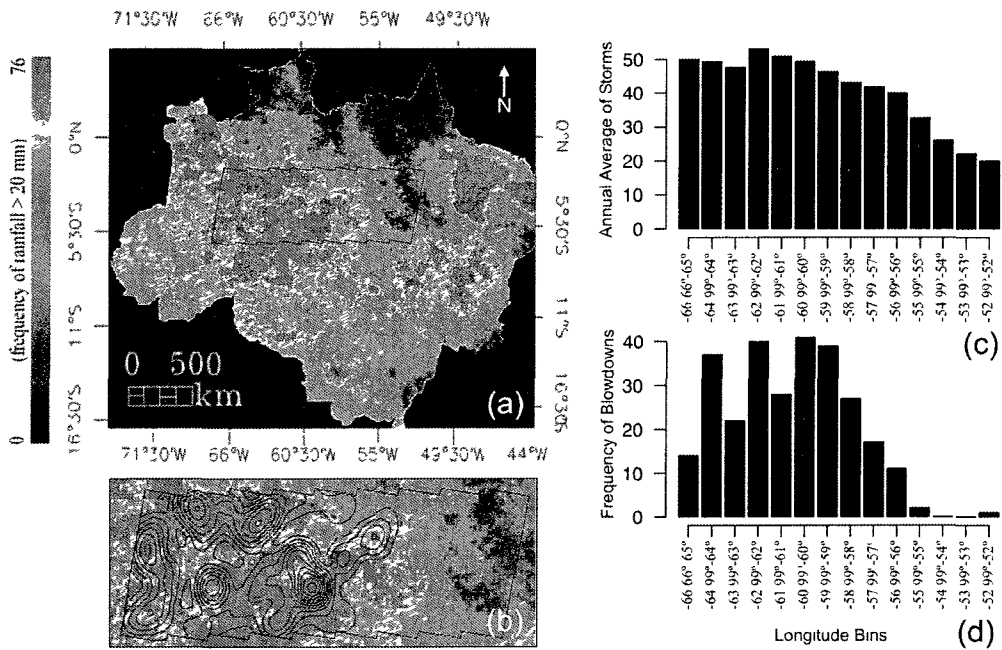


Figure 3-9: Annual frequency of intense storms in the Amazon (number of days with > 20 mm of rain) produced by 313 RTR daily images of the year 1999 (a). Clusters of large disturbances coincide with areas of more high-intensity storms (b). Frequency of the annual average of storms (c) and blow-downs (d) taken from one degree of longitude bins.

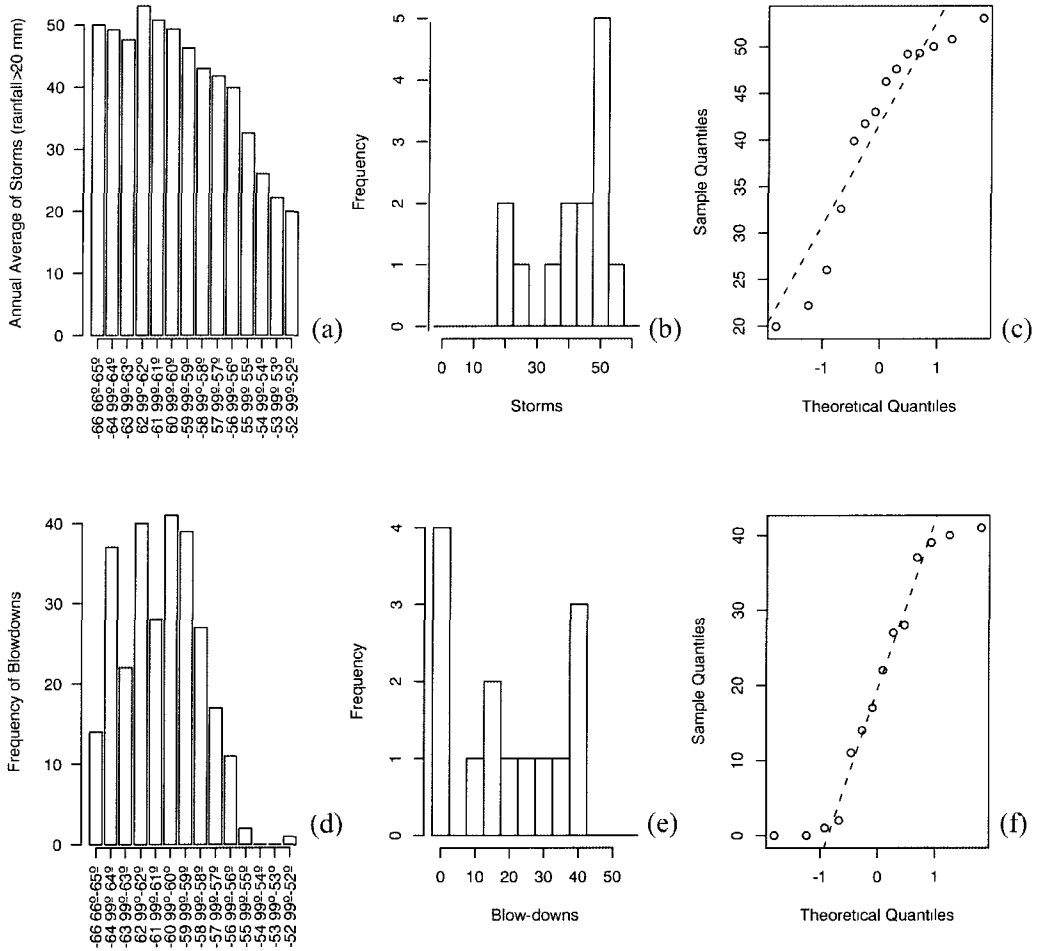


Figure 3-10: Number of events, frequency and quantile-quantile plot test of normality for blow-downs (a, b and c) and estimated storms in the Amazon (d, e and f), respectively.

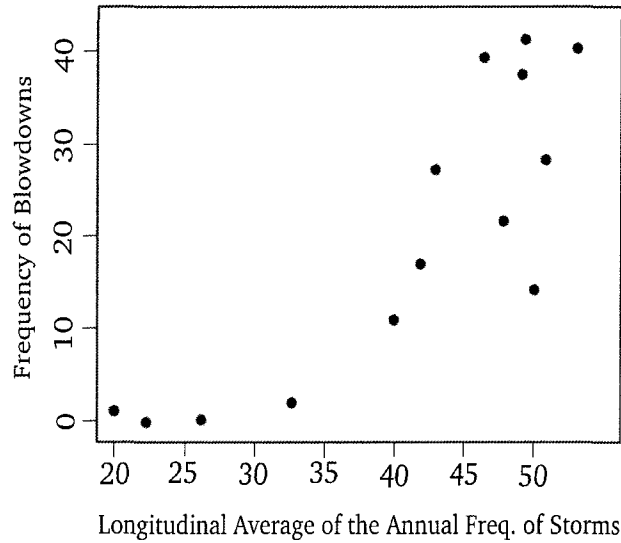


Figure 3-11: Scatter plot of storm frequency and blow-down occurrence in taken from one degree of longitude bins.

### 3.4 Estimate of Return Frequency of Large Disturbances

A comparison of the eastern and western portions of our study region (Fig. 3-8) shows a strong contrast in the blow-down recurrence intervals. Based on the occurrence of new blow-downs and the assumption of a constant disturbance rate (see section 3.2.6), we estimated the recurrence interval for blow-downs in the eastern region is 90,000 yr while it is only 27,000 yr for the western region (Table 3.1).

### 3.5 Discussion

We confirm the conclusions of the earlier study by Nelson et al. [1994] and expand on their work by using semi-automatic digital classification for detection and mapping of blow-downs in the Amazon and a satellite proxy measurement for convective storm events. In the study by Nelson et al. [1994], the threshold minimum area of disturbance was 30 ha. By using spectral unmixing and pixel by pixel classification of Landsat images we reduced

Table 3 1 Frequency, disturbed area and recurrence interval (T, in years) of blow downs

Domain	Landsat	Forest	all blow downs			new blow downs			T <sub>I</sub>
	scenes	km <sup>2</sup>	numbers	km <sup>2</sup>	proportion‡	numbers	km <sup>2</sup>	proportion‡	yr (10 <sup>3</sup> )
Full	27	793076	279	219	0 03%	90	41 1	0 01%	39
Eastern*	12	339579	21	18 5	0 01%	13	7 51	0 00%	90
Western§	15	453497	258	201	0 04%	77	33 6	0 01% <sup>nn</sup>	27

\*Eastern domain 51°51'22"W to 57°25'18"W,

§Western domain 57°25'18"W to 66°49'04"W,

‡Proportion is (blow down area – by total area of forest) × 100%,

†Assumes a constant disturbance rate and detectability of 2 years T = forest area – (new blow-down area – detectability interval) See section 3 2 6

the threshold of detection for blow downs to about 5 ha (~55 pixels) Both studies found that new plus old blow-down disturbances represented a small fraction of the entire studied area of undisturbed forests (~0 02%) Through digital processing, we were able to not only improve the spatial resolution but also improve the temporal resolution with important implications that we discuss below

We found strong indication that the occurrence of large disturbances over the Amazon region are clustered However, the selection of an appropriate bandwidth is a critical step to detect spatial patterns distributions of these events It is well known that the appropriate size of bandwidth is more important than the choice of many possible kernel functions [Bailey and Gatrell, 1995] In general, a large bandwidth will result in a large amount of smoothing and low density values, producing a generalized map On the other hand, a small bandwidth will result in less smoothing, producing a map with local variations in point densities [Bailey and Gatrell, 1995] We recognize that the choice of bandwidth in SPA is subjective and future studies are needed

The frequency distribution of storms and frequency of blow downs suggest a nonlinear relationship, which is not entirely surprising, considering that cloud top temperature is only a proxy of storm severity, and considering the spatial and temporal mismatches between

recorded blow-downs and the RTR data set. The RTR rainfall data set used provides increased spatial resolution (4 km) and higher frequency compared to earlier climatologies to isolate the importance of severe storm events. Closer linkage of blow-down events to storm conditions will require high-frequency observations of rainfall (now available) and high-frequency ground-based records of disturbance over wide areas (currently unavailable).

Although the disturbance rates are certainly higher in the Western Amazon, the estimate of recurrence interval for blow-downs remains highly uncertain. Estimating a millennial-scale recurrence interval from two years of observations (the period of detection), depends on the assumption that disturbance rates during those two years are representative of this disturbance process over millennia. Nonetheless, the east-west asymmetry in the frequency distribution of blow-downs is consistent with the geographic distribution of disturbance-adapted tree genera [ter Steege et al., 2006], suggesting that, over the long term, disturbance events are less frequent in eastern compared to western Amazon. However, long-term changes of climate [Mayle and Power, 2008] and patterns of soil fertility [Malhi et al., 2006] and geology [Rossetti, Toledo, and Goes, 2005] would be much more important environmental factors affecting the distribution of plant species and plant functional types.

Assuming that the blow-down damages all the trees and considering the average range of biomass for the Amazon is between 150 and 350 Mg ha<sup>-1</sup> [Houghton et al., 2000], we estimate that carbon emission caused by blow-down mortality (area of blow-downs x range of mean biomass) would contribute at most only 0.3 to 2 Tg C y<sup>-1</sup> for the 27 Landsat images analyzed, although, it will be compensated by the regrowth of secondary forests. Given that net deforestation releases between 200 and 300 Tg C y<sup>-1</sup> [Houghton et al., 2000] in the Amazon, blow-down disturbance events do not make an important direct contribution to carbon dioxide emissions or even for the overall forest succession process in the tropics. While the contemporary effect of large blow-downs is small with regard to carbon and

nutrient cycling, our study raises the question of the possible importance of convective storm activity as a control over the rate of forest disturbance in general across the Amazon. If convective activity is also responsible for smaller scale disturbances, this process may help explain some of the asymmetry in tree mortality and turnover rates found for the Eastern and Western areas of the Amazon forest [Phillips and Gentry, 1994]

### 3.6 Conclusions

The occurrences of large disturbances in the Amazon is still an ongoing natural phenomenon. Our recent analyses,  $\sim 10$  years after the previous study of Nelson et al [1994] confirmed the same general patterns of size class frequency and spatial distribution of blow-downs in the Amazon. In 27 Landsat ETM+ images from 1999 to 2001 large disturbances impacted a total of 21,931 ha of undisturbed old-growth forest. The largest event covered 2,223 ha of contiguous area and blow-downs smaller than 50 ha were most frequent.

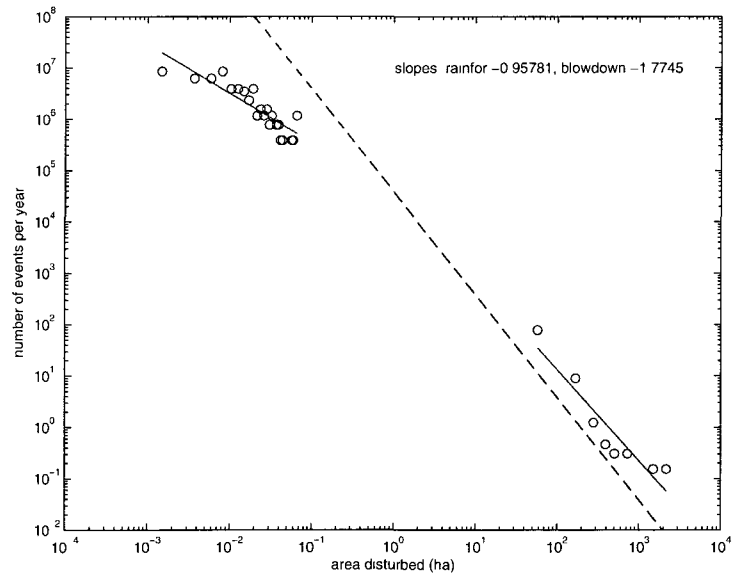
There is clear spatial association between patterns of blow-downs occurrences and high frequency of rainfall. In the Amazon most of these large disturbances occurred between  $58^{\circ}00'W$  and  $66^{\circ}49'W$ , likely associated with severe convective activity. Blow-downs were infrequent in the eastern Amazon basin ( $51^{\circ}51'W$  to  $58^{\circ}00'W$ ). Considering the east-west differences on the spatial patterns and frequency distribution of blow-downs in Amazon the turnover of blow-downs in the eastern region is 90,000 yr while it is only 27,000 yr for the western region.

Blow-down disturbance events do not have an important direct contribution to carbon dioxide emissions process in the Amazon, given the small fraction area covered by these events (0.03%) when compared with the total undisturbed forest region. Moreover, it probably is compensated by the regrowth of secondary forests around of land-use areas of the deforestation. However, considering the east-west asymmetry in tree mortality and

turnover in the Amazon, our work may also explain part of the spatial patterns of forest dynamics in the tropics.

## CHAPTER 4

# PAN AMAZON FOREST DISTURBANCE SPECTRUM AND IMPLICATIONS FOR THE TROPICAL OLD-GROWTH FOREST CARBON SINK



Dissertation chapter in preparation for Nature Geoscience



## 4.1 Introduction

There is strong evidence for a global land sink implied by the global atmospheric CO<sub>2</sub> record, fossil fuel emissions and estimates of ocean carbon uptake based on ocean surveys of dissolved inorganic carbon and water mass tracers such as chlorofluorocarbon gases [?]. Tropical forests may account for a substantial portion of the global terrestrial carbon sink [Phillips et al., 1998, 2008; Lewis et al., 2009]. The Amazon basin forest contains a large carbon pool (~100 PgC aboveground biomass [Malhi et al., 2006; Baker et al., 2004; Saatchi et al., 2007, 2011] that could be released rapidly to the atmosphere and thus substantially enhance greenhouse warming (e.g. Schimel et al. [2001]; Friedlingstein et al. [2003]). Because of its vast size the Amazon forest also has the potential to moderate global warming through enhanced carbon uptake due to growth stimulation caused by increases in atmospheric CO<sub>2</sub> [Grace et al., 1995; Cox et al., 2000]. Evidence from a tropical forest plot network (RAINFOR) indicates that old-growth Amazon forests have gained carbon over the last decades [Phillips et al., 1998, 2008; Lewis et al., 2009]. The RAINFOR plots (mostly 1ha in size) are distributed in several South American countries and in some cases provide data back three decades. Biometric measurements track the forest dynamics of growth and death of individual trees [Malhi et al., 2002].

While the old-growth forest estimates based on regular forests censuses [Phillips et al., 1998] reveal, on average, biomass gains for the 1ha plots surveyed, it is unclear to what extent these biomass gains indicate a true basin-wide trend. We ask whether the biomass gains may be an artifact of the small plots and small area sampled. Most forest stands gain biomass over decades to centuries and biomass gain is reversed only when severe disturbances kill large forest areas rapidly [Frelich, 2002]. Such severe disturbance events will release large amounts of carbon to the atmosphere over years following the event [Körner, 2004]. A sparse forest census network may not capture rare disturbance events. In that case,

the interpretation of the reported growth rate trends as a substantial carbon sink may represent a sampling bias [Fisher et al , 2008] In this paper, we assess whether the frequency spectrum (distribution) of forest disturbances versus disturbance severity, or equivalently the distribution of severity of disturbance versus its return time, for the Amazon Basin is sufficient to either validate or invalidate conclusions of carbon uptake based on the RAINFOR results

Understanding the role of forest disturbance in regional carbon budgets requires quantification of the frequency distribution of forest disturbance severity in terms of the amount of biomass lost Natural disturbances across the Amazon landscape range in size from tree-fall gaps on the order of 0.01 ha [Brokaw, 1982, Denslow, 1987] to blow-downs as large as 2,200 ha [Nelson et al , 1994, Garstang et al , 1998, Chambers et al , 2009b, Espirito-Santo et al , 2010, Negron-Juarez et al , 2010] A complete characterization and understanding of this spectrum of natural disturbances in tropical ecosystems is missing [Chambers et al , 2009b, Frohking et al , 2009] To date, carbon loss in tropical forests have been estimated based mainly on biometric data of individual trees from small plots [Pyle et al , 2008, Gloor et al , 2009] Some attempts have been made to estimate disturbance areas for tree-fall gaps [Van der Meer et al , 1994], blow-downs [Nelson et al , 1994, Espirito-Santo et al , 2010, Negrón-Juarez et al , 2010] and hurricanes [Whitmore, 1989]

We present a first synthesis of existing and new basin-wide disturbance observations and characterize their spatial distribution and temporal frequency We define disturbance broadly as all plant mortality that liberates carbon Because of the uncertainties associated with below-ground biomass, we discuss carbon losses only in terms of above-ground biomass (AGB) which probably accounts for more than 80% of biomass in Amazon Basin forests [Houghton, 2005, Malhi et al , 2006, Saatchi et al , 2007] We use records of biomass changes from a spatially distributed forest census network in the Amazon [Phillips et al , 1998, Malhi

and Román-Cuesta, 2008; Gloor et al., 2009] supplemented by two large forest plot surveys from central Eastern Amazon and an analysis of multiple satellite images to map, detect and estimate the severity of large disturbances (blow-downs). We reanalyze records of blow-downs likely caused by downdrafts associated with convective clouds [Garstang et al., 1998] covering the entire Brazilian Amazon forests using historical Landsat satellite images [Nelson et al., 1994] and a more recent East-West mosaic of Landsat scenes covering the Amazon [Espírito-Santo et al., 2010]. We combine the spatial records of blow-downs with an aboveground map of biomass developed recently for the tropics [Saatchi et al., 2007, 2011]. We analyze information on the spectrum of disturbances with an ensemble of growth rates from forests censuses using a simple stochastic forest simulator. From this analysis we seek to infer the potential effects of the observed spectrum of disturbances on estimates of forest carbon uptake.

## 4.2 Methods

### 4.2.1 Forest Inventories and Remote Sensing

The detection of forest disturbance and tree mortality that releases carbon depends upon spatial and temporal scales and observational methods. We combine data from forest censuses and the analysis of Landsat images permitting us effectively to sample disturbances across nearly all scales (Fig. 4-1 and Tab. 4.1).

For disturbances that affect less than about 0.1 ha, we combine two spatial and temporal sources of data: (1) 151  $\sim$ 1ha forest inventory plots from the RAINFOR covering 45 Amazon regions [Gloor et al., 2009]; and (2) losses of biomass in areas of branch or tree-fall gaps of two plots of 53 and 114 ha from central Eastern Amazonia. For disturbances at a landscape scale (disturbance size  $>$  5 ha) we combine three remote sensing data sets: (1) a spatially extensive record of large disturbances from blow-downs  $\geq$  30 ha from 136 Landsat

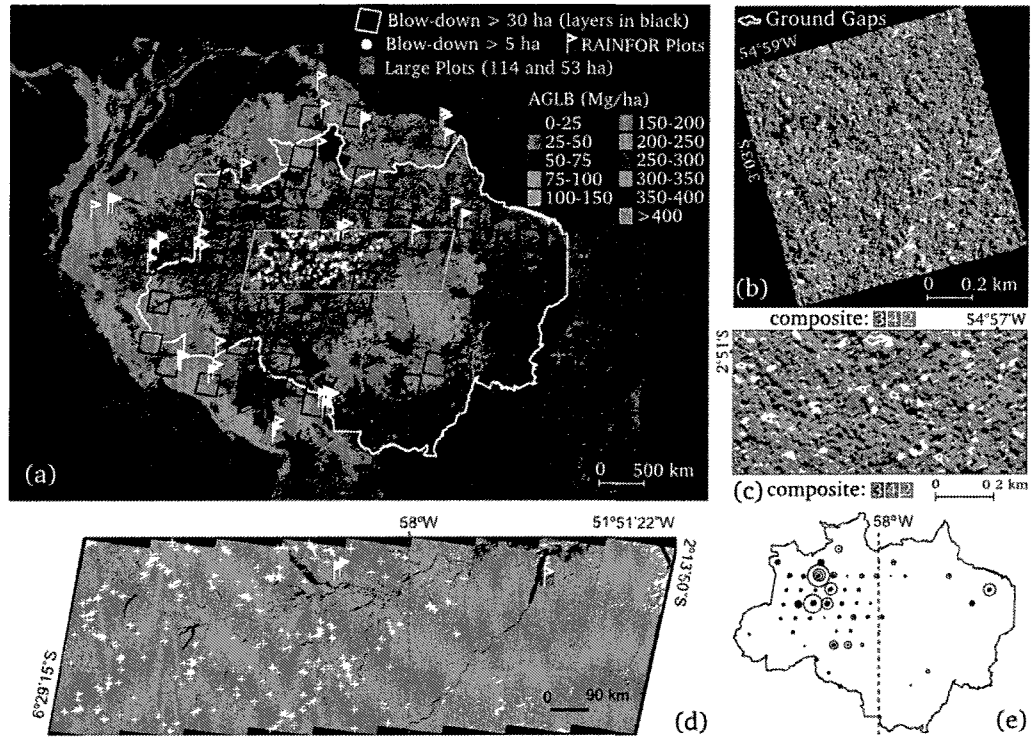


Figure 4-1: Spatial distribution of censuses RAINFOR plots ( $n=151$ ), inspected Landsat images ( $n=137$ ) with occurrences of large blow-down disturbances  $\geq 30$  ha ( $n=330$  blow-downs) and  $\geq 5$  ha ( $n=279$  blow-downs) overlapped on an aboveground biomass map of the Amazon (a). Large forest inventory plot of 114 ha with canopy gaps ( $n=55$ ) overlapped on a high resolution IKONOS-2 image acquired in 2008 in the Eastern Amazon (b). Large plot of 53 ha with canopy gaps ( $n=51$ ) over a second high resolution IKONOS-2 image acquired in 2009. Digitally classified blow-downs in an East-West mosaic of Landsat image from central Amazon (d). Areas of blow-downs  $\geq 30$  ha mapped by Landsat images (disturbance areas are proportional to the size of the circles) (e).

scenes of the Brazilian Amazon [Nelson et al., 1994] - 8 scenes are outside of the Brazilian geographic border; (2) a high resolution mapping of blow-downs  $\geq 5$ ha using 27 Landsat scenes on an east-west transect in the central Amazon [Espírito-Santo et al., 2010]; and (3) a multi-sensor remote sensing product of aboveground biomass for the tropics [Saatchi et al., 2007, 2011]. For all disturbances we estimate areas and severity defined as changes in above-ground biomass (AGB) stocks (Supplementary C-1). Disturbances in field plots were accessed from the observation of net allometric AGB changes [Gloor et al., 2009] and allometric AGB estimates in opened canopy gaps. For large disturbances [Nelson et al., 1994; Espírito-Santo et al., 2010] we estimated severity based on the area of blow-downs multiplied by a geographic biomass mean using a carbon stock map of the Amazon [Saatchi et al., 2007, 2011] assuming an upper bound on mortality rate of 100% in areas of blow-downs [Nelson et al., 1994; Chambers et al., 2009b] (See Supplementary Material for Chapter 4). This upper bound of mortality rate is an overestimate that provides a conservative estimate for assessment of the significance of natural disturbance to old-growth forest carbon accumulation rates.

Table 4.1: Statistical summary of the four data sets: 151 1ha plots distributed over the Amazon, 96 tree-fall gaps of 167 ha plot in East central Amazon, 278 blow-downs  $\geq 5$  ha detected in 27 Landsat scenes and 330 large disturbances  $\geq 30$  ha inspected in 137 Landsat scenes.

Statistic summary	RAINFOR	167 ha plot	Blow-downs in 27 images	Blow-downs in 136 images
Raw data	151	96	279	330
Min disturbance area (ha)	0 0003	0 003	5	30
Max disturbance area (ha)	0 09	0 13	2,223	2,651
Mean disturbance area (ha)	0 016	0 026	79	213
Median disturbance area (ha)	0 014	0.022	37	123
SD of disturbance area (ha)	0 013	0 018	179	279
Sum of disturbance area (ha)	2 49	2 51	21,931	70,421
Min biomass change (Mg)	0 11	0 12	649	6,136
Max biomass change (Mg)	23 38	39 81	778,263	927,752
Mean biomass change (Mg)	5 02	6 11	24,183	60,395
Median biomass change (Mg)	4 37	3 27	10,478	35,343
SD of biomass change (Mg)	3 57	7 23	62,694	85,787
Sum of biomass change (Mg)	758 27	587.35	6,747,201	19,930,460

### 4.2.2 Spatial Distribution of Large Disturbances

We reanalyzed the original data from Nelson et al. [1994] using a spatial point analysis (SPA) to quantify the clustering of disturbances (Chapter 3, subsection 3.2.5 Modeling Spatial Point Patterns of Blow-downs) over the Amazon domain [Espírito-Santo et al., 2010]. A SPA [Ripley, 1981] consists of a set of points ( $s_1, s_2, \text{etc.}$ ) in a defined study region ( $B$ ) divided into sub-regions ( $AB$ ).  $Y(A)$  is the number of events that occurred in sub-region  $A$ . In a spatial context, the number of points can be estimated by use of their expected value  $\mathbb{E}(Y(A))$ , and covariance  $COV(Y(A_i), Y(A_j))$ , given that  $Y$  is the event number in areas  $A_i$  and  $A_j$ . The intensity of an event ( $s$ ) is the frequency of points of a specific location  $s$ , where  $ds$  is the area of this region. The intensity of events, or, in our case, number of blow-downs per Landsat image, can be represented as:

$$\lambda(s) = \lim_{ds \rightarrow 0} \left\{ \frac{\mathbb{E}(Y)(ds)}{ds} \right\} \quad (4.1)$$

Because SPA only requires the spatial location of each event, we used the centroid of each classified blow-down in the Landsat images. We used a Gaussian smoothing algorithm (kernel) with a bandwidth of 50 km to determine the spatial clustering of blow-downs and a probability density function  $k$  [Ripley, 1981] to examine the spatial dependence of these events [Espírito-Santo et al., 2010].

Previous spatial analysis of large disturbances in the Amazon showed that blow-downs are extremely rare in the Eastern Amazon region [Nelson et al., 1994; Espírito-Santo et al., 2010]. To account the spatial variability of large disturbance in the Amazon we used this re-analyzed map of blow-downs to infer the return time and severity of large disturbances over the basin.

### 4.2.3 Return Time versus Disturbance Severity

Disturbance severity ( $x$ ) has been scaled as if  $x$  obeys a power law  $p(x) \propto x^{-\alpha}$  drawn from a probability distribution, normally area, where  $\alpha$  is a constant exponent or scaling parameter [Fisher et al., 2008; Chambers et al., 2009b; Negrón-Juárez et al., 2010]. However, observed quantities ( $x$ ) rarely follow a power law distribution [Clauset et al., 2009]. An alternative approach to quantify disturbance regimes by class size area is to consider the distribution of return times versus severity of disturbances, inverting an empirical cumulative probability density function (PDF). From our data we can infer the relation of return time versus disturbance severity [Gloor et al., 2009], if we assuming that we may interchange time with space. The empirical probability density  $p(A)$  that a fixed location is hit by a disturbance of area  $A$  during one year is given by:

$$p(A)\Delta A = \left( \sum_{A' \in (A, A+\Delta A)} A' \right) / A_{Amazon} \quad (4.2)$$

where  $A_{Amazon} = 8 \times 10^6 km^2$  (INPE Pan-Amazônia project, unpublished data) is the total forested area of the Amazon. The probability for the occurrence of a disturbance event per year with area loss larger than  $A$  at a fixed location is then:

$$P(X \geq A) = \sum_{A' \geq A} p(A')\Delta A' = \frac{A^{distrbd}_{tot}}{A_{Amazon}} - \sum_{A'=0}^A p(A')\Delta A' \quad (4.3)$$

using the identity:

$$\sum_{A=0}^{\infty} p(A)\Delta A = \frac{1}{A_{Amazon}} \sum_i A_i = \frac{A^{distrbd}_{tot}}{A_{Amazon}} \quad (4.4)$$

where  $A^{distrbd}_{tot} = \sum_{all-disturbances} A$  is the total annually disturbed forest area in the Amazon. Therefore an estimate for the return time  $\tau(X \geq A)$  of a disturbance event  $X$  with

forest area lost larger than  $A$  at a fixed location is given by the inverse of the cumulative PDF

$$\tau(X \geq A) = \frac{1}{P(X \geq A)} = \frac{1}{\frac{A^{distrbd}_{tot}}{A_{Amazon}} - \sum_{A'=0}^A p(A')\Delta A'} \quad (4.5)$$

An analogous equation holds for return time with respect to biomass lost associated with a disturbance event

#### 4.2.4 Forest Aboveground Biomass Simulation

Once the disturbance spectrum of aboveground biomass loss is defined we can then infer the variance introduced into an ensemble of growth rates from forests censuses using a simple stochastic forest simulator  $dM = growth \times dt - Mortality \times dt$  with  $dM$  aboveground forest biomass change per area,  $dt$  a time interval, here one year, and  $Growth$  and  $Mortality$  stochastic variables distributed according to the observed frequency distributions of tree growth and mortality (Fisher et al 2008, Gloor et al 2009). We used as input parameters growth from the 151 annually-censused plots (Gloor et al 2009) and mortality (aboveground biomass loss) from our new disturbance spectrum analysis. Moreover, differently from the previous analysis of the aboveground biomass carbon sink over the Amazon (Gloor et al 2009) we incorporate new observed forest mortality data of tree-fall gaps (167 ha plot) and intermediate sizes of blow-down disturbances  $\geq 5$  ha (Esprito-Santo et al 2010). Analysis of the biomass variance trajectory over the time allows us to assess the statistical significance of a carbon sink in old-growth forests (Gloor et al, 2009).



## 4.3 Results and Discussion

### 4.3.1 Size Frequency and Spatial Clustering

In the entire forested Brazilian Amazon ( $3.9 \times 10^6 \text{ km}^2$ ) Nelson et al (1994) found 330 blow-downs  $\geq 30$  ha distributed in 72 Landsat scenes from the total 137 scenes (Supplementary C-3) acquired between 1988 and 1991. The total area of the 330 disturbed patches was  $\sim 90 \times 10^3$  ha [Nelson et al, 1994]. Comparison of the results of Espírito-Santo et al [2010] and Nelson et al [1994] revealed that across the Amazon there are a substantial number of intermediate sized blow-downs (5-30 ha). While high resolution data of blow-downs  $\geq 5$  ha are not available for the entire Amazon, we reanalyzed the data of Nelson et al [1994] using a kernel Gaussian smoothing algorithm for cluster analysis (SPA) of large disturbances. The analysis reveals clear clustering pattern of large forest disturbances in the western Amazon basin (Fig 4-2) west of  $58^\circ$  W independently of the bandwidth size used for the analysis (Supplementary C-4 and C-5). The large disturbances cover about  $\frac{1}{4}$  of the area of the Brazilian Amazon. These results are consistent with the findings of Espírito-Santo et al [2010] who found that disturbances  $> 5$  ha were 12 times frequent more west of  $58^\circ$  W compared to the area studied to the east.

### 4.3.2 Occurrence spectrum and return time

Our data permit us to determine the frequency spectrum of forest disturbances in the Amazon basin by scaling them using frequency distribution of area to the basin. Scaling by aboveground biomass losses we found two disjoint size and severity domains (Fig 4-3). There is a lack of information on the mid-range of the spectrum in between small gap-phase disturbances and landscape scale blow-downs (Fig 4-3).

Combined data of small disturbances (RAINFOR and two large plots) over the Amazon region ( $8 \times 10^6 \text{ km}^2$ ) indicate that branch or tree-fall gaps occur at the return time between

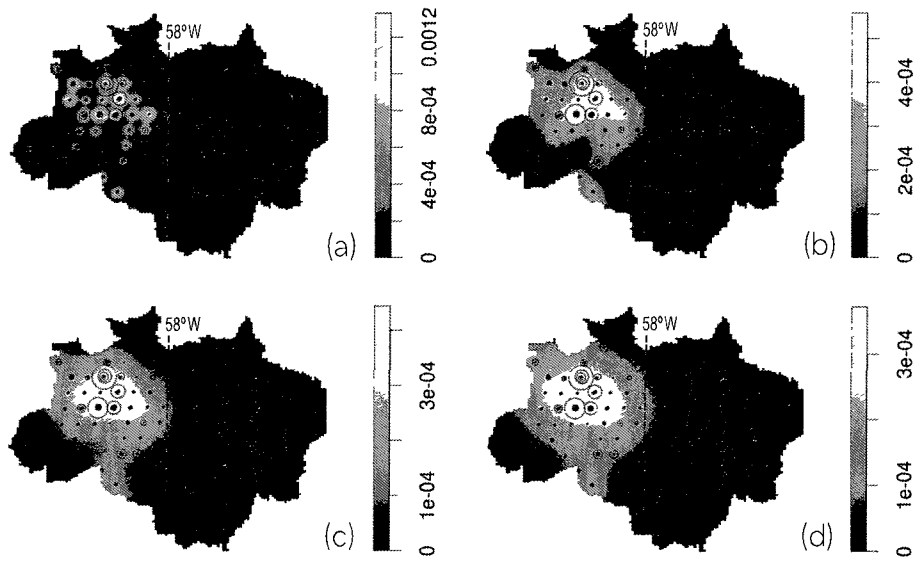


Figure 4-2: Intensity maps of blow-downs of Brazilian Amazon using a Gaussian smoothing kernel with bandwidth of 50 (a), 100 (b), 150 (c) and 200 km (d) modeled from 330 large disturbances  $\geq 30$  ha [Nelson et al., 1994] detected in 137 Landsat images over the basin. Color bar is the intensity of large disturbances in the Amazon (number of blow-downs per  $\text{km}^2$ ).

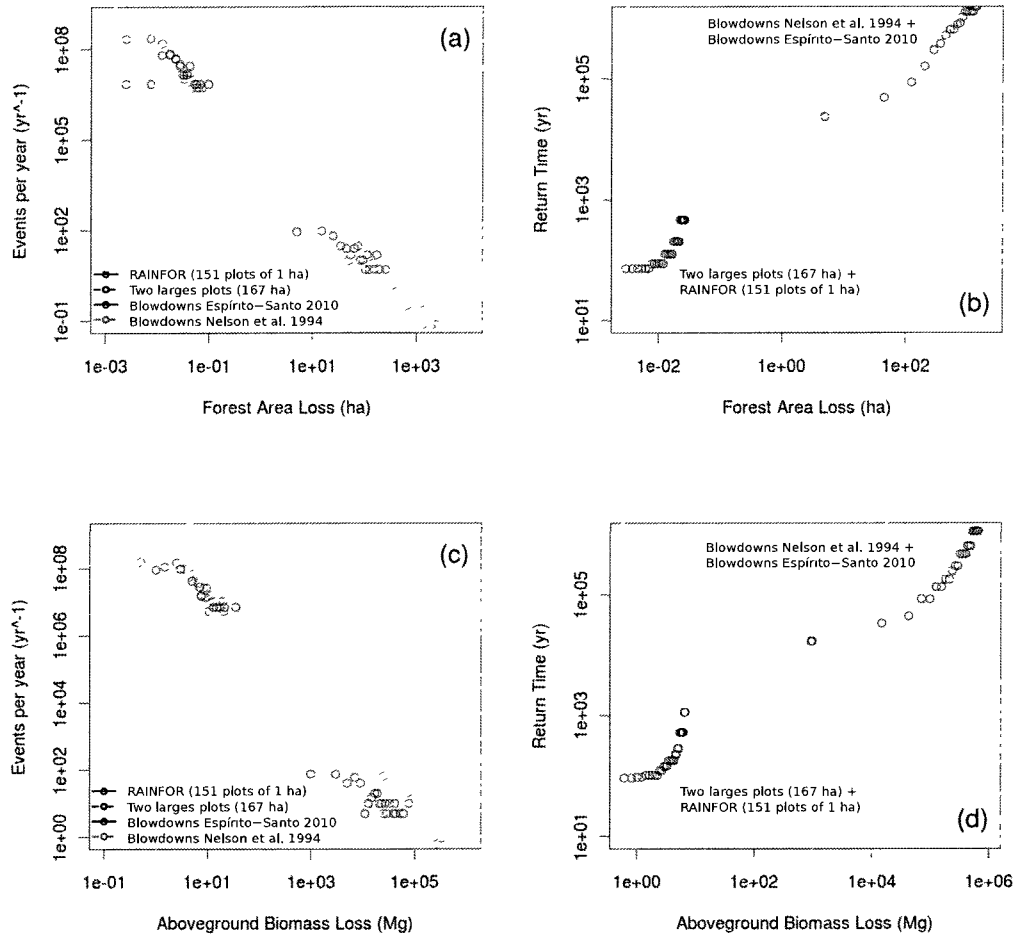


Figure 4-3: Natural forest disturbance spectrum from the Amazon basin. Number of disturbances per year (a) and return time (b) associated with area of events from tree-fall to blow-downs. Number of disturbances per year (c) and return time (d) compared to the severity of disturbances (biomass loss).

0 and 100 yrs which corroborates observed annual tree-fall disturbances rate of 1% (gap creation) from several studies in tropical forests [Van der Meer et al., 1994; Fraver et al., 1998]. The return time of large blow-downs is very rare over the Amazon region ranging from  $4 \times 10^4$  y to greater than  $10^6$  y dependent upon size. This is consistent with previous findings of forest turnover estimated by the sum of all recent blow-downs in just one Landsat image which is around  $5 \times 10^3$  y [Nelson et al., 1994] or  $3.9 \times 10^4$  y using the forested area of 27 Landsat images [Espírito-Santo et al., 2010].

### 4.3.3 Implications on Basin-Wide Old-growth Forest Carbon Sink

Having established an empirical Amazon basin-wide forest disturbance spectrum we assess its implications on the old-growth forest sink claim based on the RAINFOR forest census plot of Phillips et al. [1998, 2008]; Baker et al. [2004]; Lewis et al. [2009] following the simple stochastic simulator of aboveground biomass approach of Gloor et al. [2009].

The total area of the disturbances (mortality) of all classes for the Amazon region forest ( $8 \times 10^6$  km<sup>2</sup>) is estimated to in  $1.86 \times 10^7$  ha yr<sup>-1</sup> which represents a committed emission of  $2.53 \times 10^9$  Mg C yr<sup>-1</sup>. Total area disturbed and carbon released by small tree fall-gaps  $1.86 \times 10^7$  ha yr<sup>-1</sup> and  $2.52 \times 10^9$  Mg C yr<sup>-1</sup>. Intermediate and large blow-downs with total area of only  $4.19 \times 10^4$  ha yr<sup>-1</sup> and estimated severity of  $6.1 \times 10^6$  Mg C yr<sup>-1</sup> are essentially insignificant in budgetary terms although they have important local effects. Over the Amazon biome tree-fall gaps and tree mortality represent 99.7% of all carbon loss due to all natural mortality. Large disturbances although impressive are extremely rare (Fig. 4-3) and therefore unlikely to have a significant contribution of carbon emission at the Amazon basin confirming the view of Espírito-Santo et al. [2010].

Using the simple stochastic forest simulator framework described above how we analyze the likelihood that the basin-wide old-growth forests growth trends reported by Phillips et al.

[1998], Lewis et al [2009] are a sampling artifact caused by under-sampling of intermediate and large blow-down disturbances. The forests simulator results reveal that blow-downs are too rare to invalidate the conclusions of these studies. The variance in growth rates caused by blow-downs alone is much smaller than the forest census plot mean growth rate. This may also be inferred roughly from the return time versus disturbance severity distribution (Fig. 3d). Biomass losses per year due to blow-downs is on the order of  $10^{-5} \text{ yr}^{-1} \times 10^3 \text{ Mg yr}^{-1} \text{ ha}^{-1} = 10^{-2} \text{ Mg ha}^{-1}$  which is much smaller than the observed growth trend (Phillips et al. 2009).

#### 4.4 Concluding Remarks

The spatial concentration of blow-down disturbances observed calls into question the extrapolation of results in a recent study that estimated that a single cross-basin squall line event propagating across the Western Amazon coming from the South was responsible for a widespread Amazon forest mortality of 542 million trees or a total biomass loss of 128 Gg C [Negrón-Juárez et al., 2010]. These authors based their finding on the image classification of only  $0.034 \times 10^6 \text{ km}^2$  of high resolution Landsat image and extrapolated to the larger region ( $4.5 \times 10^6 \text{ km}^2$ ) based on meteorological data ( $\sim 10 \text{ km}$  resolution) showing the complete extent of a propagating squall line [Negrón-Juárez et al., 2010]. While blow-down disturbances are extremely rare in the Eastern Amazon, Negrón-Juárez et al. [2010] extrapolated uniformly across the squall line areas without regard to geography. At the ground level, forest inventories over the basin have also documented a clear difference in tree mortality and turnover rates for the Eastern versus Western areas of the Amazon forest [Phillips and Gentry, 1994, Phillips et al., 1998, Lewis et al., 2004, ter Steege et al., 2006] associated in part with soil depth and texture [Quesada et al., 2009].

There is a lack of quantification for disturbances from 0.13 to 5 ha (Tab. 4.1) in our spec-

trum analysis of disturbances for the Amazon. While our data suggest two clear extreme regimes of disturbances, we cannot conclude that there is not a continuous regime of disturbance in tropical forests. Currently we lack data to investigate this range of disturbance sizes. Disturbances in the 0.1 to 5 ha range would be difficult to detect with traditional forest inventory because they are probably very rare and would require extremely extensive surveys. Recently Kellner and Asner [2009] showed quantified gap frequencies from 5 areas of 1 km<sup>2</sup> in tropical forests in Costa Rica and Hawaii using airborne LiDAR technology. Chambers et al. [2009b] characterized vegetation recovery in blow-downs using satellite borne hyperspectral data (Hyperion). Given sufficient resources, either of these technologies should be useful for quantification of disturbances in the range of 0.1 to 5 ha. Our spectrum analysis (Fig. 4-3b) suggests that a 1 ha disturbance may have a return time on the order of 10<sup>4</sup> years. In order to observe a reasonable number of 1 ha events, we would probably need over 10<sup>5</sup> ha of spatially distributed airborne LiDAR or satellite hyperspectral collections.

In summary, the probability of large severe disturbances is very small. As an upper bound on the effects of such disturbances we may simply estimate a mortality based carbon flux from the probability of that disturbance  $P$  (severe disturbance)  $\times$   $M$  (mass of the severe disturbance). Even this approach suggests that severe disturbances contribute less than  $6 \times 10^{-3}$  Pg C y<sup>-1</sup>. Our findings strongly contradict the results of Fisher et al. [2008] and Chambers et al. [2009a] who denied the finding of an observed old-growth forest carbon sink in the Amazon of  $\sim 0.5$  Pg C yr<sup>-1</sup> over the last decades [Phillips et al., 1998, Lewis et al., 2009].

## CHAPTER 5

# CONCLUSIONS

### 5.1 The Balance of Natural Disturbances Processes in the Amazon

Above-ground biomass losses from natural disturbance processes are poorly understood and quantified in tropical forest areas [Uhl et al , 1988] Natural disturbances across of the Amazon landscape have occurrence ranges from branch or tree-fall gaps of 0 - 0.1 ha [Brokaw, 1982, Denslow, 1987] to large blow-downs areas of 5 - 3,000 ha [Nelson et al , 1994, Garstang et al , 1998, Chambers et al , 2009b, Espirito-Santo et al , 2010] At the plot scale tropical forest dynamics are governed by occurrences of small tree-fall gaps [Denslow, 1987] between 0.025 and 0.4 ha [Hubbell et al , 1999] In the Amazon region blow-downs greater than 30 ha [Nelson et al , 1994] produced by high-velocity downburst winds [Garstang et al , 1998] have been detected in satellite images [Nelson et al , 1994] The largest single blow-down covered 3,370 ha, with the most frequent size classes falling between 30 and 100 ha [Nelson et al , 1994]

The following questions motivated this dissertation: What is the mean coarse woody debris (CWD) or biomass change and tree mortality observed in small and large scale disturbances? What is the link between CWD observed of the several disturbances size class area and its implication for the carbon cycling? What remote sensing approaches can be applied to detect large disturbances especially blow-downs in the Amazon? How

does the turnover of these events vary across the Amazon landscape? What is the effect of blow-downs on carbon flux in the Amazon? What is the relative importance of disturbance at the local landscape scale versus disturbance at the regional scale to the dynamics of the carbon cycle in the Amazon? Is there some mechanistic process that can explain the variation and the intensity of these disturbances at local and regional scales? How can we reduce the uncertainties in carbon budgets by improvement of our knowledge of the rate of formation of small gaps and large disturbances in Amazon forests?

In this dissertation natural disturbances were examined in three ways: (1) Formation and detection of small scale disturbances was investigated in the field and with high resolution remote sensing; (2) I mapped and analyzed the spatial distribution of large disturbances (blow-downs) caused by convective cloud drafts; and (3) I characterized the spectrum of natural disturbances in tropical ecosystems.

As part of this dissertation, I showed [Espírito-Santo et al., 2010] that using digital classification of recent Landsat images enables detection of disturbances as small as 5 ha forest. These canopy disturbances revealed similar patterns of the frequency area distributions of disturbances previously registered by Nelson et al. [1994] over the Western Amazon. Blow-downs greater than 101 ha, although rare, accounted for 61.6% of total disturbance area of this region. Despite the large scale differences of area from tree-gaps to landscape blow-downs, the severity of disturbances (losses of above-ground biomass or necromass) has been rarely quantified [Frolking et al., 2009]. Quantitative studies of natural disturbances uniting all severity scales of disturbance in the Amazon were non-existent [Chambers et al., 2007a; Frolking et al., 2009] prior to my compilation achieved in Chapter 4.

In the Chapter 2 of this dissertation I documented the installation and survey of two large forest inventory plots of 114 and 53 ha in unmanaged tropical forest of the Tapajós National Forest. I mapped all gaps and collected data of coarse woody debris (CWD)



and tree mortality in both plots. I found 96 gaps in these plots and discovered that most mortality did not result in gap formation. Only about one-third of all tree mortality results in gap formation, and the carbon flux based on necromass in gaps is only about one part in six of the total CWD flux comparing with nearby permanent plots [Pyle et al., 2008; Palace et al., 2008]. On average, gap formation accounted for a minor proportion of the stocks (about 5% of the total fallen CWD) and fluxes (about 23%) of CWD carbon.

In Chapter 3, I analyzed 27 Landsat images to map large scale disturbances over the Amazon basin (canopy disturbance areas  $\geq 5$  ha) and applied a spatial pattern analysis of blow-downs apparently caused by severe storms. I found 279 patches (from 5 ha to 2,223 ha) characteristic of blow-downs and quantified that 21.931 ha of forest were disturbed in the total analysis. I found a strong correlation between occurrence of blow-downs and frequency of heavy rainfall (Spearman's rank,  $r^2=0.84$ ,  $p<0.0003$ ). The return time of blow-downs in the Amazon is about 40 thousand years. I concluded that blow-downs make an insignificant contribution to carbon cycling.

I analyzed the spectrum of disturbances in Chapter 4. I used historical data of the RAINFOR plots network in the Amazon [Phillips and Gentry, 1994; Phillips et al., 1998; Gloor et al., 2009], data from the large plots surveyed for Chapter 2, and a multi-sensor satellite image approach to study the frequency and extent of natural disturbances across the Amazon region. This study integrated the disturbance areas from small-scale (branch and tree falls) to large-scale disturbances. Assuming an upper bound of 100% of tree mortality in large disturbances and using the aboveground biomass  $\times$  area based on existing maps [Saatchi et al., 2007, 2011], I was able to estimate the severity of disturbances over the Amazon (Fig. 5-1) in carbon units. The total area of the disturbances of all classes for the Amazon region ( $8 \times 10^6$  km<sup>2</sup>) was  $1.86 \times 10^7$  ha yr<sup>-1</sup> which represents a committed emission of 2.53 Pg C yr<sup>-1</sup>. Total area disturbed and carbon released by small tree fall-gaps  $1.86 \times$

$10^7$  ha yr<sup>-1</sup> and 2.52 Pg C yr<sup>-1</sup>, respectively, is much bigger than large blow-downs with total area of only  $4.19 \times 10^4$  ha yr<sup>-1</sup> and estimated severity of 0.00006 Pg C yr<sup>-1</sup>. The number of small disturbances is about  $10^8$  yr<sup>-1</sup>, which suggests that over the Amazon biome tree-fall gaps and tree mortality represent 99% of all carbon loss due to natural mortality.

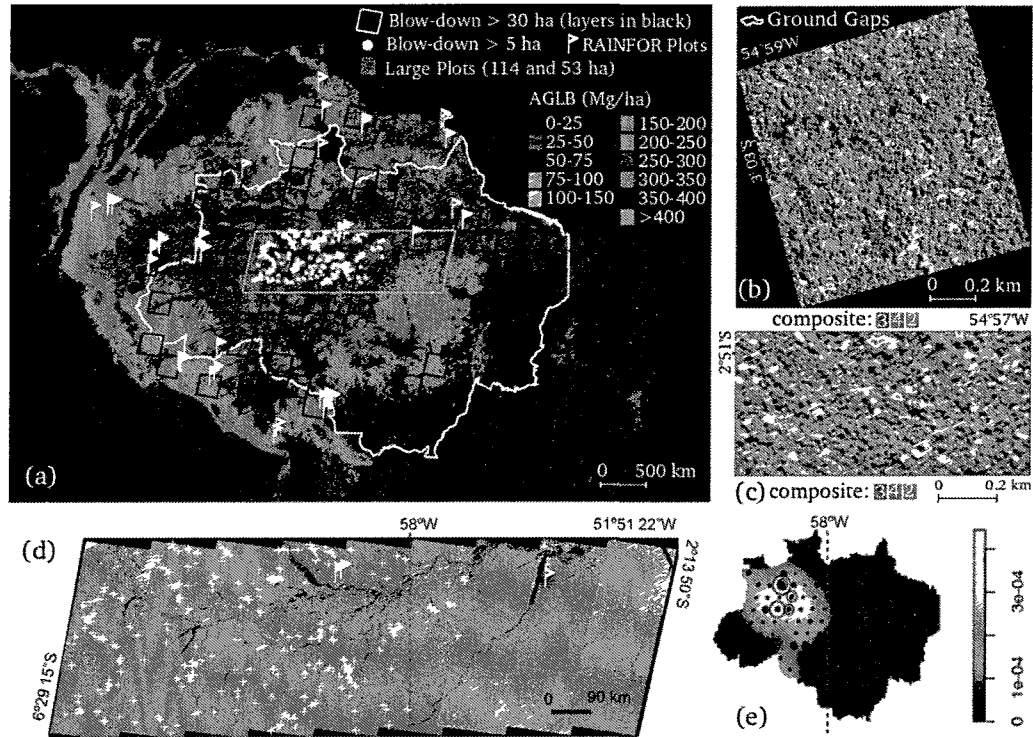


Figure 5-1: Data gathered in this dissertation or integrated into analyses for this dissertation include: The spatial distribution of RAINFOR plots of 1ha (n=151), 137 Landsat images with occurrences of large blow-downs  $\geq 30$  ha (n=330 blow-downs in 72 scenes) and  $\geq 5$  ha (n=279 events in 27 Landsat scenes discussed in Chapter 3) superimposed on a map of aboveground biomass in the Amazon (a); a large forest inventory plot of 114 ha with canopy gaps (n=55) shown superimposed on a high resolution IKONOS-2 imaged (2008) in the Tapajós National Forest (Chapter 2) (b); a large plot of 53 ha with canopy gaps (n=51) over a second high resolution IKONOS-2 image (2009) in the Tapajós National Forest (Chapter 2); a digital classification of blow-downs in an East-West mosaic of Landsat images from central Amazon (Chapter 3)(d); and the spatial distribution of blow-downs (size of the circles proportional to the disturbance area) detected in 129 images inside of the Brazilian Amazon.

## 5.2 Open Questions on Disturbance Area and Severity

The severity of natural disturbances defined as the change in aboveground biomass may be estimated using forest disturbance areas times a mean aboveground biomass stock [Espírito-Santo et al., 2010; Negrón-Juárez et al., 2010] from a nearby stand source [Phillips and Gentry, 1994; Phillips et al., 1998, 2004; Gloor et al., 2009] or a data-product of aboveground biomass [Saatchi et al., 2007, 2011]. However the contribution of mortality to carbon loss in each event normally is unknown [Nelson et al., 1994; Froking et al., 2009] and therefore there is a large source of uncertainty in severity data sets of natural disturbances. My analysis of mass loss used in Chapter 4 was based on the conservative assumption of a direct proportionality between carbon loss and mortality scaled to plot areas  $\{mean\ biomass\ of\ the\ plot\ (Mg\ ha^{-1})\} \div \{aboveground\ biomass\ loss\ of\ a\ event\ (Mg)\}$ . Based on this assumption, the relation between disturbance area (ha) and severity (Mg) is linear. However, direct measurements of the correlation between disturbance area and severity in the two large plots with a total area of 167 ha (Fig. 5-2, see Chapter 2) suggests that the relation between area and severity is subject to uncertainty ( $r=0.71$ ,  $p<0.001$ ).

Estimates of biomass loss assuming 100% mortality within the blow-downs fall within the 95% of confidence interval limits of this regression. However, I caution that this extrapolation is hazardous. First, the logarithmic equation is well outside of the data set for which it was fit and second because large blow-downs do not result in 100% mortality (M. Keller personal observation; [Nelson et al., 1994; Chambers et al., 2009b]). Defining the relation between disturbance area and mortality remains a research challenge.

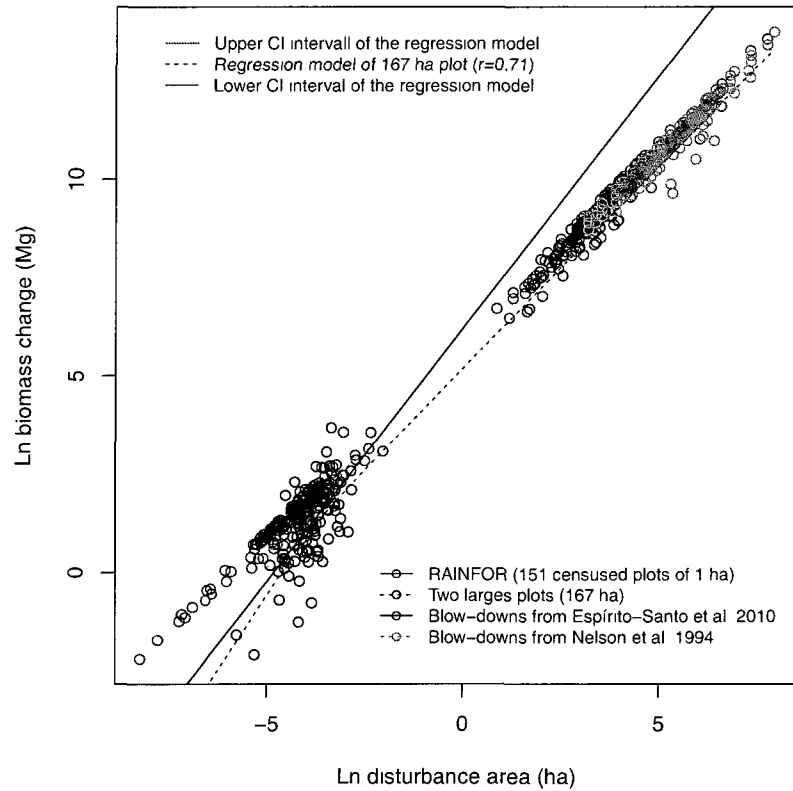


Figure 5-2: Logarithmic graph of empirical relation between disturbance area (ha) and aboveground biomass loss (Mg) for 96 tree-branch fall disturbances from 167 ha plot of forest disturbances in the Amazon. Data sets combined cover scales from branch falls to landscape blow-downs. A regression based on data from 96 tree-fall gaps (0.003 - 1.3 ha) where both area and aboveground biomass were measured at the same time was  $\text{Ln biomass} = 6.2102 + 1.29(\text{Ln area})$  ( $r^2 = 0.71$ ).

### **5.3 An Equation to Relate Disturbance Area and Biomass Loss**

Few studies of canopy dynamics have attempted to map the distribution of small, frequent gaps in tropical forest [Hubbell et al , 1999] and few, if any, have attempted to relate the occurrence of natural disturbances with production of CWD which generates a large pool of carbon [Denslow, 1987, Clark et al , 2002, Rice et al , 2004, Keller et al , 2004, Chambers et al , 2004, Palace et al , 2007] and nutrients [Clark et al , 2002] In Chapter 2, I discovered that no study in the tropical forest literature estimated the relation between the area of gaps (area, perimeter or any gap geometry) and the amount of CWD produced by natural tree or branch fall disturbances I developed the first equation to relate the severity of canopy disturbances to carbon loss by mortality However, considering the high diversity of forests in the Amazon, this equation may be valid for only a limited area of the central Amazon area More data of gap geometry and coarse woody debris for several regions are necessary

### **5.4 Limitations and Future Work on Natural Disturbances for Carbon Cycling**

Large natural disturbances in old-growth tropical forests (area  $\geq 1$  ha) are caused by a variety of mechanisms such as landslides [Walker et al , 1996], floods [Wittmann et al , 2002], fires [Cochrane, 2003], wind [Nelson et al , 1994], and cyclonic storms [Lugo, 1995] Chapter 4 points out that there is a lack of quantification for disturbances from 0.13 to 5 ha in the spectrum analysis of disturbances for the Amazon While our data looks at the extremes of the disturbance regimes, we cannot conclude that there is not a continuous regime of disturbance in tropical forests if we do not have a method to investigate the gap

in our data. Intermediate disturbance class sizes (0.1 to 5 ha) are difficult to detect with traditional forest inventory methods because of the large areas that would be required to be surveyed on the ground.

As a first guess, my spectrum analysis suggests that a 2 ha disturbance may have a return time on the order of  $10^3$  years. In order to observe a reasonable number of 1 ha events, we would probably need over  $10^5$  ha of survey. Recently Kellner and Asner [2009] examined the spectrum of gap frequency using airborne LiDAR remote sensing. Their analysis of 100 ha areas of 5 forests in Costa Rica and Hawaii. As a result, they had a cut-off in detected gap size of 0.01 to 0.1 ha, dependent upon their gap definition. Collection of larger airborne LiDAR data sets is feasible but currently costly. Such collections would be useful to quantify intermediate scale disturbances.

One of the main questions of this dissertation was: Can one analyze forest dynamics by observation of gap formation instead of a conventional analysis of individual tree mortality? From my results in Chapter 3, I learned that gap forming disturbances only account  $\sim 30\%$  of the total flux of CWD carbon. This result suggests that even a highly accurate system to monitor forest disturbances in the tropics (e.g. airborne LiDAR) there is a substantial amount of tree mortality that may not be observed. The monitoring of large forest areas in the tropics remains a challenge for tropical ecologists.

# APPENDICES

# APPENDIX A

## FREQUENTLY USED ABBREVIATIONS

CSR	Complete Spatial Randomness
CHM	Canopy Height Model
CO	Canopy Openness
CWD	Coarse Woody Debris
ETM+	The Enhanced Thematic Mapper Plus
GF	Gap Fraction
GV	Green Vegetation
INPE	Brazilian National Institute for Space Research
LAI	Leaf Area Index
LBA	Large Scale Biosphere-Atmosphere Experiment in the Amazon
MS	Multi-Spectral Image
NASA	US National Aeronautics and Space Administration
NESSF	NASA Earth System Science Fellowship
NDVI	Normalized Difference Vegetation Index
NPV	Nonphotosynthetic Vegetation
PAN	Panchromatic Image
PRODES	Brazilian Deforestation Project
RS	Remote Sensing
RTR	Real-Time Rainfall
SD	Shade
SMA	Spectral Mixture Analysis
SPA	Spatial Point Patterns Analysis



APPENDIX B  
SUPPLEMENTAL MATERIAL FOR  
CHAPTER 2

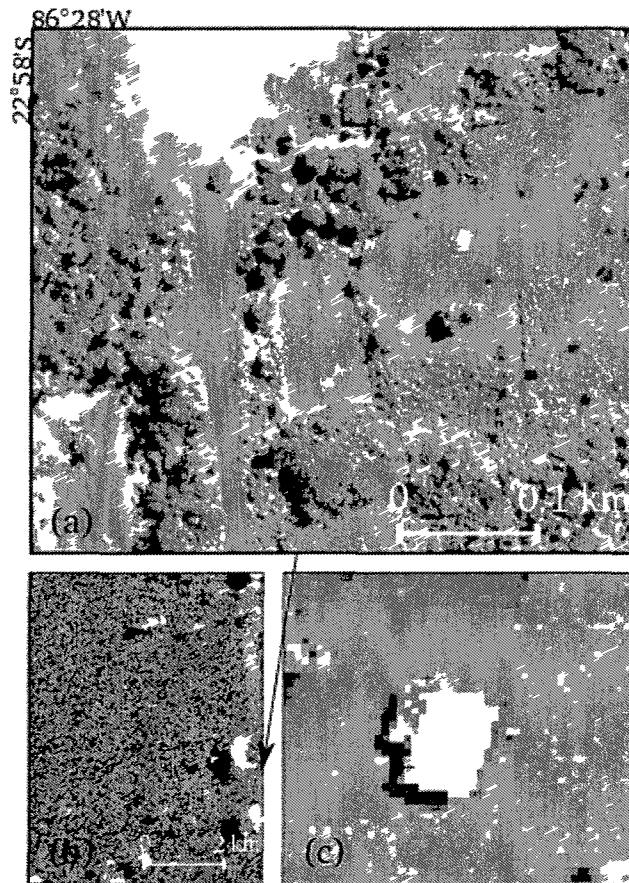


Figure B-1 GPS ground validation (red dots) of the ortorectification IKONOS image. Building construction objects (a) were used as target for GPS measurements (b). Roofs of houses (c) were used only for a general check of the ground validation.

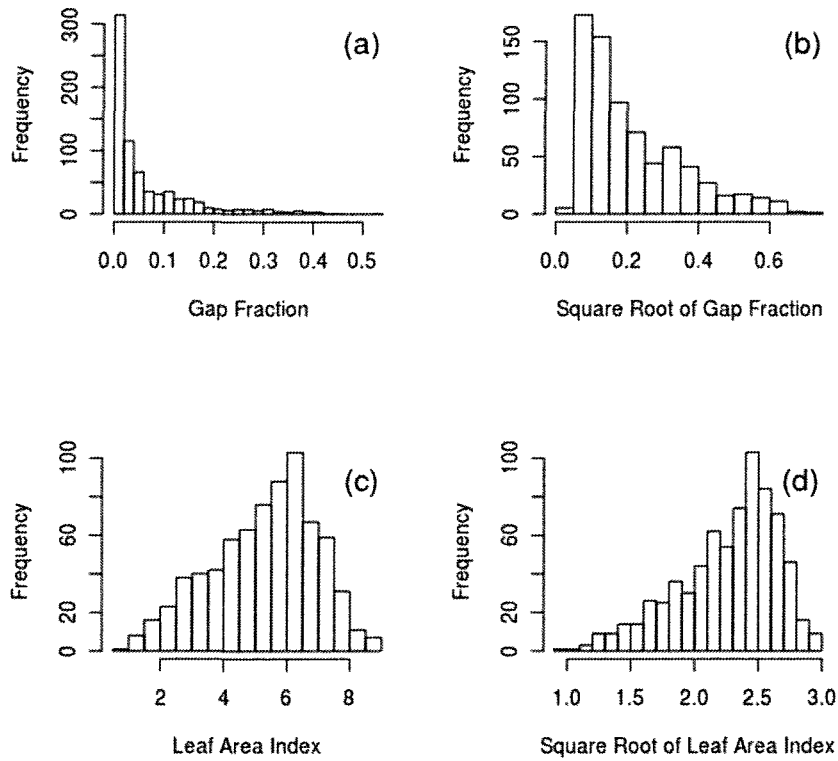


Figure B-2: Frequency distributions of ground collection of LAI-2000 PCA in the 114 ha plot (n=731). Positive skewed frequency distribution of diffuse non-interceptance (DIFN) light or canopy openness (CO) (a). Square root transformation of CO to reduce the skewed data distribution (b). Negative skewed data distribution of LAI (c) and its square root transformation (d).

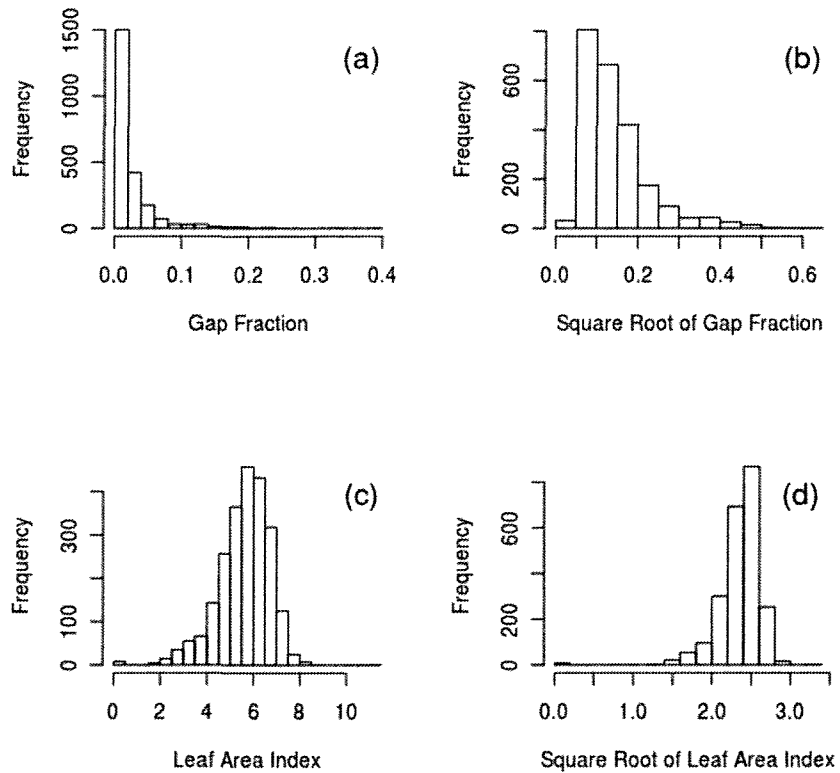


Figure B-3: Frequency distributions of ground collection of LAI-2000 PCA in the 53 ha plot (n=2315). Positive skewed frequency distribution of diffuse non-interceptance (DIFN) light or canopy openness (CO) (a). Square root transformation of CO to reduce the skewed data distribution (b). Negative skewed data distribution of LAI (c) and its square root transformation (d).

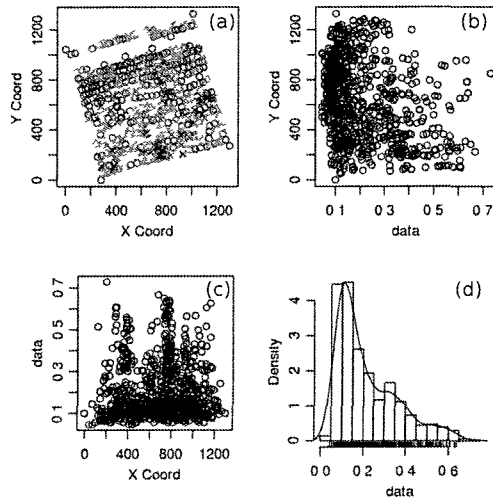


Figure B-4: Spatial distribution of gap fraction (n=731) in the 114 ha plot (a), scatter plot between data and spatial coordinates Y (b) and X (c) and frequency distribution of gap fraction data (d).

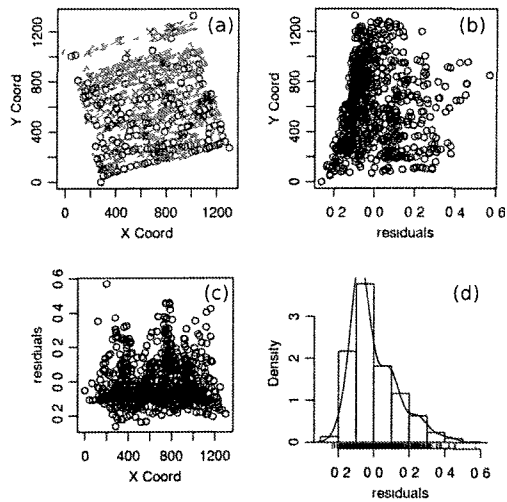


Figure B-5: Spatial distribution of gap fraction (n=731) in the 114 ha plot (a), scatter plot between data and removed spatial trends of the coordinates Y (b) and X (c) and frequency distribution of gap fraction residuals (d). The global spatial trend was removed from the original data (square root of gap fraction) by polynomial linear model (Spatial trend =  $X + Y + Y^2$ ) where the regression between the two variable revealed a trend of  $r^2 = 0.12$ .

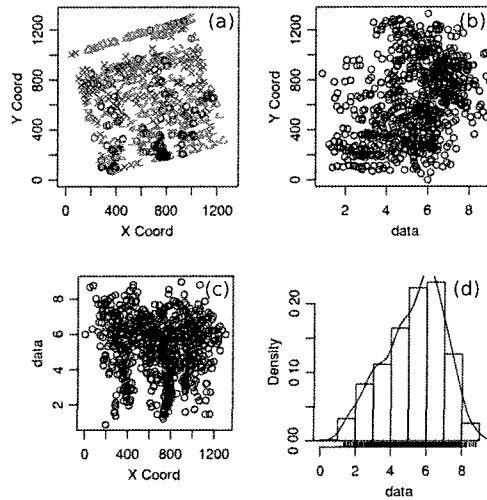


Figure B-6: Spatial distribution of leaf area index ( $n=731$ ) in the 114 ha plot (a), scatter plot between data and spatial coordinates Y (b) and X (c) and frequency distribution of leaf area index data (d).

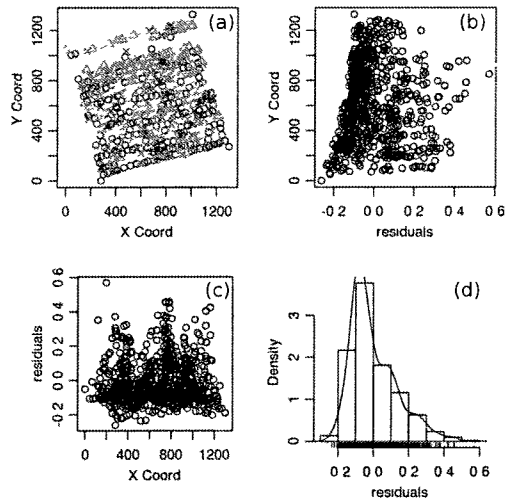


Figure B-7: Spatial distribution of leaf area index ( $n=731$ ) in the 114 ha plot (a), scatter plot between data and removed spatial trends of the coordinates Y (b) and X (c) and frequency distribution of leaf area index residuals (d). The global spatial trend was removed from the original data (leaf area index) by polynomial linear model (Spatial trend =  $X + Y + Y^2$ ) where the regression between the two variable revealed a trend of  $r^2 = 0.17$ .

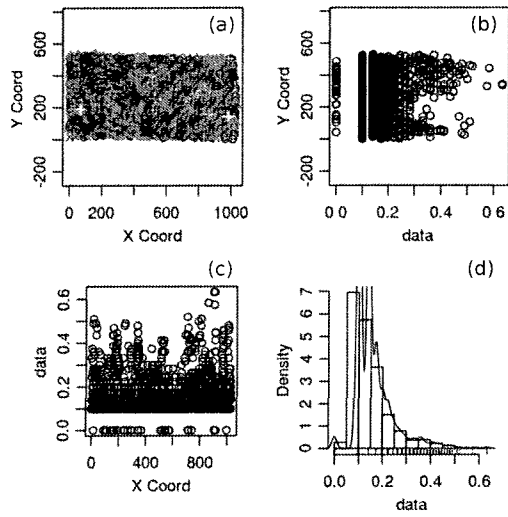


Figure B-8: Spatial distribution of gap fraction ( $n=2315$ ) in the 53 ha plot (a), scatter plot between data and spatial coordinates Y (b) and X (c) and frequency distribution of gap fraction data (d).

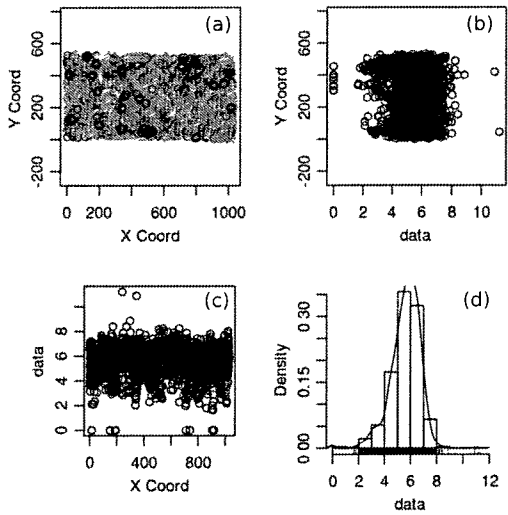


Figure B-9: Spatial distribution of leaf area index ( $n=2315$ ) in the 53 ha plot (a), scatter plot between data and spatial coordinates Y (b) and X (c) and frequency distribution of leaf area index data (d).

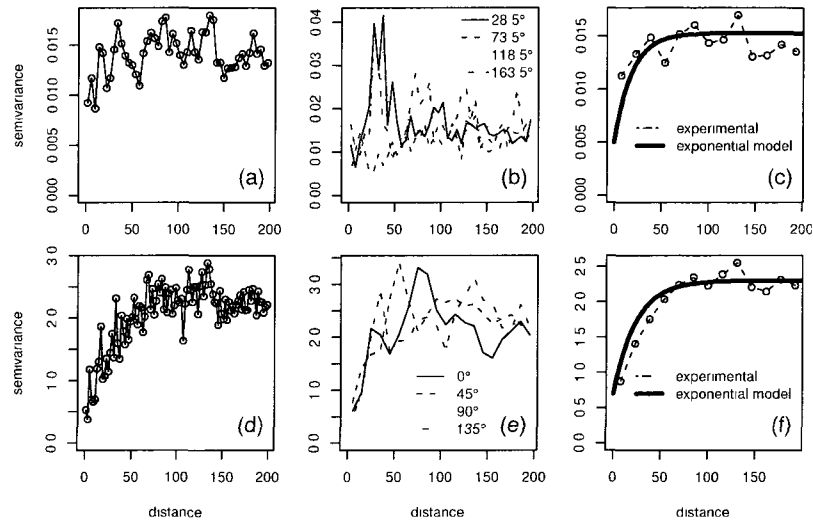


Figure B-10: Geostatistics analysis of ground remote sensing collections of 114 ha plot. Experimental semivariograms of canopy openness (square root of CO): unidirectional (a), multi-directional (b) and modeled exponential semivariogram (c). Experimental semivariograms for LAI: unidirectional (d), multi-directional (e) and modeled exponential semivariogram (f).

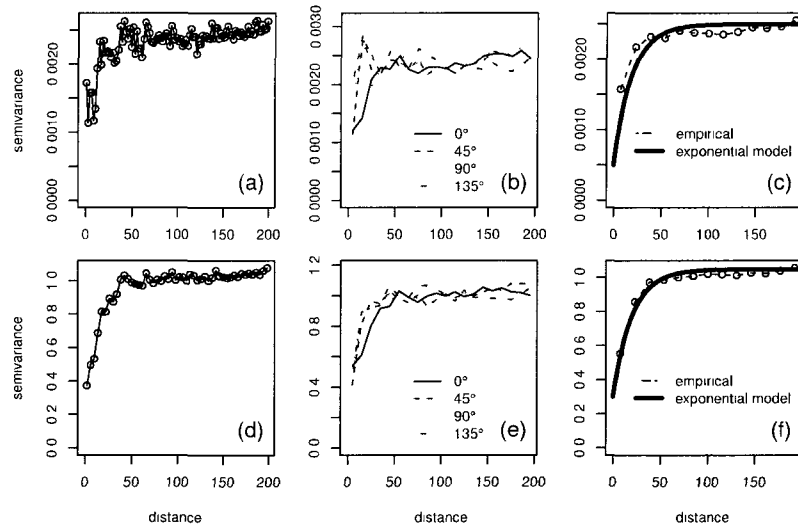


Figure B-11: Geostatistics analysis of ground remote sensing collections of 50 ha plot. Experimental semivariograms of canopy openness (square root of CO): unidirectional (a), multi-directional (b) and modeled exponential semivariogram (c). Experimental semivariograms for LAI: unidirectional (d), multi-directional (e) and modeled exponential semivariogram (f).

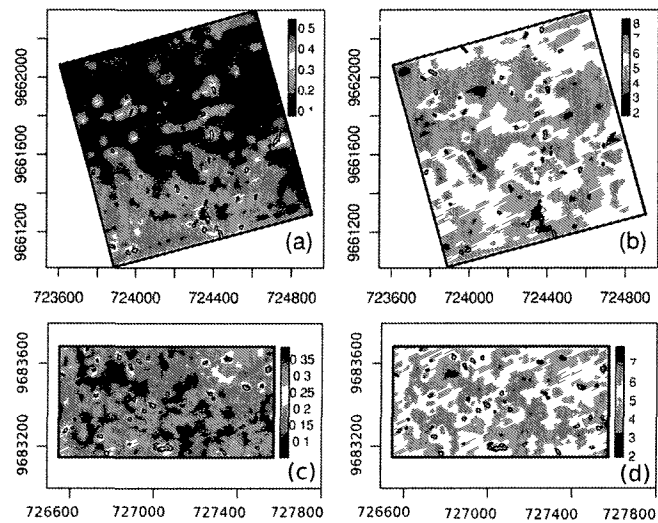


Figure B-12 Interpolated canopy openness (square root of CO) (a) and leaf area index (LAI) (b) in 100 ha plot ( $n=731$ ) using an exponential semivariogram model. The same maps of canopy openness (square root of CO) (c) and leaf area index (LAI) (d) in other large forest inventory plot of 53 ha ( $n=2315$ ). Gap areas (black polygons) are present in areas of high fraction of canopy openness for both plots (a and c). The leaf area index drop considerably (2 to 4) around of tree fall gaps (b and d).

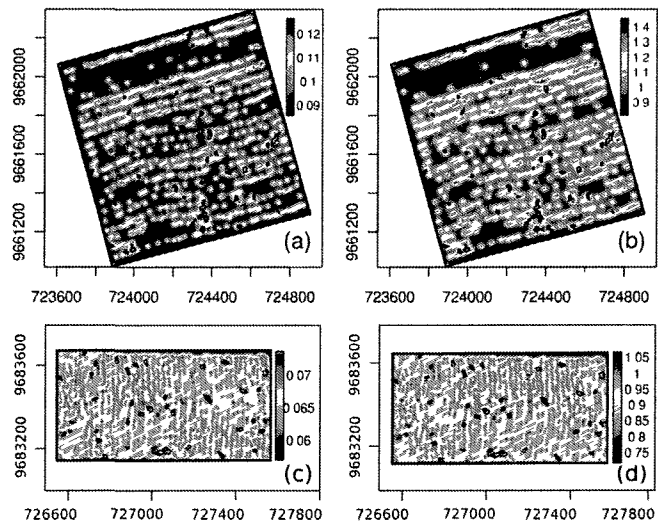


Figure B-13 Interpolation uncertainty (standard error) of canopy openness (a) and LAI (b) of the 114 ha plot ( $n=731$ ). The same maps of uncertainties of canopy openness (c) and LAI (d) but for 53 ha plot ( $n=2315$ ).



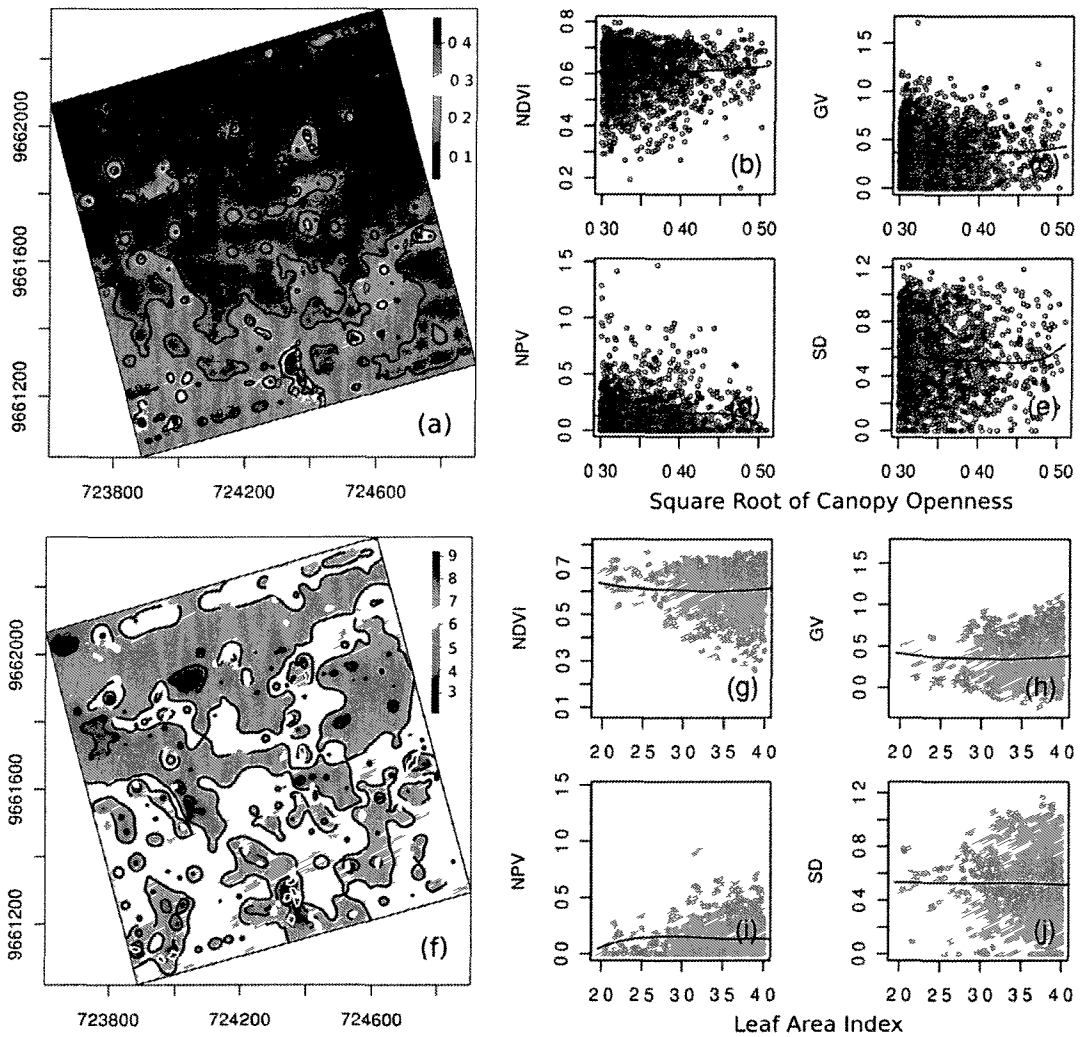


Figure B 14 Contour map of canopy openness (square root of CO) in 114 ha forest area (4 meter grid plot) showing increasing of  $CO \geq 0.3$  (yellow grid spots) in areas of tree fall gaps (red polygons) Regression analysis of the between grid areas with  $CO \geq 0.3$  (square root) or  $0.09 CO$  and remote sensing products ( $n=1817$  pixels of 4 m) NDVI (b), green vegetation (c), nonphotosynthetic vegetation (d) and shade (e) Contour map of geostatistics interpolation of LAI showing decreasing of leaf area index  $\leq 4$  (dark blue grid spots) in regions of tree-fall gaps (white polygons) Cross correlation analysis between areas with  $LAI \leq 4$  and remote sensing products ( $n=1869$  pixels of 4 m) and cross correlation with NDVI (g), green vegetation (h), nonphotosynthetic vegetation (i) and shade (j)

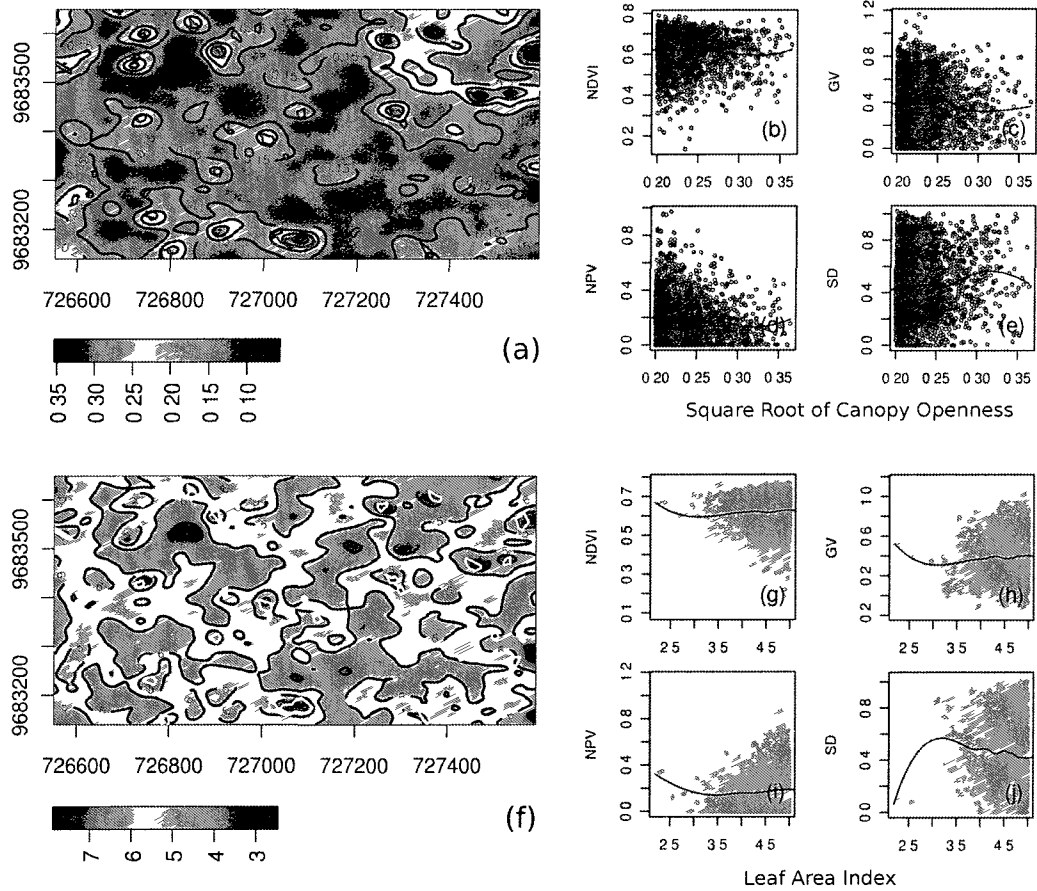


Figure B-15 Contour map of canopy openness (square root of CO) in 53 ha forest area (4 meter grid plot) showing increasing of  $CO \geq 0.23$  (yellow grid spots) in areas of tree fall gaps (red polygons) Regression analysis of the between grid areas with  $CO \geq 0.23$  (square root) and remote sensing products ( $n=1102$  pixels of 4 m) NDVI (b), green vegetation (c), nonphotosynthetic vegetation (d) and shade (e) Contour map of geostatistics interpolation of LAI showing decreasing of leaf area index  $\leq 4$  (light blue grid spots) in regions of tree-fall gaps (white polygons) Cross correlation analysis between areas with  $LAI \leq 5$  and remote sensing products ( $n=3764$  pixels of 4 m) and cross correlation with NDVI (g), green vegetation (h), nonphotosynthetic vegetation (i) and shade (j)

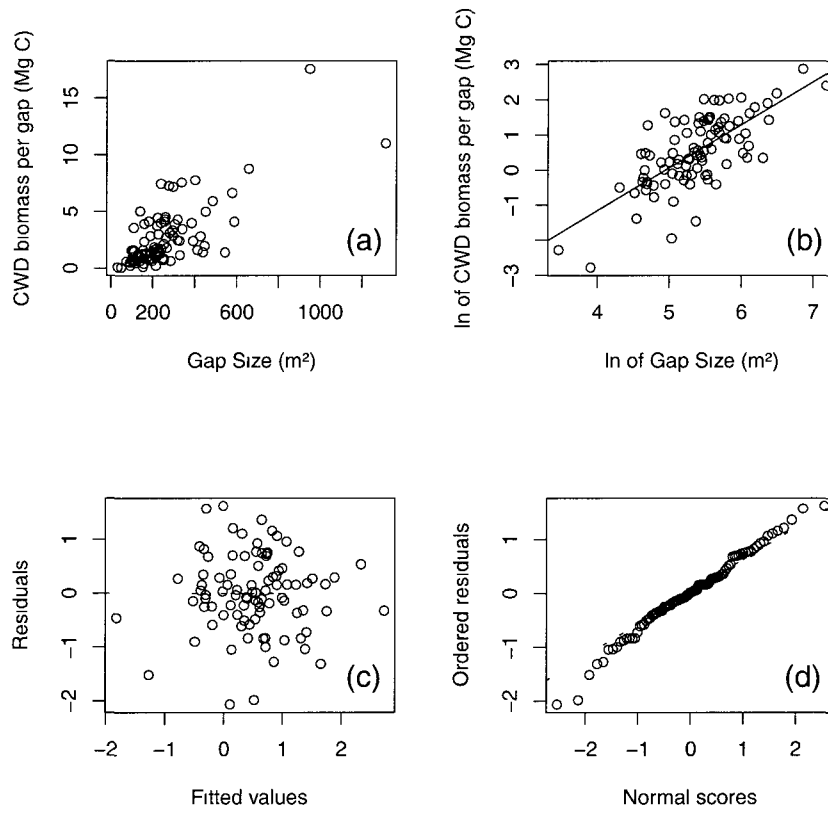


Figure B-16 Linear regression analysis between gap size area ( $m^2$ ) and coarse woody debris CWD (Mg C) of two large plots (167 ha and  $n=92$ ) (a) Log log graph of gap area and CWD (b) Diagnostic regression analysis tests of residuals (c) and its theoretical normalized quantiles (d) Pearson correlation  $r=0.72$ , fitted adjusted regression model  $R^2=0.53$  and  $p\text{-value}<0.01$  Intercept and slope are respectively, 0.1551 and 0.0108

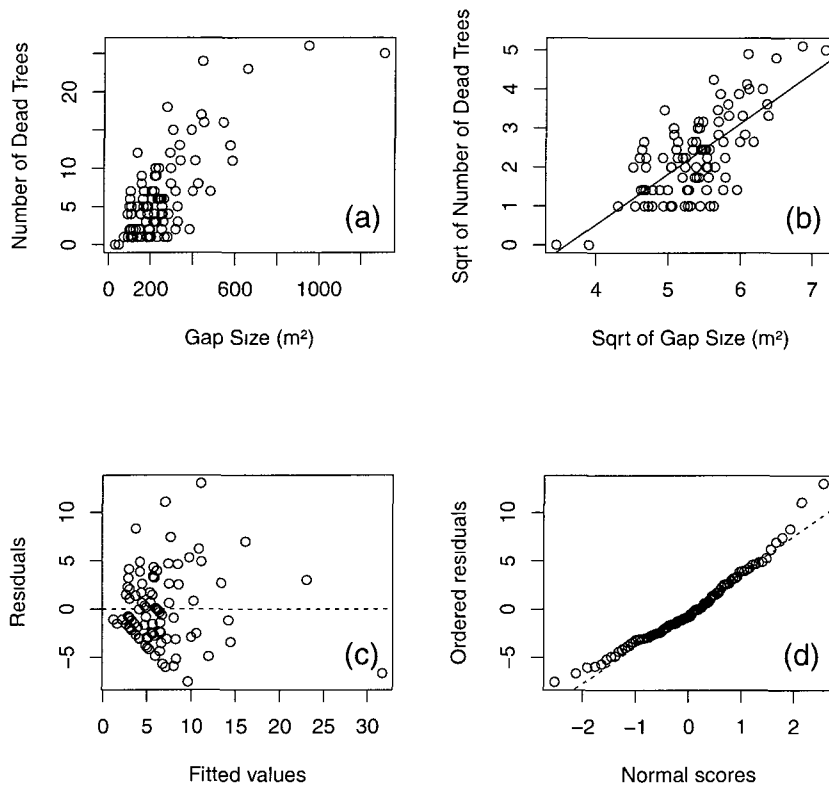


Figure B-17: Linear regression analysis between gap size area (m<sup>2</sup>) and number of dead trees of two large plots (167 ha and n=92) (a). Square root transformation graph of gap area and number of dead trees (b). Diagnostic regression analysis tests of residuals (c) and its theoretical normalized quantiles (d). Pearson correlation  $r=0.74$ , fitted adjusted regression model  $R^2=0.56$  and  $p\text{-value}<0.01$ . Intercept and slope are respectively, 0.3485 and 0.0238.

# APPENDIX C

## SUPPLEMENTAL MATERIAL FOR CHAPTER 4

### C.1 Data Integration

We used the extensive historical data set of the RAINFOR plots [Phillips et al., 2004] based on net changes in biomass ( $\text{t ha}^{-1} \text{ yr}^{-1}$ ) which account two above-ground biomass terms: biomass gain (from tree growth and recruitment) and biomass losses (from tree mortality). The biomass losses from these plots were assessed to provide information of tree mortality across the Amazon basin. Those plots are typically 1 ha in size and measurements details have been described elsewhere [Phillips et al., 2004; Baker et al., 2004; Lewis et al., 2004]. All plots ( $n=151$ ) cover a total area of 226.2 ha with a mean census interval of 3.2 years. We used 151 plots with census interval between 0.5 and 1.5 years to estimate tree mortality over the Amazon (Fig. 4-1). All trees with diameter larger than 10 cm have been monitored over a mean period of 11.3 years. Above-ground biomass was estimated by allometric equations [Chambers et al., 2001]. Mortality rate have been corrected for census-interval effects [Malhi and Wright, 2004]

RAINFOR data do not account for biomass losses (disturbances) that do not result in complete tree mortality (e.g. CWD produced by partial crown-falls). To evaluate carbon losses, we installed and surveyed two large forest inventory plots of 114 and 53 ha, in unmanaged forest area in the eastern central Amazon (Tapajós National Forest) (Supplementary C-1). The first plot was installed in 2008 and the second in 2009. We adopted an intense protocol of ground measurements of gap-formation and related those areas with the amount of CWD measured in each gap. We mapped all gaps in both large plots using the gap definition of Runkle (1981) that includes areas directly and indirectly affected by the canopy opening. We defined the modes of gap-formation based on the type of disturbance: (a) partial or complete crown-fall (from either live or dead standing trees), (b) snapped bole-fall, and (c) uprooted tree-fall. We classified all gaps within two age classes: (a)  $< 1$  year, for gaps caused by recent disturbances, and (b)  $\geq 1$  year. For each gap identified in the field we measured the volume of all CWD in each ground gap. CWD were separated into categories of complete dead trees or wood pieces. For snapped bole-falls and uprooted tree-falls, dead trees with diameter  $> 10$  cm were recorded for diameter. For complete crown-falls only crown-fall trunks were recorded. The majority of CWD production in this area was caused by single or multiple tree-falls. We used the allometric equation [Brown, 1997] as approximation of woody biomass losses by fresh treefalls and snapped bole falls. For gaps with partial crown-fall we recorded the diameters of all wood pieces greater than 10 cm (the end diameters of the logs) and length of the woody material. CWD in the gaps was classified according to its decomposition status [Harmon et al., 1995] into five classes from freshest (class 1) to most rotten (class 5) [Keller et al., 2004; Palace et al., 2007, 2008]. We used an average of wood density measured for each decay class specifically developed for

this site [Keller et al , 2004] We calculated the sectional volume of each segment of CWD and the mass of section of CWD was determined from the product of the volume of material and the respective density for the material class [Keller et al , 2004, Palace et al , 2007, 2008]

We developed a spatially explicit analysis of large disturbances (blow-downs) in the Brazilian Amazon tropical forest biome based on extensive samples of Landsat satellite images (30 m) We assessed the occurrence of 330 events of large disturbances or blow-downs ( $\geq 30$  ha) during the period from 1986 to 1989 of the 135 Landsat images (Supplementary C-3) using the original raw data from the first study that described the occurrence of blow-downs in the Amazon [Nelson et al , 1994] We also analyzed the pattern of 278 large forest disturbances ( $\geq 5$  ha) from 1999 to 2001 apparently caused by severe storms in a mostly unmanaged portion of the Brazilian Amazon using 27 Landsat images and modern techniques of digital image processing (Espírito-Santo et al [2010] Chapter 2) For each blow-down event, we estimated the biomass loss using the area of each disturbances and its respective mean above-ground biomass extracted from the regional map of biomass stock of the Amazon region (Fig 4-1) (n=578, sum of blow-down records from Nelson et al [1994] and Espírito-Santo et al [2010]) From tree-fall gaps to landscape blow-downs we characterized the size-area distribution (Supplementary C-6), biomass losses (Supplementary C-7) and relation between disturbance area and severity (Supplementary C-8)

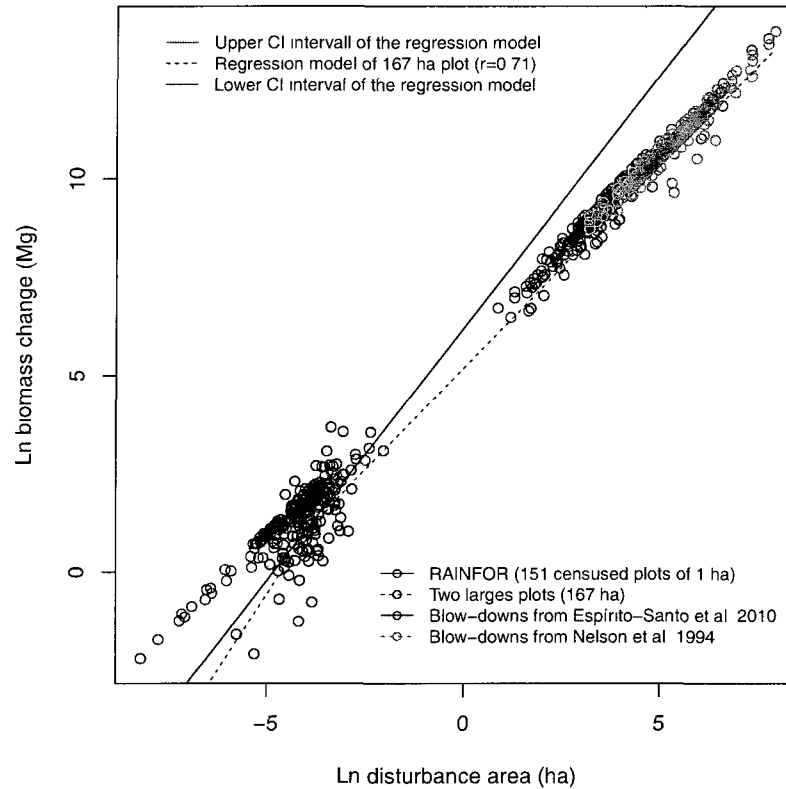


Figure C-1: Relation between disturbance area and severity (change in aboveground biomass) of forest disturbances in the Amazon. Data sets combined from several studies of disturbances across the Amazon, from branch and tree falls to landscape scale blow-downs. Small disturbances: (1) in red, forest plot inventories ( $n=151$  1ha plot, Gloor et al. 1999) distributed over the Amazon and (2) in black, 96 tree-fall gaps (Chapter 2) from two large forest inventory plots (total area 167 ha) in the Tapaj's National Forest. Large disturbances: (3) in blue, 279 blow-downs bigger than 5 ha from a East-West mosaic of 27 Landsat scenes of the Amazon; and (4) in green, 330 blow-downs greater than 30 ha from 136 Landsat scenes in the Brazilian Amazon. A relation between area and severity of disturbances (Mg aboveground biomass loss) was tested from 96 tree-fall gaps (0.003 - 0.13 ha) where both area and aboveground biomass were measured. A regression fit is  $\text{Ln biomass} = 6.2102 + 1.29(\text{Ln area})$ , for biomass change in Mg and disturbance area in ha).

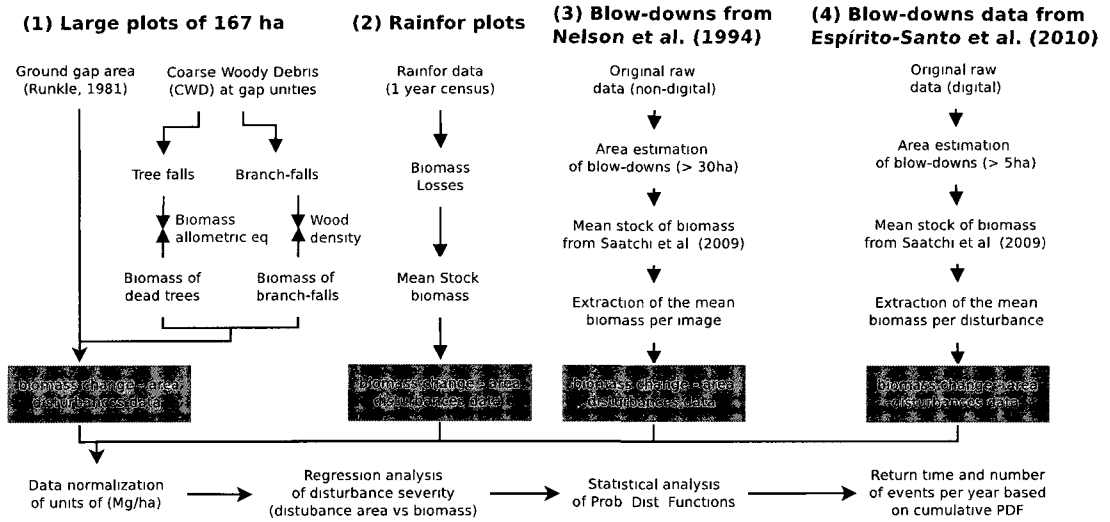


Figure C-2: Schematic outline of the main processing steps carried out to integrate several sources of disturbance data over the Amazon basin.

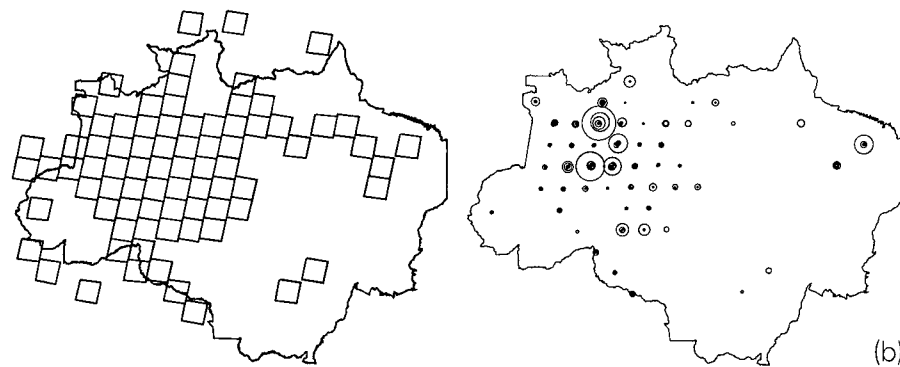


Figure C-3: Spatial distribution of 72 Landsat scenes with the occurrence of blow-down from the total 136 scenes inspected by Nelson et al. (1994) for the Brazilian Amazon (a). The area of blow-downs disturbance is proportional to the size of the circles (b). Landsat images with blow-downs outside of the Brazilian Amazon border were omitted from the spatial point analysis.



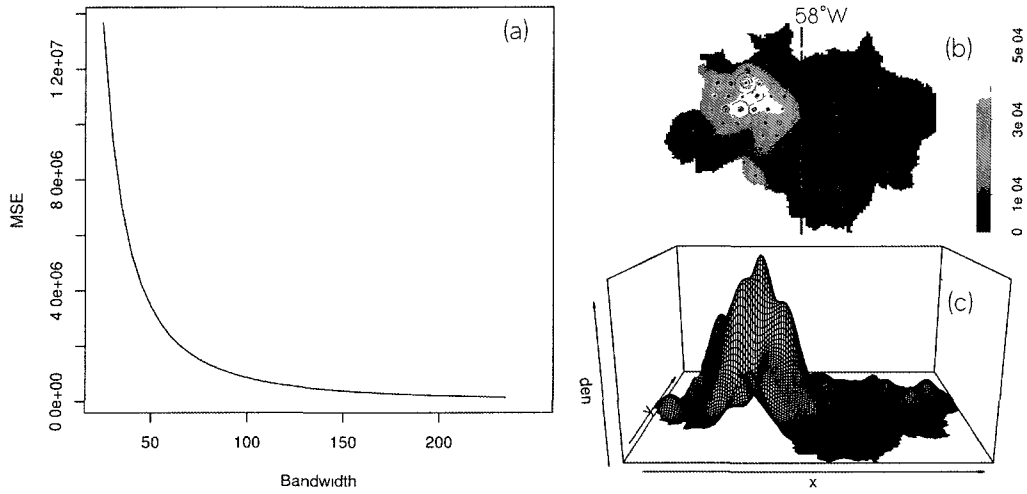


Figure C-4: Mean square error (MSE) of the Gaussian kernel smoothing algorithm (a) from the spatial distribution of 330 blow-downs from Nelson et al. (1994). The bandwidth with smaller MSE around 150 km (b) is the less biased bandwidth for this spatial data. East-West perspective graph of the intensity of blow-downs in the Amazon (c) produced by a smoothing kernel interpolation.

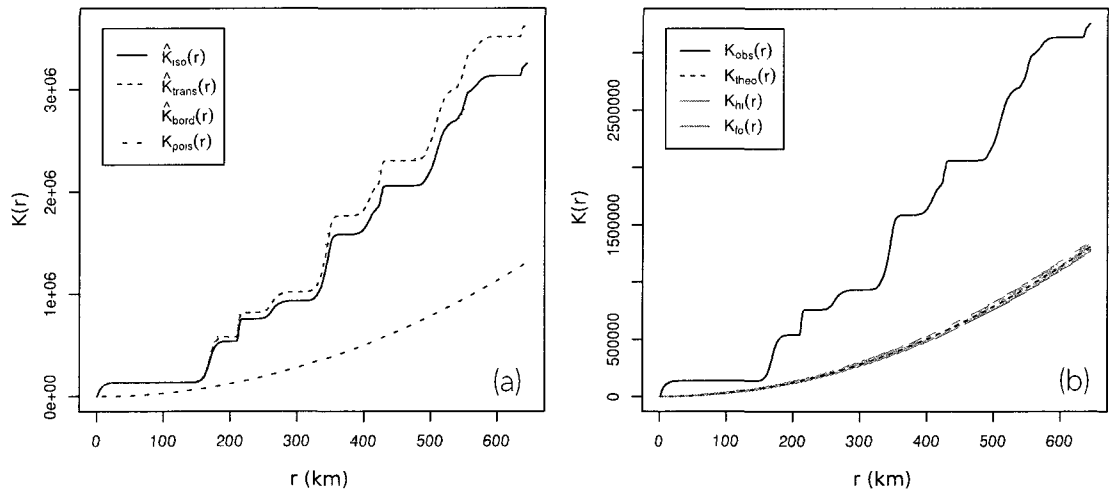


Figure C-5: K-function (a) and simulated envelopes of the spatial distribution of 330 blow-downs from Nelson et al. (1994) (a). Monte Carlo simulation ( $T=1000$ ) of the K-function (b). Black line is the original K-function and the colored lines are the upper and lower envelopes. Graphic shows that for all situations the occurrences of blow-downs are clustered.

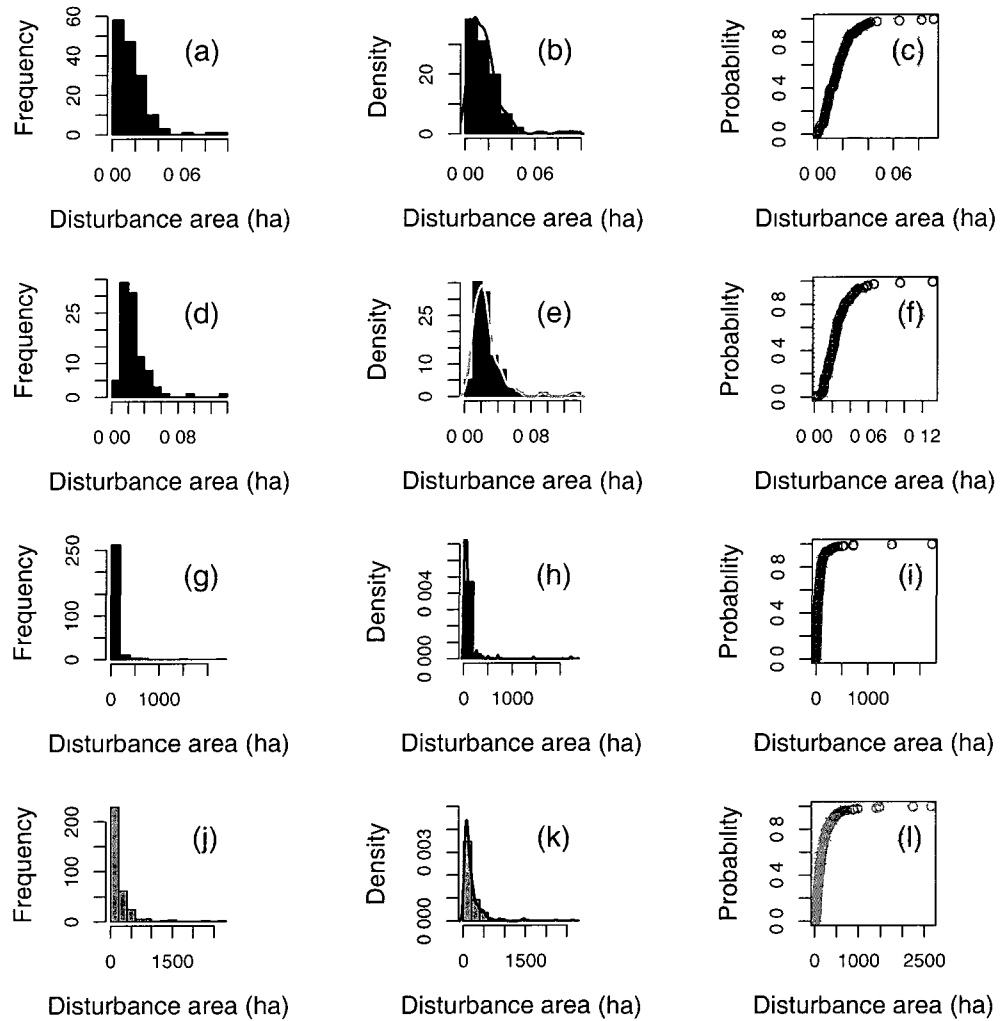


Figure C-6: Frequency, probability density function (PDF) and cumulative PDF of area from four sources of natural disturbances data sets. Small disturbances: (1) in red, RAINFOR 151 1ha plots (a-c); and (2) in black, 96 tree-branch fall disturbances from 167 ha plot (d-f). Large disturbances: (3) in blue, 279 blow-downs bigger than 5 ha from Esprito-Santo et al. (2010) (g-i); and (4) in green, 330 blow-downs greater than 30 ha from Nelson et al. (1994) (j-l).

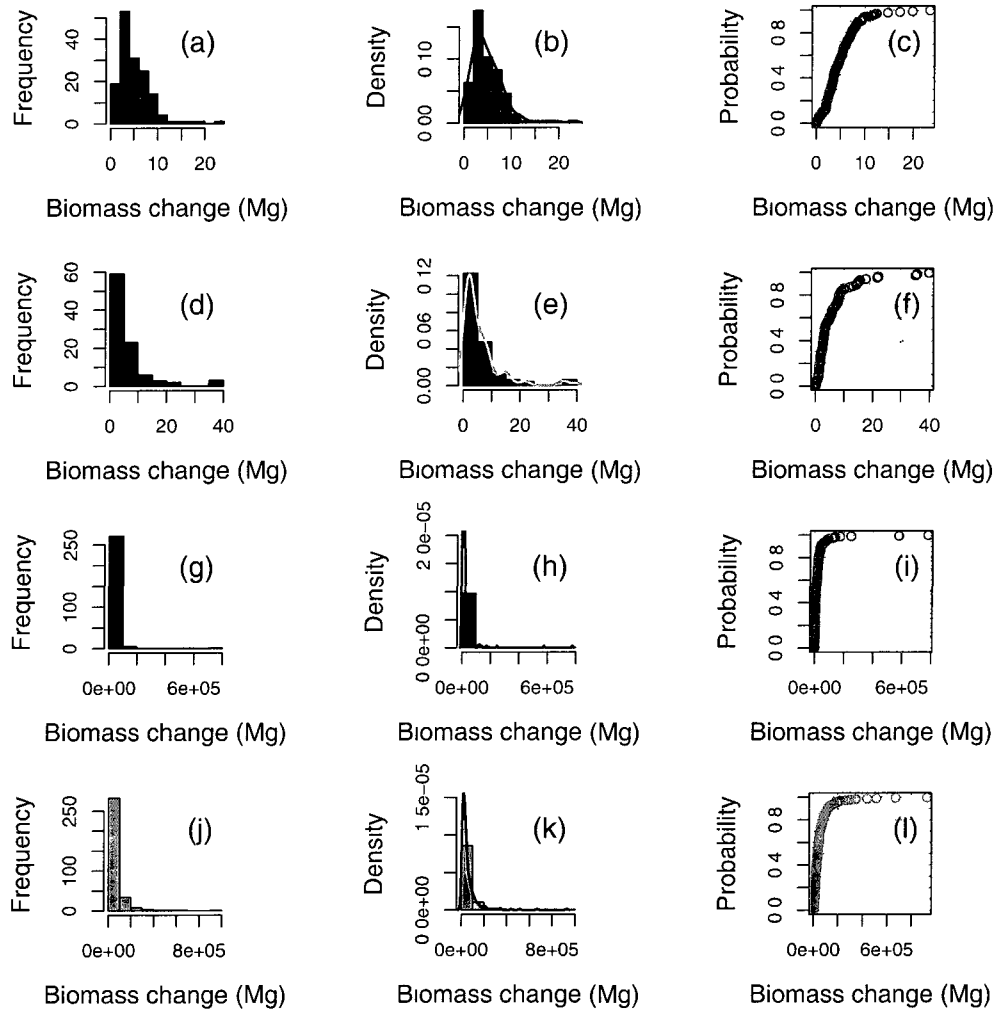


Figure C-7: Frequency, probability density function (PDF) and cumulative PDF of severity (change in aboveground biomass) from four sources of natural disturbances data sets. Small disturbances: (1) in red, RAINFOR 151 1ha plots (a-c); and (2) in black, 96 tree-branch fall disturbances from 167 ha plot (d-f). Large disturbances: (3) in blue, 279 blow-downs bigger than 5 ha from Esprito-Santo et al. (2010) (g-i); and (4) in green, 330 blow-downs greater than 30 ha from Nelson et al. (1994) (j-l).

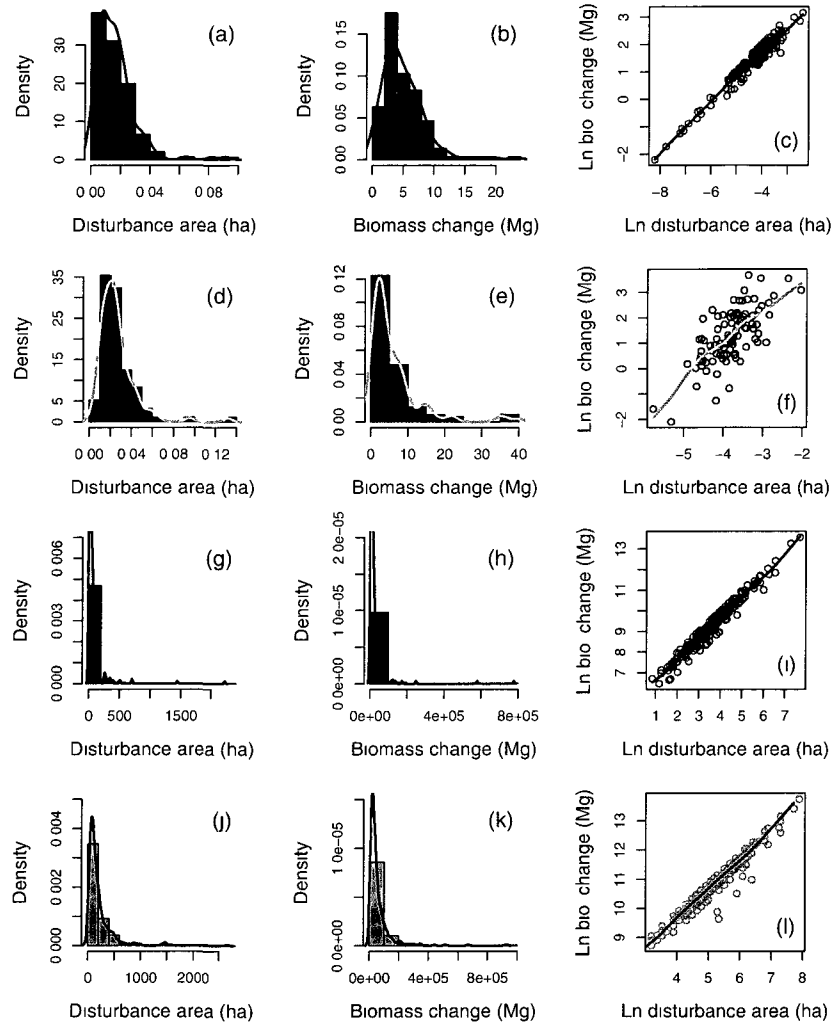


Figure C-8: Probability density function (PDF) for area and severity from four sources of natural disturbances data sets. Small disturbances: (1) in red, RAINFOR 151 1ha plots (a-c); and (2) in black, 96 tree-branch fall disturbances from 167 ha plot (d-f). Large disturbances: (3) in blue, 279 blow-downs bigger than 5 ha from Esprito-Santo et al. (2010) (g-i); and (4) in green, 330 blow-downs greater than 30 ha from Nelson et al. (1994) (j-l).

# APPENDIX D

## DOCTOR PUBLICATIONS (2005 - 2011)

### D.1 Articles in Preparation

Espírito-Santo, F.D.B, Keller, M., Linder, E., Oliveira Júnior, R.C., Pereira, C., Oliveira, G.C., Yuan, C. (2011) Gap formation in large forest plots of Brazilian Amazon: Effects on carbon cycling and measurement using high resolution optical remote sensing. *Journal of Geophysical Research - Biosciences*.

Espírito-Santo, F.D.B, Gloor, M., Keller, M., Phillips, O. and RAINFOR Group. (2011) First Pan Amazon forest disturbance spectrum and implications on the tropical old-growth carbon sink. *Nature Geoscience*.

### D.2 Articles Submitted Recently

Adami M., Bernardes, S., Arai E., Miura A.K., Freitas R.M., Shimabukuro Y., Espírito-Santo F.D.B., Moreira M.A., & Rudorff B.F. (2010) Vegetation seasonality over several terrestrial regions of South America. *Journal of Environmental Management*.

Espírito-Santo F.D.B., Shimabukuro Y.E., Santos J.R., Kuplich T.M. & Aragão, L.E.O.C. (2010) Age and aboveground biomass accumulation of secondary forest in Amazon: an explicit semi-automatic classification of multitemporal satellite images. *Remote Sensing of Environment*.

### D.3 Peer-Reviewed Journal Articles

Espírito-Santo F.D.B, Keller M., Braswell B., Nelson B.W., Frohling S., & Vicente G. (2010) Storm intensity and old-growth forest disturbances in the Amazon region. *Geophysical Research Letters* 37: L11403 [doi:10.1029/2010GL043146].

Chambers J.Q., Asner G.P., Morton D.C., Anderson L.O., Saatchi S.S., Espírito-Santo F.D.B., Palace M., & Souza C. (2006) Regional ecosystem structure and function: ecological insights from remote sensing of tropical forests. *Trends in Ecology and Evolution* 22: 414-423.

Morton C.D., DeFries R.S., Shimabukuro Y.E., Anderson L.O., Arai E., Espírito-Santo F.D.B., Freitas R., & Morisette J. (2006) Cropland expansion changes deforestation dynamics in the southern Brazilian Amazon. *The Proceedings of the National Academy of Sciences* 103: 1463714641.

Morton D.C., Defries R.S., Shimabukuro Y.E., Anderson L.O., Espírito-Santo F.D.B., Hansen M., & Carroll M. (2005) Rapid Assessment of Annual Deforestation in the Brazilian Amazon Using MODIS Data. *Earth Interactions* 9: 1-22.

Espírito-Santo F.D.B., Shimabukuro Y.E., & Kuplich T.M. (2005) Mapping forest successional stages following deforestation in Brazilian Amazonia using multi-temporal Landsat images. *International Journal of Remote Sensing* 26: 635-642.

Espírito-Santo F.D.B., Shimabukuro Y.E., Aragão L.E.O.C., & Machado E.L.M. (2005) Analysis of the floristic and phytosociologic composition of Tapajós National Forest with geographic support of satellite images. *Acta Amazonica* 35: 167-185.

Espírito-Santo F.D.B. & Shimabukuro Y.E. (2005) Validation of tropical forest area mapping using aerial videography images and data from field work survey. *Revista Árvore* 29: 227-239.

Aragão L.E.O.C., Shimabukuro Y.E., Espírito-Santo F.D.B., & Williams M. (2005) Landscape pattern and spatial variability of leaf arean index in Eastern Amazonia. *Forest Ecology and Management* 211: 240-256.

Aragão L.E.O.C., Shimabukuro Y.E., Espírito-Santo F.D.B., & Williams M. (2005) Spatial Validation of the Collection 4 MODIS LAI Product in Eastern Amazonia. *IEEE Transactions on Geosciences and Remote Sensing* 43: 2526-2973.

Lefsky M.A., Harding D.J., Keller M., Cohen W.B., Carabajal C.C., Espírito-Santo F.D.B., Hunter M.O., Oliveira R., & Camargo P.B. (2005) Estimates of forest canopy height and aboveground biomass using ICESat. *Geophysical Research Letters* 32: L22S02.

# BIBLIOGRAPHY

- Aragão, L. E. O. C., Shimabukuro, Y. E., Espírito-Santo, F. D. B., and Williams, M. (2005). Spatial validation of the collection 4 modis lai product in eastern amazonia. *IEEE Transactions on Geoscience and Remote Sensing*, 43(11), 2526–534.
- Ashton, P. (1995). What can be learned from a 50 ha plot which cannot be learned any other way? In Lee, H., Ashton, P., and Ogino, K., editors, *Long Term Ecological Research of Tropical Rain Forest in Sarawak. Proceedings of the Workshop on "Long Term Ecological Research in relation to Forest Ecosystem Management" Kuching Sarawak Malaysia*, vol. Vol. II-3, pp 207–220. Ehime University, Japan, Studies of Global Environmental Change with Special Reference to Asia and Pacific Regions
- Asner, G. P., Knapp, D. E., Broadbent, E. N., Oliveira, P. J. C., Keller, M., and Silva, J. N. (2005). Selective logging in the brazilian amazon. *Science*, 310, 480–482.
- Asner, G. P., Palace, M., Keller, M., Pereira Jr., R., Silva, J. N. M., and Zweede, J. C. (2002). Estimation canopy structure in an amazon forest from laser range finder and ikonos satellite observations. *Biotropica*, 34(4), 483–492.
- Asner, G. P. and Warner, A. S. (2003) Canopy shadow in ikonos satellite observations of tropical forests and savannas. *Remote Sensing of Environment*, 83(1), 521–533.
- Asner, G. P., Wessman, C. A., and Schimel, D. S. (1998). Heterogeneity of savanna canopy structure and function from imaging spectrometry and inverse modeling. *Ecological Applications*, 8(4), 1022–1036.
- Baddeley, A. and Turner, R. (2005). spatstat: An r package for analyzing spatial point patterns. *Journal of Statistical Software*, 6(12), 1–42
- Baddeley, A. and Turner, R. (2006). *Case Studies in Spatial Point Process Modeling*, chap. Modelling spatial point patterns in R, pp. 23–74. Springer, New York, NY.
- Bailey, T. C. and Gatrell, A. C. (1995). *Interactive spatial data analysis*. Longman Scientific & Technical, Harlow.
- Baker, T. R., Phillips, O. L., Malhi, Y., Almeida, S., Arroyo, L., Di Fiore, A., Erwin, T., Killeen, T. J., Laurance, S. G., Laurance, W. F., Lewis, S. L., Lloyd, J., Monteagudo, A., Neill, D. A., Patino, S., Pitman, N. C. A., Silva, N. M., and Martinez, R. V. (2004). Variation in wood density determines spatial patterns in amazonian forest biomass. *Global Change Biology*, 10, 545–562.
- Baltzer, J. L., Davies, S. J., Noor, N. S. M., Kassim, A. R., and LaFrankie, J. V. (2007). Geographical distributions in tropical trees: can geographical range predict performance and habitat association in co-occurring tree species? *Journal of Biogeography*, 34, 1916–1926.
- Baxter, P. W. J. and Getz, W. M. (2005). A model-framed evaluation of elephant effects on tree and fire dynamics in african savannas. *Ecological Applications*, 15(4), 1331–1341.

- Boardman, J. W. (1993). Automating spectral unmixing of aviris data using convex geometry concepts. In *Summaries of the Fourth Annual JPL Airborne Geoscience Workshop*, pp. 11–14. JPL, Pasadena, CA.
- Boardman, J. W., Kruse, F. A., and Green, R. O. (1995). Mapping target signatures via partial unmixing of aviris data. In *Summaries of the Fifth Annual JPL Airborne Geoscience Workshop*, pp. 23–26. JPL, Pasadena, CA.
- Bolzan, M. J. A., Ramos, F. M., Sa, L. D. A., Neto, C. R., and Rosa, R. R. (2002). Analysis of fine-scale canopy turbulence within and above an amazon forest using tsallis' generalized thermostatics rid c-9126-2011. *Journal of Geophysical Research-atmospheres*, *107*(D20), 8063.
- Bormann, F. and Likens, G. E. (1994). *Pattern and Process in a Forested Ecosystem: Disturbance, Development and the Steady State Based on the Hubbard Brook Ecosystem Study*. Springer, 1st ed. 1979. corr. 2nd printing ed.
- Brokaw, N. V. L. (1982). The definition of treefall gap and its effect on measures of forest dynamics. *Biotropica*, *14*, 158–160.
- Brokaw, N. V. L. and Scheiner, S. M. (1989). Species composition in gaps and structure of a tropical forest. *Ecology*, *70*(3), 538–541.
- Brown, S. (1997). Estimating biomass and biomass change of tropical forests: a primer. Tech. Rep. FAO Forest Paper 134, Food and Agriculture Organization of the United Nations (FAO), Rome, Italy.
- Canham, C. D., Denslow, J. S., Platt, W. J., Runkle, J. R., Spies, T. A., and White, P. S. (1990). Light regimes beneath closed canopies and tree-fall gaps in temperate and tropical forests. *Canadian Journal of Forest Research-revue Canadienne De Recherche Forestiere*, *20*(5), 620–631.
- Chambers, J., Negrn-Jurez, R., , Hurtt, G., Marra, D., and Higuchi, N. (2009a). Lack of intermediate-scale disturbance data prevents robust extrapolation of plot-level tree mortality rates for old-growth tropical forests. *Ecology Letters*, *12*(12), E22–E25.
- Chambers, J. Q., Asner, G. P., Morton, D. C., Anderson, L. O., Saatchi, S. S., Esprito-Santo, F. D. B., Palace, M., and Souza, C. (2007a). Regional ecosystem structure and function: ecological insights from remote sensing of tropical forests. *Trends in Ecology & Evolution*, *22*(8), 414–423.
- Chambers, J. Q., Fisher, J. I., Zeng, H., Chapman, E. L., Baker, D. B., and Hurtt, G. C. (2007b). Hurricane katrinas carbon footprint on u.s. gulf coast forests. *Science*, *318*, 1107–1108.
- Chambers, J. Q., Higuchi, N., Teixeira, L. M., Santos, J., Laurance, S. G., and Trumbore, S. E. (2004). Response of tree biomass and wood litter to disturbance in a central amazon forest. *Oecologia*, *141*(4), 596–611.
- Chambers, J. Q., Higuchi, N., Tribuzy, E. S., and Trumbore, S. E. (2001). Carbon sink for a century: Intact rainforests have a long-term storage capacity. *Nature*, *410*, 429.



- Chambers, J. Q., Robertson, A., Carneiro, V., Lima, A., Smith, M.-L., Plourde, L., and Higuchi, N. (2009b). Hyperspectral remote detection of niche partitioning among canopy trees driven by blowdown gap disturbances in the central amazon. *Oecologia*, *160*(1), 107–117.
- Clark, D. (1990). *The reproductive biology of tropical plants*, vol. 20, chap. The role of disturbance in the regeneration of neotropical moist forests, pp. 291–315. Man and the Biosphere Series. The Pathenon, London.
- Clark, D. A. (2002). Are tropical forests an important carbon sink? reanalysis of the long-term plot data. *Ecological Applications*, *12*(1), 3–7.
- Clark, D. B., Castro, C. S., Alvarado, L. D. A., and Read, J. M. (2004a). Quantifying mortality of tropical rain forest trees using high-spatial-resolution satellite data. *Ecology Letters*, *7*, 52–59.
- Clark, D. B. and Clark, D. A. (1996). Abundance, growth and mortality of very large trees in neotropical lowland rain forest. *Forest Ecology and Management*, *80*(1-3), 235–244.
- Clark, D. B. and Clark, D. A. (2000). Landscape-scale variation in forest structure and biomass in a tropical rain forest. *Forest Ecology and Management*, *137*, 185–198.
- Clark, D. B., Clark, D. A., Brown, S., Oberbauer, S. F., and Veldkamp, E. (2002). Stocks and flows of coarse woody debris across a tropical rain forest nutrient and topography gradient. *Forest Ecology and Management*, *164*(1-3), 237–248.
- Clark, D. B., Read, J. M., Clark, M. L., Cruz, A. M., Dotti, M. F., and Clark, D. A. (2004b). Application of 1-m and 4-m resolution satellite data to ecological studies of tropical rain forests. *Ecological Application*, *14*(1), 61–74.
- Clauset, A., Shalizi, C. R., and Newman, M. E. J. (2009). Power-law distributions in empirical data. *SIAM Review*, *51*, 661.
- Cochrane, M. A. (2003). Fire science for rainforests. *Nature*, *417*, 913–919.
- Condit, R., Aguilar, S., Hernandez, A., Perez, R., Lao, S., Angehr, G., Hubbell, S. P., and Foster, R. B. (2004). Tropical forest dynamics across a rainfall gradient and the impact of an el nino dry season. *Journal of Tropical Ecology*, *20*, 51–72.
- Condit, R., Hubbell, S. P., Lafrankie, J. V., Sukumar, R., Manokaran, N., Foster, R. B., and Ashton, P. S. (1996). Species-area and species-individual relationships for tropical trees: a comparison of three 50-ha plots. *Journal of Ecology*, *84*(4), 549–562.
- Cox, P. M., Betts, R. A., Jones, C. D., Spall, S. A., and Totterdell, I. J. (2000). Accelerating of global warming due to carbon-cycle feedbacks in a coupled climate model. *Nature*, *401*(9), 184–187.
- Crawley, M. J. (2007). *The R book*. John Wiley & Sons, US.
- Cressie, N. (1993). *Statistics for Spatial Data (Wiley Series in Probability and Statistics)*. Wiley-Interscience, revised edition ed.

- Delaney, M., Brown, S., Lugo, A. E., TorresLezama, A., and Quintero, N. B. (1997). The distribution of organic carbon in major components of forests located in five life zones of Venezuela. *Journal of Tropical Ecology*, *13*, 697–708.
- Denslow, J. S. (1987). Tropical rainforest gaps and tree species diversity. *Annual Review of Ecology and Systematics*, *18*, 431–451.
- Dial, G., Bowen, H., Gerlach, F., Grodecki, J., and Oleszczuk, R. (2003). Ikonos satellite, imagery, and products. *Remote Sensing of Environment*, *88*(1-2), 23–36.
- Dial, G. and Grodecki, J. (2005). Rpc replacement camera models. In *ASPRS*. Baltimore, Maryland.
- Diggle, P. J. (1983). *Statistical Analysis of Spatial Point Patterns*. Academic Press, US.
- Eidt, R. C. (1968). *Biogeography and ecology in South America*, chap. The climatology of South America, pp. 54–81. W. Junk Publishers, Boston.
- Espírito-Santo, F. D. B., Keller, M., Braswell, B., Nelson, B. W., Froking, S., and Vicente, G. (2010). Storm intensity and old-growth forest disturbances in the Amazon region. *Geophysical Research Letters*, *37*(11), L11403.
- Fields-Team (2006). Tools for spatial data. national center for atmospheric research.
- Fisher, J., Hurtt, G., Thomas, Q. R., and Chambers, J. C. (2008). Clustered disturbances lead to bias in large-scale estimates based on forest sample plots. *Ecology Letters*, *11*, 554–563.
- Fraser, C., Baltasvias, E., and Gruen, A. (2001). Ikonos geo stereo images: Geometric potential and suitability for 3d building reconstruction. In *ISPRS Ankara Workshop*. Ascona, Switzerland.
- Fraver, S., Brokaw, N. V. L., and Smith, A. P. (1998). Delimiting the gap phase in the growth cycle of a Panamanian forest. *Journal of Tropical Ecology*, *14*, 673–681.
- Frazer, G., Canham, C., and Lertzman, K. (1999). *Gap Light Analyzer (GLA): Imaging software to extract canopy structure and gap light transmission indices from true-colour fisheye photographs, users manual and program documentation*. Simon Fraser University, Burnaby, British Columbia, and the Institute of Ecosystem Studies, Millbrook, New York.
- Frazer, G. W., Fournier, R. A., Trofymow, J. A., and Hall, R. J. (2001). A comparison of digital and film fisheye photography for analysis of forest canopy structure and gap light transmission. *Agricultural and Forest Meteorology*, *109*(4), 249–263.
- Frazer, G. W., Trofymow, J. A., and Lertzman, K. P. (2000). Canopy openness and leaf area in chronosequences of coastal temperate rainforests. *Canadian Journal of Forest Research-revue Canadienne De Recherche Forestiere*, *30*(2), 239–256.
- Frelich, L. E. (2002). *Forest dynamics and disturbance regimes studies from temperate evergreen-deciduous forests*. Cambridge University Press, Cambridge.
- Friedlingstein, P., Dufresne, J. L., Cox, P. M., and Rayner, P. (2003). How positive is the feedback between climate change and the carbon cycle? *Tellus Series B-chemical and Physical Meteorology*, *55*(2), 692–700.

- Frolking, S , Palace, M W , Clark, D B , Chambers, J Q , Shugart, H H , and Hurtt, G C (2009) Forest disturbance and recovery A general review in the context of spaceborne remote sensing of impacts on aboveground biomass and canopy structure *Journal of Geophysical Research-biogeosciences*, 114, G00E02
- Fujita, T T (1985) The downburst Microburst and macroburst Tech rep Satellite and Mesometeorology Research Project (SMRP), The University of Chicago
- Garstang, M , White, S , Shugart, H H , and Halverson, J (1998) Convective cloud downdrafts as the cause of large blowdowns in the amazon rainforest *Meteorology and Atmospheric Physics*, 67, 199–212
- Gloor, M , Phillips, O , Lloyd, J , Lewis, S , Malhi, Y , Baker, T , Lopez-Gonzalez, G , Peacock, J , Almeida, S , Oliveira, A , Alvarez, E , Amaral, I , Arroyo, L , Aymard, G , Banki, O , Blanc, L , Bonal, D , Brando, P , Chao, K -J , Chave, J , Dvila, N , Erwin, T , Silva, J , Fiore, A , Feldpausch, T , Freitas, A , Herrera, R , Higuchi, N , Honorio, E , Jimnez, E , Killeen, T , Laurance, W , Mendoza, C , Monteagudo, A , Andrade, A , Neill, D , Nepstad, D , Vargas, P , Peuela, M , Cruz, A , Prieto, A , Pitman, N , Quesada, C , Salomo, R , Silveira, M , Schwarz, M , Stropp, J , Ramirez, F , Ramirez, H , Rudas, A , Steege, H , Silva, N , Toires, A , Terborgh, J , Vsquez, R , and Heyden, G (2009) Does the disturbance hypothesis explain the biomass increase in basin-wide amazon forest plot data? *Global Change Biology*, 15, 2418–2430
- Goward, S N , Townshend, J R G , Zanon, V , Polcelli, F , Stanley, T , Ryan, R , Holekamp, K , Underwood, L , Pagnutti, M , and Fletcher, R (2003) Acquisition of earth science remote sensing observations from commercial sources lessons learned from the space imaging ikonos example *Remote Sensing of Environment*, 88(1-2), 209–219
- Grace, J , Lloyd, J , McIntyre, J , Miranda, A C , Meir, P , Miranda, H S , Nobre, C , Moncrieff, J , Massheder, J , Malhi Y , Wright, I , and Gash, J (1995) Carbon-dioxide uptake by an undisturbed tropical rain-forest in southwest amazonia, 1992 to 1993 *Science*, 270(5237), 778–780
- Hall, F G , Shimabukuro, Y E , and Huemmerich, K F (1995) Remote sensing of forest biophysical structure using mixture decomposition and geometric reflectance models *Ecological Application*, 5(4), 993–1013
- Harmon, M E , Whigham, D F , Sexton, J , and Olmsted, I (1995) Decomposition and mass of woody detritus in the dry tropical forests of the northeastern yucatan peninsula, mexico *Biotropica*, 27(3), 305–316
- Houghton, R A (2005) Aboveground forest biomass and the global carbon balance *Global Change Biology*, 11, 945–958
- Houghton, R A , Skole, D L , Nobre, C A , Hackler, J L , Lawrence, K T , and Chomentowski, W H (2000) Annual fluxes of carbon from deforestation and regrowth in the brazilian amazon *Nature*, 403(20), 301–304
- Hubbell, S P , Foster, R B , O'Brien, S T , Harms, K E , Condit, R , Wechsler, B , Wright, S J , and Loo de Lao, S (1999) Light-gap disturbances, recruitment limitation, and tree diversity in a neotropical forest *Science*, 283, 554–557

- Hurtt, G., Xiao, X., Keller, M., Palace, M., Asner, G. P., Braswell, R., Brondizio, E. S., Cardoso, M., Carvalho, C. J. R., Fearon, M. G., Guild, L., Hagen, S., S, T., Schloss, A., Vonotetis, G., Wickel, A. J., Moore III, B., and Nobre, C. (2003). Ikonos imagery for the large scale biosphereatmosphere experiment in amazonia (lba). *Remote Sensing of Environment*, 88, 111–127.
- INPE (1998). Instituto nacional de pesquisas espaciais, prodes (projeto de desflorestamento da amazonia).
- Journal, A. G. (1986). Constrained interpolation and qualitative information - the soft kriging approach. *Mathematical Geology*, 18(3), 269–305.
- Kayitakire, F., Hamel, C., and Defourny, P. (2006). Retrieving forest structure variables based on image texture analysis and ikonos-2 imagery. *Remote Sensing of Environment*, 102(3-4). 390–401.
- Keller, M., Palace, M., Asner, G., Pereira, R., and Silva, J. N. (2004). Coarse woody debris in undisturbed and logged forests in the eastern brazilian amazon. *Global Change Biology*, 10(5), p784–795.
- Kellner, J. and Asner, G. (2009). Convergent structural responses of tropical forests to diverse disturbance regimes. *Ecology Letters*, 12, 887–897.
- Körner, C. (2004). Through enhanced tree dynamics carbon dioxide enrichment may cause tropical forests to lose carbon. *Philosophical Transactions of the Royal Society: Biological Science*, 359, 493–498.
- Krige, D. G. (1951). A statistical approach to some basic mine valuation problems on the witwatersrand. *Journal of the Chemical, Metallurgical and Mining Society*, 52(4), 119–139.
- Laurance, W. F., Oliveira, A. A., Laurance, S. G., Condit, R., Nascimento, H. E. M., Sanchez-Thorin, A. C., Lovejoy, T. E., Andrade, A., D'Angelo, S., Ribeiro, J. E., and Dick, C. W. (2004). Pervasive alteration of tree communities in undisturbed amazonian forests. *Nature*, 428, 171–175.
- Lawton, R. O. and Putz, F. E. (1988). Natural disturbance and gap-phase regeneration in a wind-exposed tropical cloud forest. *Ecology*, 69(3), 764–777.
- Lefsky, M. A., Harding, D. J., Keller, M., Cohen, W. B., Carabajal, C. C., Esprito-Santo, F. D. B., Hunter, M. O., Oliveira, R., and Camargo, P. B. (2005). Estimates of forest canopy height and aboveground biomass using icesat. *Geophysical Research Letters*, 32(22), L22S02.
- Leigh, E. G. (1975). Structure and climate in tropical rain forest. *Ann. Rev. Ecol. Syst.*, 6, 67–86.
- Lewis, S. L., Lopez-Gonzalez, G., Sonke, B., Affum-Baffoe, K., Baker, T. R., Ojo, L. O., Phillips, O. L., Reitsma, J. M., White, L., Comiskey, J. A., Djuikouo, M. N., Ewango, C. E. N., Feldpausch, T. R., Hamilton, A. C., Gloor, M., Hart, T., Hladik, A., Lloyd, J., Lovett, J. C., Makana, J. R., Malhi, Y., Mbago, F. M., Ndangalasi, H. J., Peacock, J., Peh, K. S. H., Sheil, D., Sunderland, T., Swaine, M. D., Taplin, J., Taylor, D., Thomas,

- S. C., Votere, R., and Woll. H. (2009). Increasing carbon storage in intact african tropical forests. *Nature*, 457(7232), 1003–U3.
- Lewis, S. L., Phillips, O. L., Douglas, S., Barbara, V., R., B. T., Sandra, B., W., G. A., Niro, H., W., H. D., F., L. W., Jean, L., Yadvinder, M., Abel, M., Nez, V. P., Bonaventure, S., M.N.Nur, S., W., T. J., and Vsquez, M. R. (2004). Tropical forest tree mortality, recruitment and turnover rates: calculation, interpretation and comparison when census intervals vary. *Journal of Ecology*, 92, 929–9444.
- LI-COR (1992). *LAI-2000 plant canopy analyzer: operation manual*. Lincoln, Nebraska US.
- Lieberman, D., Lieberman, M., Peralta, R., and Hartshorn, G. S. (1985). Mortality patterns and stand turnover rates in wet tropical forest in costa rica. *Journal of Ecology*, 73, 915–924.
- Lieberman, M. and Lieberman, D. (1989). Forests are not just swiss cheese: canopy stereogeometry of non-gaps in tropical forests. *Ecology*, 70(3), 550–552.
- Lu, L. X., Denning, A. S., da Silva-Dias, M. A., da Silva-Dias, P., Longo, M., Freitas, S. R., and Saatchi, S. (2005). Mesoscale circulations and atmospheric co2 variations in the tapajos region, para, brazil. *Journal of Geophysical Research-atmospheres*, 110(D21), D21102.
- Lugo, A. E. (1995). Reconstructing hurricane passages over forests: a tool for understanding multiple-scale responses to disturbance. *Trends in Ecology & Evolution*, 10(3), 98–99.
- Lugo, A. E., Applefield, M., Pool, D. J., and Mcdonald, R. B. (1983). The impact of hurricane david on the forests of dominica. *Canadian Journal of Forest Research*, 13, 201–211.
- Lugo, A. E. and Helmer, E. (2004). Emerging forests on abandoned land: Puerto ricos new forests. *Forest Ecology and Management*, 190, 145–161.
- Malhi, Y. and Grace, J. (2000). Tropical forests and atmospheric carbon dioxide. *Trends in Ecology & Evolution*, 15(8), 332–337.
- Malhi, Y., Phillips, O. L., Lloyd, J., Baker, T., Wright, J., Almeida, S., Arroyo, L., Frederiksen, T., Grace, J., Higuchi, N., Killeen, T., Laurance, W. F., Leano, C., Lewis, S., Meir, P., Monteagudo, A., Neill, D., Vargas, P. N., Panfil, S. N., Patino, S., Pitman, N., Quesada, C. A., Rudas-Ll, A., Salomao, R., Saleska, S., Silva, N., Silveira, M., Sombroek, W. G., Valencia, R., Martinez, R. V., Vieira, I. C. G., and Vinceti, B. (2002). An international network to monitor the structure, composition and dynamics of amazonian forests (rainfor). *Journal of Vegetation Science*, 13(3), 439–450.
- Malhi, Y. and Román-Cuesta, R. M. (2008). Analysis of lacunarity and scales of spatial homogeneity in ikonos images of amazonian tropical forest canopies. *Remote Sensing of Environment*, 112(5), 2074–2087.
- Malhi, Y., Wood, D., Baker, T. R., Wright, J., Phillips, O. L., Cochrane, T., Meir, P., Chave, J., Almeida, S., Arroyo, L., Higuchi, N., Killeen, T. J., Laurance, S. G., Laurance, W. F., Lewis, S. L., Monteagudo, A., Neill, D. A., Vargas, P. N., Pitman, N. C. A., Quesada,

- C A , Salomao, R , Silva, J N M , Lezama, A T , Terborgh, J , Martinez, R V , and Vinceti, B (2006) The regional variation of aboveground live biomass in old-growth amazonian forests *Global Change Biology*, 12(7) 1107–1138
- Malhi, Y and Wright, J (2004) Spatial patterns and recent trends in the climate of tropical rainforest regions *Philosophical Transactions of the Royal Society Biological Science*, 359, 3113–29
- Markham, B L and Barker, J L (1987) Radiometric properties of u s processed landsat mss data *Remote Sensing of Environment*, 22(1), 39–71
- Mayle, F E and Power, M J (2008) Impact of a drier early-mid holocene climate upon amazonian forests *Philosophical Transactions of the Royal Society B-biological Sciences*, 363(1498), 1829–1838
- Melillo, j m , mcguire, a d , kicklighter, d w , moore, b , vorosmarty, c j , and schloss, a l (1993) Global climate change and terrestrial net primary production *Nature*, 363(6426), 234–240
- Miller, S D , Goulden, M L , and Da Rocha, H R (2007) The effect of canopy gaps on subcanopy ventilation and scalar fluxes in a tropical forest *Agricultural and Forest Meteorology*, 142(1), 25–34
- Nascimento, H E M , Laurance, W F , Condit, R , Laurance S G , D'Angelo, S , and Andrade, A C (2005) Demographic and life history correlates for amazonian trees *Journal of Vegetation Science*, 16 625–634
- Negron-Juarez, R I , Chambers, J Q , Guimaraes, G , Zeng, H , Raupp, C F M , Marra, D M , Ribeiro, G H P M , Saatchi, S S , Nelson, B W , and Higuchi, N (2010) Widespread amazon forest tree mortality from a single cross-basin squall line event *Geophysical Research Letters*, 37(16), L16701
- Nelson, B W , Kapos, V , Adams, J B , Oliveira, W J , Braun, O P G , and Amaral, I L (1994) Forest disturbance by large blowdowns in the brazilian amazon *Ecology*, 75(3), 853–858
- NOAA (2010) Estimated value of magnetic declination
- Nobis, M and Hunziker, U (2005) Automatic thresholding for hemispherical canopy photographs based on edge detection *Agricultural and Forest Meteorology*, 128(3-4), 243–250
- Numata, I , Soares, J V , Roberts, D A , Leonidas, F C , Chadwick, O A , and Batista, G T (2003) Relationships among soil fertility dynamics and remotely sensed measures across pasture chronosequences in rondonia, brazil *Remote Sensing of Environment*, 87(4), 446–455
- Palace, M , Keller, M , Asner, G P , Silva, J N M , and Passos, C (2007) Necromass in undisturbed and logged forests in the brazilian amazon *Forest Ecology Management*, 238, 309–318
- Palace, M , Keller, M , and Silva, H (2008) Necromass production Studies in undisturbed and logged amazon forests *Ecological Applications*, 18(4), 873–884

- Parker, G. G., Harmon, M. E., Lefsky, M. A., Chen, J., Pelt, R. V., Weis, S. B., Thomas, S. C., Willian, E. W., Shaw, D. C., and Frankling, J. F. (2004). Three-dimensional structure of an old-growth pseudotsuga-tsuga canopy and its implications for radiation balance, microclimate, and gas exchange. *Ecosystems*, 4(5), 440–453.
- Phillips, O. L., Baker, T. R., Arroyo, L., Higuchi, N., Killeen, T. J., Laurance, W. F., Lewis, S. L., Lloyd, J., Malhi, Y., Monteagudo, A., Neill, A. A., Vargas, P. N., Silva, J. N. M., Terborgh, J., Martnez, R. V., Alexiades, M., Almeida, S., Brown, S., Chave, J., Comiskey, J. A., Czimczik, C. I., Di Fiore, A., Erwin, T., Kuebler, C., Laurance, S. G., Nascimento, H. E. M., Olivier, J., Palacios, W., Patino, S., Pitman, N. C. A., Quesada, C. A., Saldias, M., Lezama, A. T., and Vinceti, B. (2004). Pattern and process in amazon tree turnover, 19762001. *Philosophical Transactions of the Royal Society: Biological Science*, 359, 477–491.
- Phillips, O. L. and Gentry, A. H. (1994). Increasing turnover through time in tropical forests. *Science*, 263, 954–958.
- Phillips, O. L., Lewis, S. L., Baker, T. R., Chao, K. J., and Higuchi, N. (2008). The changing amazon forest. *Philosophical Transactions of the Royal Society B-biological Sciences*, 363(1498), 1819–1827.
- Phillips, O. L., Malhi, Y., Higuchi, N., Laurance, W. F., Nnez, P. V., Vsquez, R. M., Laurance, S. G., Ferreira, L. V., Stern, M., Brown, S., and Grace, J. (1998). Changes in the carbon balance of tropical forests: evidence from long-term plots. *Science*, 282, 439–442.
- Phillips, O. L., Malhi, Y., Vicenti, B., Baker, T., Lewis, S. L., Higuchi, N., Laurance, W. F., Nes Vargas, P., Vquez Matinez, R., Laurance, S., Ferreira, L. V., Stern, M., Brown, S., and Grace, J. (2002). Changes in growth of tropical forests: Evaluating potential biases. *Ecological Applications*, 12(2), 576–587.
- Pyle, E. H., Santoni, G. W., Nascimento, H. E. M., Hutyra, L. R., Vieira, S., Curran, D. J., van Haren, J., Saleska, S. R., Chow, V. Y., Carmago, P. B., Laurance, W. F., and Wofsy, S. C. (2008). Dynamics of carbon, biomass, and structure in two amazonian forests. *Journal of Geophysical Research*, 113(G1), G00B08.
- Quesada, C. A., Lloyd, J., Schwarz, M., Baker, T. R., Phillips, O. L., Patio, S., Czimczik, C., Hodnett, M. G., Herrera, R., Arneith, A., Lloyd, G., Malhi, Y., Dezzeo, N., Luizo, F. J., Santos, A. J. B., Schmerler, J., Arroyo, L., Silveira, M., Priante Filho, N., Jimenez, E. M., Paiva, R., Vieira, I., Neill, D. A., Silva, N., Peuela, M. C., Monteagudo, A., Vsquez, R., Prieto, A., Rudas, A., Almeida, S., Higuchi, N., Lezama, A. T., Lpez-Gonzlez, G., Peacock, J., Fyllas, N. M., Alvarez Dvila, E., Erwin, T., di Fiore, A., Chao, K. J., Honorio, E., Killeen, T., Pea Cruz, A., Pitman, N., Nez Vargas, P., Salomo, R., Terborgh, J., and Ramrez, H. (2009). Regional and large-scale patterns in amazon forest structure and function are mediated by variations in soil physical and chemical properties. *Biogeosciences Discussions*, 6(2), 3993–4057.
- R-Team (2005). R: A language and environment for statistical computing, reference index version 2.2.1. r foundation for statistical computing.

- RADAMBRASIL (1976). Folha as.21- santarm. geologia, geomorfologia, pedologia, vegetação e uso potencial da terra (levantamento dos recursos naturais, v. 10). Tech. rep., Departamento Nacional de Produção Mineral, Rio de Janeiro, Brazil.
- Ramsey III, E. W., Hodgson, M. E., Sapkota, S. K., and Nelson, G. A. (2001). Forest impact estimated with noaa avhrr and landsat tm data related to an empirical hurricane wind-field distribution. *Remote Sensing of Environment*, 77(3), 279–292.
- Read, J. M., Clark, D. B., Venticinque, E. M., and Moreira, M. P. (2003). Application of merged 1-m and 4-m resolution satellite data to research and management in tropical forests. *Journal of Applied Ecology*, 40(3), 592–600.
- Ribeiro, P. and Diggle, P. J. (2001). geor: A package for geostatistical analysis. *R News*, 1(2), 14–18.
- Rice, A. H., Pyle, E. H., Saleska, S. R., Hutyyra, L., Camargo, P. B., Portilho, K., Marques, D. F., Palace, M., Keller, M., and Wofsy, S. C. (2004). Carbon balance and vegetation dynamics in an old-growth amazonian forest. *Ecological Applications*, 14(4), S55–S71.
- Rich, P. M. (1989). *A Manual for Analysis of Hemispherical Canopy Photography (CANOPY PROGRAM)*. Los Alamos National Laboratory is operated by the University of California for the United States Department of Energy under contract W-7405-ENG-36.
- Ripley, B. D. (1981). *Spatial statistics*. John Wiley & Sons, US.
- Rossetti, D. D., Toledo, P. M., and Goes, A. M. (2005). New geological framework for western amazonia (brazil) and implications for biogeography and evolution. *Quaternary Research*, 63(1), 78–89.
- Runkle, J. R. (1981). Gap regeneration in some old-growth forests of the eastern-united-states. *Ecology*, 62(4), 1041–1051.
- Saatchi, S. S., Harris, N. L., Brown, S., Lefsky, M., Mitchard, E. T. A., Salas, W., Zutta, B. R., Buermann, W., Lewis, S. L., Hagen, S., Petrova, S., White, L., Silman, M., and Morel, A. (2011). Benchmark map of forest carbon stocks in tropical regions across three continents. *Proceedings of the National Academy of Sciences of the United States of America*, 108(24), 9899–9904.
- Saatchi, S. S., Houghton, R. A., Alvala, R. C. D. S., Soares, J. V., and Yu, Y. (2007). Distribution of aboveground live biomass in the amazon basin. *Global Change Biology*, 13(4), 816–837.
- Saleska, S. R., Miller, S. D., Matross, D. M., Goulden, M. L., Wofsy, S. C., da Rocha, H. R., de Camargo, P. B., Crill, P., Daube, B. C., de Freitas, H., Hutyyra, L., Keller, M., Kirchhoff, V., Menton, M., Munger, J. W., Pyle, E. H., Rice, A. H., and Silva, H. (2003). Carbon in amazon forests: Unexpected seasonal fluxes and disturbance-induced losses. *Science*, 302, 1554–1557.
- Sanford, R. L., Braker, E. H., and Hartshorn, G. S. (1986). Canopy openings in a primary neotropical lowland forest. *Journal of Tropical Ecology*, 2(3), 277–282.



- Schimel, D. S., House, J. I., Hibbard, K. A., Bousquet, P., Ciais, P., Peylin, P., Braswell, B. H., Apps, M. J., Baker, D., Bondeau, A., Canadell, J., Churkina, G., Cramer, W., Denning, A. S., Field, C. B., Friedlingstein, P., Goodale, C., Heimann, M., Houghton, R. A., Melillo, J. M., Moore, B., Murdiyarso, D., Noble, I., Pacala, S. W., Prentice, I. C., Raupach, M. R., Rayner, P. J., Scholes, R. J., Steffen, W. L., and Wirth, C. (2001). Recent patterns and mechanisms of carbon exchange by terrestrial ecosystems. *Nature*, *414*(6860), 169–172.
- Schowengerdt, R. A. (1997). *Remote Sensing: Models and Methods for Image Processing*, vol. 2. Academic Press, MA.
- Sheil, D., Burslem, D.F.P., and Alder, D. (1995). The interpretation and misinterpretation of mortality-rate measures. *Journal of Ecology*, *83*(2), 331–333.
- Shimabukuro, Y. E. and Smith, J. A. (1991). The least-squares mixing models to generate fraction images derived from remote sensing multispectral data. *IEEE Transactions on Geoscience and Remote Sensing*, *29*(1), 16–20.
- Shugart, H. (1984). *A theory of forest dynamics: the ecological implications of forest succession models*. Springer-Verlag, NY.
- Shugart, H. H. (2000). Importance of structure in the longer-term dynamics of landscapes. *Journal of Geophysical Research-atmospheres*, *105*(D15), 20065–20075.
- Silver, W. L., Neff, J., McGroddy, M., Veldkamp, E., Keller, M., and Cosme, R. (2000). Effects of soil texture on belowground carbon and nutrient storage in a lowland amazonian forest ecosystem. *Ecosystems*, *3*(2), 193–209.
- Skole, D. and Tucker, C. (1993). Tropical deforestation and habitat fragmentation in the amazon - satellite data from 1978 to 1988. *Science*, *260*(5116), 1905–1910.
- Smith, B. and Sandwell, D. (2003). Accuracy and resolution of shuttle radar topography mission data. *Geophysical Research Letters*, *30*(9), 1467.
- Souza, C. and Barreto, P. (2000). An alternative approach for detecting and monitoring selectively logged forests in the amazon. *International Journal of Remote Sensing*, *21*(1), 173–179.
- Taylor, M. (2009). Ikonos planetary reflectance and mean solar exoatmospheric irradiance. Tech. rep., GeoEye.
- ter Steege, H. and Hammond, D. S. (2001). Character convergence, diversity, and disturbance in tropical rain forest in guyana. *Ecology*, *82*(11), 3197–3212.
- ter Steege, H., Pitman, N. C. A., Phillips, O. L., Chave, J., Sabatier, D., Duque, A., Molino, J.-F., Prvost, M.-F., Spichiger, R., Castellanos, H., von Hildebrand, P., and Vsquez, R. (2006). Continental-scale patterns of canopy tree composition and function across amazonia. *Nature*, *443*, 444–447.
- Toan, T. L., Quegan, S., Woodward, I., Lomas, M., Delbart, N., and Picard, G. (2004). Relating radar remote sensing of biomass to modelling of forest carbon budgets. *Climatic Change*, *67*(2-3), 379–402.

- Toutin, T (2001) Geometric processing of ikonos geo images with dem In *Joint ISPRS Workshop High Resolution Mapping from Space 2001* ISPRS, Hannover, Germany
- Toutin, T (2004) Review article Geometric processing of remote sensing images models, algorithms and methods *International Journal of Remote Sensing*, 25(10), 1893–1924
- TRFIC (2001) Tropical rain forest information center Orthorectified landsat atlas dvd series
- Tucker, C J (1979) Red and photographic infrared linear combinations for monitoring vegetation *Remote Sensing of Environment*, 8(2), 127–150
- Turner, M G (2010) Disturbance and landscape dynamics in a changing world *Ecology* 91(10), 2833–2849
- Uhl, C , Clark, K , Dezzio, N , and Maquirino, P (1988) Vegetation dynamics in amazon treefall gaps *Ecology*, 69(3), 751–763
- Van der Meer, P J and Bongers, F (1996) Formation and closure of canopy gaps in the rain forest at nouragues, french guiana *Vegetatio*, 126(2), 167–179
- Van der Meer, P J , Bongers, F , Chatrou, L , and Riera, B (1994) Defining canopy gaps in a tropical rain-forest - effects on gap size and turnover time *Acta Oecologica-international Journal of Ecology*, 15(6), 701–714
- van Nieuwstadt, M G L and Sheil, D (2005) Drought fire and tree survival in a borneo rain forest, east kalimantan, indonesia *Journal of Ecology*, 93, 191201
- Vandermeer, J , Cerda, I G , Bouglas, D , Perfecto, I , and Ruiz, J (2000) Hurricane disturbance and tropical tree species diversity *Science*, 290, 788–791
- Vicente, G A , Scofield, R A , and Menzel, W P (1998) The Operational goes infrared rainfall estimation technique *Bulletin of the American Meteorological Society*, 79(9), 1883–1898
- Walker, L R , Zarin, D J , Fetcher, N , Myster, R W , and Johnson, A H (1996) Ecosystem development and plant succession on landslides in the caribbean *Biotropica*, 28(4), 566–576
- Welles, J and Norman, J (1991) Instrument for indirect measurement of canopy architecture *Agronomy Journal*, 83, 818–825
- Whigham, D F , Olmsted, I , Cano, E C , and Harmon, M E (1991) The impact of hurricane gilbert on trees, litterfall, and woody debris in a dry tropical forest in the northeastern yucatan peninsula *Biotropica*, 23(4), 434–441
- Whitmore, T C (1989) Canopy gaps and the two major groups of forest trees *Ecology*, 70(3), 536–538
- Wittmann, F , Anhof, D , and Junk, W J (2002) Tree species distribution and community structure of central amazonian varzea forests by remote-sensing techniques *Journal of Tropical Ecology*, 18, 805820